
Low-frequency dynamics in complex liquid systems

A thesis
submitted in partial fulfillment of the requirements for the degree of

Doctor of Philosophy

By:

Sneha Banerjee

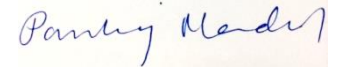
(ID: 20122027)



Department of Chemistry
Indian Institute of Science Education and Research
Pune

Certificate

Certified that the work incorporated in the thesis entitled “**Low Frequency Dynamics in Complex Liquid Systems**” submitted by **Sneha Banerjee** was carried out by the candidate, under my supervision. The work presented here or any part of it has not been included in any other thesis submitted previously for the award of any degree or diploma from any other university or institution.



(Dr. Pankaj Mandal)

Date: June 04, 2021

Declaration of Authorship

I hereby certify that the work which is being presented in the thesis entitled “**Low Frequency Dynamics in Complex Liquid Systems**” in partial fulfillment of the requirements for the award of the Degree of **Doctor of Philosophy** and submitted in the Department of Chemistry of the Indian Institute of Science Education and Research Pune is an authentic record of my own work carried out during a period from August, 2014 to June, 2021 under the supervision of Prof. Pankaj Mandal, Associate Professor, Department of chemistry, Indian Institute of Science Education and Research Pune. The matter presented in the thesis has not been submitted by me for the award of any other degree of this or any other institute.

Date: June 04,
2021



(Sneha Banerjee)

I have frequently been questioned, especially by women, of how I could reconcile family life with a scientific career. Well, it has not been easy.
– Marie Curie

Synopsis

Why study intermolecular interaction dynamics in liquid?

It is essential to understand the low-frequency dynamics in liquid systems because most of the chemical reactions occur in the liquid phase. The catalysis of drug synthesis and how a protein folds all depend on how the solvent molecule interacts with solutes and surfaces. Therefore, the fundamental questions that we need to probe are why there is such complex dependence of chemical phenomena on solvent properties? Can this relative importance of each solute-solvent interaction be identified and quantified? Furthermore, what happens to the interactions in solvent mixtures?

So, where do we see these intermolecular interactions manifesting in our real life?

Intermolecular interactions are an essential part of all aspects of our daily life. For example, in the case of protein misfolding and aggregation, the stability of the native and the denatured state depend on the delicate balance of intermolecular interactions occurring between the polar and the non-polar moieties of the protein with the solvent molecules. In our daily life, we see this denaturation when we fry an egg. When we fry an egg, we are not breaking any covalent bonds; the frying process rearranges the intermolecular interactions so that the albumin protein gets denatured. Rearrangements and fluctuations in the dynamic solute-solvent interactions occur in the fast femtosecond-picosecond timescales. Therefore, ultrafast spectroscopy allows intermolecular interactions to be probed in real-time in these fast timescales.

One of the most popular forms of spectroscopy that probes these dynamics in ultrafast timescales is the Terahertz time-domain spectroscopy (THz-TDS). Another non-resonant kind of spectroscopy called the Optical Kerr Effect (OKE) spectroscopy has also been successful in probing the low-frequency dynamics in liquid systems.

In **Chapter 2** of this thesis, we present the optical setup of the ultrafast THz-TDS and OKE spectroscopy that has been utilized in our lab.

Chapter 3 investigates the intermolecular interaction dynamics that occur in molecular liquid, benzene, and methanol in our case and in their binary mixtures of varying concentrations. One of the fascinating problems in chemistry is the formation of an azeotrope. Although azeotrope formation can be explained in terms of non-ideality, the microscopic picture remains a mystery.

Using the ultrafast spectroscopic techniques, we were able to shed light on the low-frequency dynamics of these solvent mixtures and how they differ from the azeotrope.

In **Chapter 4**, we explored the water dynamics using Optical Kerr Effect spectroscopy and changes occurring on the addition of a chaotropic solute, urea. The effect urea has on water structure is a highly debated problem in modern biochemistry. It is important to understand how urea affects the water structure because understanding this would help solve more complex problems in biology like protein denaturation. Analysis of our OKE data shows that urea does disrupt the water structure at higher concentrations.

Chapter 5 explores the water dynamics in the presence of three different types of proteins of different hydrophobicities and how these interactions change on denaturation of the protein with urea. Using ultrafast OKE spectroscopy, we saw that the mechanism behind the urea denaturation process is concentration-dependent and depends on the type of protein studied.

Acknowledgement

Foremost, I would like to thank my supervisor, Dr. Pankaj Mandal, without whose constant guidance and persistence this thesis would not have been possible. Above all, he has always been extremely patient and understanding in dealing with all his students, especially the difficult ones ;) ! I am highly appreciative of his support and that he always believes in his students. It was no easy journey, but it was manageable with having him as a mentor and a friend. Thank you, Sir!

I thank my Research Advisory Committee members, Dr. Sayan Bagchi and Dr. Arnab Mukherjee, for their critical suggestions during the annual RAC meetings. Discussions with them provided significant insights on various topics I worked on. I express my gratitude especially towards Dr. Sayan Bagchi, who provided space in his lab to finish my work when our lasers were down.

Indian Institute of Science Education and Research, Pune has undeniably provided the best research atmosphere. I sincerely thank its former and present Director for providing state-of-the-art research facilities and generous funding required to build a high-tech Laser lab. I also thank Dr. H.N. Gopi, Chair Chemistry, for his support.

Valuable time has been saved by Mayuresh and Tushar by their immense help in administrative tasks; I am much grateful to them and wish best to them for the future.

Of course, a good work environment is a prerequisite to thriving in academia. I want to thank my lab members – Avinash, Shabnum, and Aman, for supporting me throughout. I have always found solace in whining about the ups and downs of life with them. I promise to always be there to listen to you guys complain about literally anything. I also want to thank the newer/temporary members – Mayank, Ziyad, and Riteeka for being absolute sweethearts.

Most importantly, I want to thank my senior colleagues, Dr. Sohini Sarkar, and Dr. Y.G. Reddy. They bore the brunt of setting up an ultrafast spectroscopy lab and also mentored me throughout the process. Especially Sohini, who made me believe that things are often not as difficult as they seem.

A special thank you to Dr. Sayan Bagchi's group members- Deborin, Tapas, Somnath, Sushil, and Samadhan who helped during my experiments in NCL and always made me feel welcome.

This acknowledgment cannot be completed without the mention of my friends, Sulagna, Chandreyee, Aratrika, Nirajita, Priya, Sapna, and Surabhi, were with me before I embarked on this

journey, and they all checked in and constantly uplifted me to make sure that I complete this one. Kunal, Nandi, Maddy, Harshini, Aditya, Ravi, Sunil, Shabnum, Avinash, and Aman, provided an eventful Ph.D. life and everlasting memories. Thank you guys for making this possible. A special shout-out to the different all-girls gangs that I have made throughout different phases of my life; thank you for getting me out of my head and motivating me enough to finish this.

Last and most importantly, I want to thank my parents, who played a significant role in this journey. I can't thank them enough for making me the person I am today and supporting me through thick and thin. A special mention to my in-laws, who have always constantly supported all my decisions.

Also, a special shout-out to Kunal and my mother for constantly nagging and irritating me so much that I had no other option but to cry and finish this thesis.

Contents

Chapter 1 Introduction.....	4
1.1 Intermolecular Interactions.....	5
1.2 Spectroscopy in the THz regime.....	6
1.3 Optical Kerr Effect Spectroscopy.....	8
1.4 Understanding low-frequency liquid dynamics.....	9
1.5 References.....	13
Chapter 2 Experimental Methods and Data Analysis	17
2.1 Optical Kerr Effect (OKE) spectroscopy.....	18
2.2 THz-TDS setup using air-photonics for generation and detection of THz radiation....	26
2.3 References.....	29
Chapter 3 Structural fluctuations in an azeotrope: Understanding the benzene-methanol azeotrope.....	31
3.1 Introduction	32
3.2 Experimental Methods	35
3.2.1 Samples	35
3.2.2 Optical Kerr Effect (OKE) spectroscopy	36
3.2.3 THz-Time Domain Spectroscopy	36
3.3 Result and Discussion	36
3.3.1 Spectral Density and the dielectric loss spectra	36
3.3.2 Excess dielectric loss spectra	43
3.3.3 Excess and reduced spectral densities	44
3.4 Conclusion	55
3.5 References	56
Chapter 4 Water and water-urea dynamics.....	59
4.1 Introduction	60
4.2 Experimental Methods	63
4.2.1 Samples	63

4.2.2	Optical Kerr Effect Spectroscopy	63
4.3	Result and Discussion	63
4.4	Conclusion	70
4.5	References	71
Chapter 5	Protein-water interactions and protein denaturation by urea.....	76
5.1	Introduction	77
5.2	Experimental Methods	79
5.2.1	Samples	79
5.2.2	Optical Kerr Effect Spectroscopy	79
5.3	Result and Discussion	79
5.3.1	Protein-water dynamics	79
5.3.1 a)	Lysozyme	79
5.3.1 b)	Bovine serum albumin (BSA)	83
5.3.1 c)	Trypsin	87
5.3.2	Protein dynamics in urea solutions	89
5.4	Conclusion	94
5.5	References	95
Chapter 6	Summary and Outlook.....	100
6.1	The Bigger Picture	101

To
My depression, without which this thesis could have been completed maybe a year ago.

Also,
To
SSRIs, with which I was able to complete this. 😊

1

Introduction

1.1 Intermolecular Interactions

Intermolecular interactions are the forces between molecules that define the physical states of matter. Molecules attract at long distances (which is why solids and liquids exist) and repel each other at small separations (which is why their densities are finite) [1]. Interest in understanding intermolecular interactions go way back to Democritus, a Greek philosopher (ca. 460 B.C. – ca. 370 B.C.), who first hypothesized that matter existed due to interaction between small indivisible particles (“atoms”). Around 1899-1900, the work of Diderik van der Waals, Barth, and Leipzig focused on the importance of intermolecular forces in gases and liquids. For his seminal work in this field, intermolecular interactions are also called van der Waals interactions. Maurice Huggins was the first to reference the concept of hydrogen bond, in his undergraduate term paper in 1919 (unpublished) [2]. Although the origin of hydrogen bond is mostly credited to Latimer and Rodebush, the term “hydrogen bond” was probably first coined by G.N. Lewis in 1923 [2], [3]. Using simple theoretical electrostatic models, Pauling was able to reproduce H-bond energies [4] and explained the role of hydrogen bonding in forming structures. The quantum mechanical picture for intermolecular interaction, especially the dispersion forces, was given by Fritz London in 1930 [5].

Intermolecular interactions are important because they influence the physical, chemical, and biological properties of molecules, and in their absence, all matter would exist only in the gaseous phase, and life as we know it would cease to exist. The study of intermolecular interaction is vital in understanding the condensed phase dynamics, like properties of liquids and liquid mixtures, solvation, electrochemistry, structure-function correlation of bio-molecules, aggregation of molecules, and many such physical phenomena.

It would be impossible to describe in detail the broad field of intermolecular interactions in its entirety. Data on intermolecular interaction is mainly obtained from four primary sources 1) spectroscopy, 2) quantum mechanical calculations, 3) molecular beam scattering, and 4) transport and equilibrium properties of gases. In this thesis, we probe intermolecular dynamics in complex liquid systems using ultrafast spectroscopy.

Liquid dynamics are challenging to study at the molecular level because of the presence of multiple timescales pertaining to inter- and intra-molecular interactions. This results in the broadening of

the spectral signatures making it difficult to probe the molecular interactions. It is therefore essential to develop new spectroscopic tools that can separate out the spectral details. It is crucial to have a clear understanding of liquid dynamics because most of the chemical reactions occur in the liquid state. Not only that, from catalysis for drug synthesis to how proteins fold, they all depend on how the solvent molecule interacts with solutes and surfaces. The reason behind this complex dependence is the presence of different types of intermolecular forces existing between molecules. Depending on the molecules, the intermolecular forces can be long-range, which would include Columbic interactions, induced interaction, and dispersion; or short-range- charge transfer interaction and exchange repulsion.

Electrostatic forces are generally very strong and can be either attractive or repulsive. Unequal sharing of electrons in molecules due to differences in electronegativity leads to the formation of dipoles. Two dipoles can interact with one another with opposite ends attracting and like ends repelling each other. Hydrogen bonding is a special case of dipole-dipole interaction. Any molecule with a dipole moment can now distort the electron density of a nearby molecule, thereby inducing a temporary dipole in that molecule, this type of interaction is always attractive. Molecules also resonate, electrons in spherical atoms also fluctuate in time. Fluctuation of electron density causes dipole moments also to fluctuate. Therefore all molecules can be perceived as dipoles oscillating in time. Molecules that are in close proximity couple, and the movement of their electrons become correlated. The electrostatic attractive forces between these coupled fluctuating dipoles are called dispersive forces. The important thing to note here is that all these intermolecular interactions, their fluctuations, and rearrangements, like the hydrogen-bond vibrations or their making and breaking, they all occur in the femtosecond-picosecond timescales. Ultrafast spectroscopy allows intermolecular forces and dynamics of complex liquid systems to be observed directly in real-time at these fast fs-ps timescales. One of the most popular techniques to be used is the THz time-domain spectroscopy (THz-TDS) which has immense potential to probe the dynamics of various systems at these timescales. Another non-resonant technique covered in this thesis is the Optical Kerr effect (OKE) spectroscopy, which has been particularly successful in probing the molecular dynamics of liquid systems.

1.2 Spectroscopy in the THz regime

The terahertz (THz) frequency range spanning from 0.1 to 20 THz contains valuable information on the low-frequency relaxation dynamics of molecular liquids, biomolecules, and other condensed phase systems. Spectroscopy in the THz regime has emerged as a powerful tool to probe the low frequency vibrational and rotational modes in different molecules, molecular assemblies, and also in crystalline solids. Low energy phonon modes and charge carrier dynamics in electronic materials can also be probed using THz spectroscopy. THz radiation can be used to obtain the dielectric constant of various materials in this low-frequency regime. The THz region has also generated substantial interest in the medical community. Experiments are able to differentiate between healthy and cancerous cells by determining the water content in the cells. The non-invasive and non-ionizing nature of THz radiation makes it suitable for biomedical imaging and to be used as body scanners. With the advent of ultrafast lasers, it has become possible to map the temporal evolution of various physical phenomena at picosecond and sub-picosecond timescales. The generation and detection of THz pulses and thereby THz spectroscopy were pioneered by David Auston, Martin Nuss [6], and Dan Grischkowsky [7] using photoconductive antennas (PCA). Non-resonant, nonlinear processes like Optical Rectification (OR) and electro-optic (E.O.) sampling have also been used to generate and detect THz pulses [8-10]. Generation and detection of THz radiation using air plasma has been deemed the most successful in realizing a broadband THz spectrum [11]. An intense laser light (typically the output of a Ti-Sapphire amplifier, 800nm) and its second harmonic are focused in ambient air, creating a plasma at the focal point due to ionization. This plasma acts as a non-linear medium and emits electromagnetic radiation, including THz radiation.

The THz region lies between the microwave and the infrared region of the electromagnetic spectrum. Only with the advent of ultrafast lasers, it became possible to probe this spectral region, which was commonly referred to as the "THz gap." In a typical THz experiment, THz pulses are created using ultrafast pulses (10fs-100fs) from a Ti-Sapphire oscillator or amplifier system. The pulse duration of the THz pulse generated is ~ 1 ps. 1 THz is typically defined as 33.3 cm^{-1} in wavenumber, $300 \text{ }\mu\text{m}$ in wavelength, and 4.14 meV in energy. One of the advantages of THz-time domain spectroscopy (THz-TDS) is that it measures the transient electric field and not just its intensity. A Fourier transform of the time-dependent THz electric field determines the amplitude

and phase of the spectral components that make up the pulse. The absorption coefficient and the refractive index of the sample (and hence complex dielectric function) can be calculated from the amplitude and phase information without calling for the complicated Kramer-Kronig analysis. Using an additional ultrafast pump beam, the THz-TDS setup can be modified to a pump-probe experiment to be used for time-resolved studies on various systems.

1.3 Optical Kerr Effect Spectroscopy

Kerr effect, first discovered in 1875, stated that a static electric field could induce changes in the optical properties of a liquid [12]. It was found later that intense optical fields could also induce measurable changes in the dielectric properties of a liquid; this was called the Optical Kerr Effect [13], and the first successful experiment was demonstrated in 1963 [14], [15]. With the introduction of pulsed lasers, spectroscopic research in the picosecond and sub-picosecond timescales became possible. With a pulsed laser, it was possible to get a broad spectral bandwidth extending up to 20-30 THz; the bandwidth solely dependent on the pulse duration. Another significant advancement was the introduction of the optical heterodyne detection [16]. The optically heterodyne detected – optical Kerr effect (OHD-OKE) has substantially improved signals in terms of signal-to-noise ratio [17] and control on the stray birefringence effects in the signal [18]. The first OKE experiment using sub-picosecond laser pulses and heterodyned detection was realized in the 1980s [19-22], which led to more research groups investigating the fast dynamics of simple molecular liquids using OHD-OKE, complex dynamics like that of molecular liquids approaching phase transition, liquid crystals, and glass formers have also been investigated using this technique [23].

The Optical Kerr effect is a third-order non-linear process, and it measures the derivative of the time-correlation function of the anisotropic part of the polarizability tensor, unlike THz-TDS, which measures the two-point correlation function of the dipole moment. The advantage of doing an OKE and THz-TDS study together is that it is possible to get complementary information on the same dynamics of a system [24].

$$S_{OKE}(t) \propto \frac{d}{dt} \langle \alpha(0) \alpha(t) \rangle ;$$

$$S_{THz-TDS}(t) \propto \frac{d}{dt} \langle \mu(0) \mu(t) \rangle ;$$

When an intense laser light beam propagates in a material, it is accompanied by the orientation of the electric charges along the electric field. The polarization of the electrons is instantaneous and follows the oscillations of the electric field, even at optical frequencies. If the molecules have permanent or an induced dipole moment, they reorient along the direction of propagation of the field. This motion is slow relative to the oscillation of the optical field. After electronic and nuclear reorientation, the material is no longer isotropic, and therefore the refractive index along the optical electric field is not the same as that in the other directions. This photo-induced birefringence is the Optical Kerr Effect (OKE). Once the electric field is interrupted, the electronic birefringence ceases immediately, while the decay of the nuclear birefringence requires molecular reorientation. The measurement of the temporal variation of the nuclear birefringence is used to get information on the dynamics of liquids.

1.4 Understanding low-frequency liquid dynamics:

The rotational and vibrational spectra of many liquids and gases lie in the electromagnetic spectrum's THz region. One of the most studied liquids in the history of OKE spectroscopy is benzene. It was also seen that the molecular shape and polarizability affected the shapes of the OKE spectra more than the intermolecular dynamics, which was the reason behind benzene and pyridine having similar spectral densities [25] [26]. From simulations and OKE experiments, it was concluded that the high-frequency portion of the spectral density had contributions from molecular librations [25] [27], while the 20 cm^{-1} low-frequency shoulder had contributions that were both translational and rotational in character. The orientational diffusion timescales from the exponential fits measured by different groups were around 3 ps, and the faster intermediate timescale ranged from 0.7- 1 ps. The slow diffusive timescales were found to be proportional to the inverse square root of the tumbling moment of inertia, which also suggested a strong translational-rotational coupling in benzene [28]. Using a short enough pulse (35 fs), it has also been possible to obtain an OKE spectrum till 20 THz, which resolves the intramolecular in-plane ring deformation mode of benzene [29]. Earlier studies also tried to interpret the vibrational dynamics of benzene in terms of phonon modes, basing it on the fact that the molecules in a liquid are not random but are ordered in short times. Each molecule will be surrounded by other molecules forming cage-like clusters fading into the bulk. The oscillator lineshapes used to fit

these normal modes explain the spectra in terms of a mixture of inhomogeneously broadened, underdamped and overdamped librations and intermolecular vibrations [19]. A recent study by Farrell et al. has tried to simplify the spectral density (S.D.) of benzene and other alkanes by utilizing a four-component model to fit the data. The α and the β relaxation correspond to the orientational and translational diffusion and have been fitted to the Debye and Cole-Cole functions. The cage rattling motion is known as the fast β process. The fast β , in this case, fits well with a Brownian oscillator. And the other oscillator is used to account for the librational motions [30]. Although this type of fitting procedure makes the analysis look simplistic and ignores the fact that these underlying dynamics are not separate processes but correlated to each other, they have still been able to describe the underlying dynamics of a wide range of liquids.

One of the other most studied systems using THz-TDS is the properties of water vapor [31], liquid water, and its mixtures with other molecular liquids [32, 33]. The dielectric properties of liquids depend on the interaction of dipoles, permanent and induced, and their relaxations. Hydrogen bonding has a significant effect on these dipoles and hence on the THz response. The reorientation of these dipoles in liquids happens in picosecond timescales, and a knowledge of the dynamics is essential for both chemical reaction rates and biological functions. Two Debye functions have been called to model the dielectric spectra of water, with timescales of roughly 200 fs and 8 ps [34], [35]. The addition of another liquid changes these dynamics. A third Debye function has to be used to fit the water-ethanol data [36]. THz-TDS has also been used to understand the water dynamics in the presence of ions. The ions not only slow down the dynamics [37], but in some cases, their effects propagate to water molecules beyond the first solvation shell because of water's extensive hydrogen-bonding network. OKE spectrum of water shows a relaxation peak attributed to translational diffusion or cage-rattling motion (β relaxation), water has two additional intermolecular modes corresponding to the hydrogen bond bend or the transverse acoustic (T.A.) phonon mode and the hydrogen bond stretch or the longitudinal acoustic (L.A.) phonon mode. Beyond 20 THz librational bands start appearing [24].

As mentioned earlier, the advantage of doing a THz-TDS and OKE experiment together on the same system is that it is possible to get complementary information on the same dynamics. Comparing the dielectric loss spectrum and susceptibility spectrum for water show that both the spectra look different at first glance. A relaxation peak dominates the dielectric loss spectrum at low frequencies spanning up to 400GHz. The loss spectrum is fitted to two Debye with timescales

8.38 ps and 1.1 ps and four damped harmonic oscillators. The interesting thing is, after removing the slowest, most dominant peak, the shape of the loss spectrum looks similar to the Raman spectrum. One single relaxation and four oscillators were used to fit the Raman spectrum. The correlation between both these spectra suggests that these intermolecular modes in the loss and the susceptibility spectra have the same molecular origin [38].

Understanding water dynamics on its own and in the presence of different biologically important solutes is fundamental because water plays a crucial role in many biological functions. The addition of solutes does not affect the librational dynamics of water as much; for hydrophilic solutes, the hydrogen bond stretch and bending modes only start getting affected when half the water molecules are inside the solvation shell. For solutes with hydrophobic moieties, the bimodal character of the spectral density of water persists till even higher concentrations [39, 40]. On the other hand, the translational diffusive timescales show retardation by a factor of 4, which is evident even at low concentrations of the solute. A recent study explores the water spectrum from picosecond to nanosecond timescales to have a more generalized picture of the slowdown of the water dynamics over a wide range of solutes. To focus on water dynamics, the solutes are chosen so that they do not contribute to the OKE spectrum much [40].

Recent OKE experiments on biological samples have also shown the presence of underdamped vibrational modes even in physiological conditions. The general assumption was that any low-frequency vibrational modes, if present in these samples, would be highly overdamped due to interaction with water, and the spectra at large would represent the change in water dynamics with the addition of these solutes. However, this is not the case, as delocalized phonon-like modes have been observed in proteins, enzymes, enzyme-inhibitor complexes, and DNA [41, 42]. OKE experiments on different oligomers dissolved together (association) and separately (minimizing the probability of association) have been used to identify different underdamped phonon bands that correspond to interstrand hydrogen-bond modes of single and double-strand DNA. Understanding the dynamics of these phonon modes is essential because breaking these hydrogen bonds is the initial step that leads to the formation of the transcription bubble, which facilitates the transcription and replication processes in DNA [42]. Low-frequency vibrational modes in G-quadruplexes have also been investigated using optical Kerr effect spectroscopy. A summation of Debye, Cole-Cole and several Brownian oscillators are generally called upon to fit these GHz-THz spectra. OKE spectra can be used to resolve different low-frequency modes of doubly-

stranded DNA and G quadruplexes, which shows that changes in the stiffness of the molecules can also bring about a change in its low-frequency dynamics [43].

One of the interesting ways in which intermolecular interactions manifests, is in the formation of an azeotrope. While the physical interpretation of why azeotropes occur can be explained in terms of non-ideality, azeotropes remain a mystery at a molecular level. In Chapter 3 of this thesis, we use ultrafast spectroscopic techniques on the azeotrope and other mixtures of benzene and methanol throughout the composition range, which not only gives us information about the relaxation and librational dynamics at ultrafast timescales but provides experimental proof that the formation of an azeotrope is a temperature-driven process.

Water, especially interfacial water, has a significant effect on the protein's internal structure and dynamics. OKE spectral density can resolve protein water dynamics from 100GHz to up to 10THz, including relaxation and librational dynamics of bulk water and water-protein interactions. Urea is a chaotropic agent and a well-known denaturant for proteins. The molecular picture of the interaction of urea with the water hydrogen bond network and the chemical denaturation of the proteins is still ambiguous. Analysis of the spectral densities of urea solutions obtained from OKE spectroscopy shows the presence of two types of environments depending on the molarity of the solution. In Chapters 4 and 5, we have used OKE spectroscopy to investigate the effect urea has on the water hydrogen bond network and mapped out the structural changes occurring in three different proteins on the addition of urea.

1.5 References

1. A D Buckingham, a. and B.D. Utting, *Intermolecular Forces*. Annual Review of Physical Chemistry, 1970. **21**(1): p. 287-316.
2. Balaram, P., *Bonds: Chemical, Hydrogen and Others*. Current Science, 2013. **104**(5): p. 567-568.
3. Latimer, W.M. and W.H. Rodebush, *POLARITY AND IONIZATION FROM THE STANDPOINT OF THE LEWIS THEORY OF VALENCE*. Journal of the American Chemical Society, 1920. **42**(7): p. 1419-1433.
4. Pauling, L., *he nature of the chemical bond and the structure of molecules and crystals: An introduction to modern structural chemistry*. 1944, Ithaca, N.Y: Cornell University Press
5. London, F., *Zur Theorie und Systematik der Molekularkräfte*. Zeitschrift für Physik, 1930. **63**(3): p. 245-279.
6. Auston, D.H. and M.C. Nuss, *Electrooptical generation and detection of femtosecond electrical transients*. IEEE Journal of Quantum Electronics, 1988. **24**(2): p. 184-197.
7. Gallot, G. and D. Grischkowsky, *Electro-optic detection of terahertz radiation*. Journal of the Optical Society of America B, 1999. **16**(8): p. 1204-1212.
8. Hu, B.B., et al., *Free-space radiation from electro-optic crystals*. Applied Physics Letters, 1990. **56**(6): p. 506-508.
9. Carrig, T.J., et al., *Scaling of terahertz radiation via optical rectification in electro-optic crystals*. Applied Physics Letters, 1995. **66**(2): p. 121-123.
10. Nahata, A., A.S. Weling, and T.F. Heinz, *A wideband coherent terahertz spectroscopy system using optical rectification and electro-optic sampling*. Applied Physics Letters, 1996. **69**(16): p. 2321-2323.
11. Karpowicz, N., X. Lu, and X.C. Zhang, *Terahertz gas photonics*. Journal of Modern Optics, 2009. **56**(10): p. 1137-1150.
12. Kerr, J., *XL. A new relation between electricity and light: Dielectrified media birefringent*. The London, Edinburgh, and Dublin Philosophical Magazine and Journal of Science, 1875. **50**(332): p. 337-348.

13. Buckingham, A.D., *Birefringence Resulting from the Application of an Intense Beam of Light to an Isotropic Medium*. Proceedings of the Physical Society. Section B, 1956. **69**(3): p. 344-349.
14. Mayer, G.a.G., R. , *The effect of an intense light beam on the index of refraction of liquids*. 258: 2039. C.R. Acad. Sci., 1963. **258**: p. 2039.
15. Maker, P.D., R.W. Terhune, and C.M. Savage, *Intensity-Dependent Changes in the Refractive Index of Liquids*. Physical Review Letters, 1964. **12**(18): p. 507-509.
16. Ippen, E.P. and C.V. Shank, *Picosecond response of a high-repetition-rate CS₂ optical Kerr gate*. Applied Physics Letters, 1975. **26**(3): p. 92-93.
17. Levenson, M.D. and G.L. Eesley, *Polarization selective optical heterodyne detection for dramatically improved sensitivity in laser spectroscopy*. Applied physics, 1979. **19**(1): p. 1-17.
18. Waldeck, D., et al., *Picosecond pulse induced transient molecular birefringence and dichroism*. The Journal of Chemical Physics, 1981. **74**(6): p. 3381-3387.
19. McMorro, D., W.T. Lotshaw, and G.A. Kenney-Wallace, *Femtosecond optical Kerr studies on the origin of the nonlinear responses in simple liquids*. IEEE Journal of Quantum Electronics, 1988. **24**(2): p. 443-454.
20. Kalpouzos, C., et al., *Femtosecond laser-induced Kerr responses in liquid carbon disulfide*. The Journal of Physical Chemistry, 1987. **91**(8): p. 2028-2030.
21. Greene, B.I., et al., *Microscopic dynamics in simple liquids by subpicosecond birefringences*. Physical Review A, 1984. **29**(1): p. 271-274.
22. Greene, B.I. and R.C. Farrow, *The subpicosecond kerr effect in CS₂*. Chemical Physics Letters, 1983. **98**(3): p. 273-276.
23. Smith, N.A. and S.R. Meech, *Optically-heterodyne-detected optical Kerr effect (OHD-OKE): Applications in condensed phase dynamics*. International Reviews in Physical Chemistry, 2002. **21**(1): p. 75-100.
24. Turton, D.A., et al., *Rattling the cage: Micro- to mesoscopic structure in liquids as simple as argon and as complicated as water*. Journal of Molecular Liquids, 2011. **159**(1): p. 2-8.
25. Heisler, I.A. and S.R. Meech, *Low-frequency isotropic and anisotropic Raman spectra of aromatic liquids*. The Journal of Chemical Physics, 2010. **132**(17): p. 174503.

26. Zhong, Q. and J.T. Fourkas, *Optical Kerr Effect Spectroscopy of Simple Liquids*. The Journal of Physical Chemistry B, 2008. **112**(49): p. 15529-15539.
27. Ryu, S. and R.M. Stratt, *A Case Study in the Molecular Interpretation of Optical Kerr Effect Spectra: Instantaneous-Normal-Mode Analysis of the OKE Spectrum of Liquid Benzene*. The Journal of Physical Chemistry B, 2004. **108**(21): p. 6782-6795.
28. Manfred, K., X. He, and J.T. Fourkas, *Assessing the Role of Moment of Inertia in Optical Kerr Effect Spectroscopy*. The Journal of Physical Chemistry B, 2010. **114**(37): p. 12096-12103.
29. Kakinuma, S. and H. Shirota, *Dynamic Kerr Effect Study on Six-Membered-Ring Molecular Liquids: Benzene, 1,3-Cyclohexadiene, 1,4-Cyclohexadiene, Cyclohexene, and Cyclohexane*. The Journal of Physical Chemistry B, 2015. **119**(13): p. 4713-4724.
30. Farrell, A.J., et al., *Low-Frequency (Gigahertz to Terahertz) Depolarized Raman Scattering Off n-Alkanes, Cycloalkanes, and Six-Membered Rings: A Physical Interpretation*. The Journal of Physical Chemistry B, 2020. **124**(35): p. 7611-7624.
31. van Exter, M., C. Fattinger, and D. Grischkowsky, *Terahertz time-domain spectroscopy of water vapor*. Optics Letters, 1989. **14**(20): p. 1128-1130.
32. Rønne, C., P.-O. Åstrand, and S.R. Keiding, *THz Spectroscopy of Liquid H_2O and D_2O* . Physical Review Letters, 1999. **82**(14): p. 2888-2891.
33. Venables, D.S. and C.A. Schmuttenmaer, *Far-infrared spectra and associated dynamics in acetonitrile–water mixtures measured with femtosecond THz pulse spectroscopy*. The Journal of Chemical Physics, 1998. **108**(12): p. 4935-4944.
34. Thrane, L., et al., *THz reflection spectroscopy of liquid water*. Chemical Physics Letters, 1995. **240**(4): p. 330-333.
35. Kindt, J.T. and C.A. Schmuttenmaer, *Far-Infrared Dielectric Properties of Polar Liquids Probed by Femtosecond Terahertz Pulse Spectroscopy*. The Journal of Physical Chemistry, 1996. **100**(24): p. 10373-10379.
36. Møller, U., et al., *Terahertz reflection spectroscopy of Debye relaxation in polar liquids [Invited]*. Journal of the Optical Society of America B, 2009. **26**(9): p. A113-A125.
37. Tielrooij, K.J., et al., *Cooperativity in Ion Hydration*. Science, 2010. **328**(5981): p. 1006-1009.

38. Fukasawa, T., et al., *Relation between dielectric and low-frequency Raman spectra of hydrogen-bond liquids*. Physical Review Letters, 2005. **95**(19).
39. Heisler, I., K. Mazur, and S. Meech, *THz Raman spectra of aqueous solutions of hydrophiles and amphiphiles*. SPIE OPTO. Vol. 8623. 2013: SPIE.
40. Ramakrishnan, G., et al., *Spectrum of Slow and Super-Slow (Picosecond to Nanosecond) Water Dynamics around Organic and Biological Solutes*. The Journal of Physical Chemistry Letters, 2017. **8**(13): p. 2964-2970.
41. Turton, D.A., et al., *Terahertz underdamped vibrational motion governs protein-ligand binding in solution*. Nature Communications, 2014. **5**(1): p. 3999.
42. González-Jiménez, M., et al., *Observation of coherent delocalized phonon-like modes in DNA under physiological conditions*. Nature Communications, 2016. **7**(1): p. 11799.
43. González-Jiménez, M., G. Ramakrishnan, and K. Wynne, *Low-frequency vibrational modes in G-quadruplexes reveal the mechanical properties of nucleic acids*. bioRxiv, 2020: p. 2020.03.16.993873.

2

Experimental Methods and Data Analysis

2.1 Optical Kerr Effect (OKE) spectroscopy

The experimental setup for OHD-OKE is relatively straightforward compared to other forms of pump-probe spectroscopies.

A part of the beam from a Ti: Sapphire amplified laser (Spitfire Pro XP, Spectra-Physics) with a central wavelength of 800 nm and a repetition rate of 1 kHz is split into a pump and a weak probe beam using a beam splitter. The pump power is kept below 1 mW to avoid pulse distortion due to nonlinear processes. To probe the ultrafast dynamics of the molecules, the pulse duration should be less than 100fs; the shorter the pulse, the broader is the spectral bandwidth obtained.

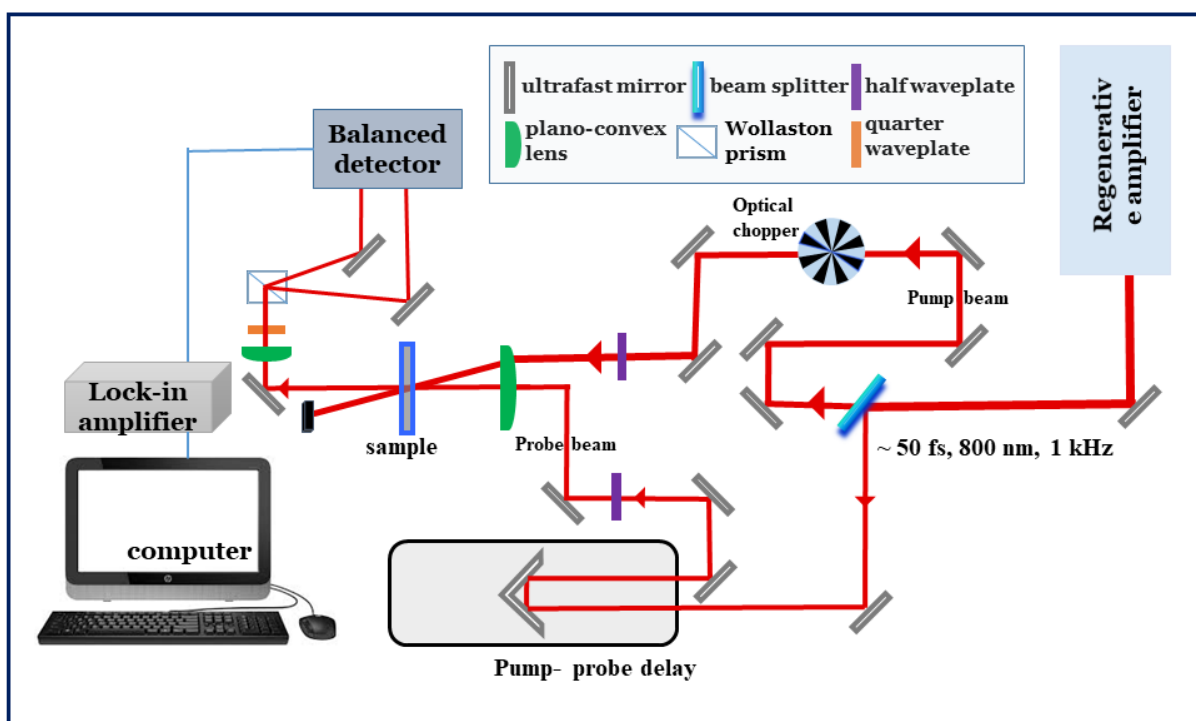


Figure 1: Experimental setup for OHD-OKE spectroscopy

The pump passes through a mechanical chopper, a half-wave plate, and is routed and focused onto the sample. The probe beam transverses a delay line and passes through a half-wave plate before reaching the sample. The pump and probe beams are polarized 45° to each other. Both the pump and the probe beam must be focused and spatially overlapped onto the sample. The temporal overlap is controlled with the delay stage. The pump beam is blocked after the sample, and the probe passes through a quarter-wave plate, which makes the probe light elliptically polarized, followed by a Wollaston prism, which separates it into its parallel and perpendicular components and sends it to a balanced photodetector [1]. The detector is a pair of photodiodes that are balanced prior to the experiment without the pump excitation. Since the signal is obtained by electronically subtracting the horizontal from the vertical component, the detection is automatically heterodyned [2]. The detector's output is measured using a lock-in amplifier locked to the frequency of the chopper placed in the pump path. The computer software records the modulated signal as a function of pump-probe delay.

In some cases, a double modulation technique is also used to obtain a better signal-to-noise ratio where both the pump and probe beams are modulated, and the lock-in is referenced to the sum or difference frequency of modulation [3]. The raw transients obtained as a function of time delay contain essential information about the ultrafast dynamics of the molecules at a microscopic level. Multiple long scans up to 100 ps were taken and averaged to give a better signal-to-noise ratio. The data was then extrapolated to 300 ps before doing a Fourier Transform deconvolution as mentioned by Mcmorrow and Lotshaw [4] to give us the spectral density (SD). The SD thus obtained is equivalent to the Bose-Einstein corrected depolarized Raman spectrum [5], [6].

The intense electric field distorts the electron clouds of the molecules; this response is instantaneous and is seen as the strong, intense peak at zero delay in the OKE signal (Figure 3). The remainder of the decay is known collectively as the nuclear response. The electric field also disturbs the random orientational distribution of the molecules and causes them to align along the field's direction. This causes a transient anisotropy in the sample, which causes the birefringence. After the excitation process is done and the pump has moved away, spontaneous rotational diffusion tries to reorient the molecules back; this process happens at timescales typical of rotational diffusion and can be obtained from the OKE data itself. The schematic is shown in Figure 2.

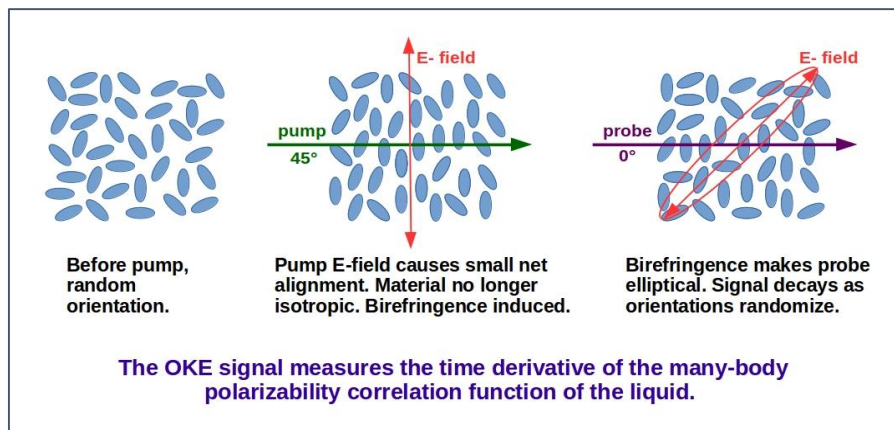


Figure 2: The propagation of an intense electric field through a liquid sample, a schematic.

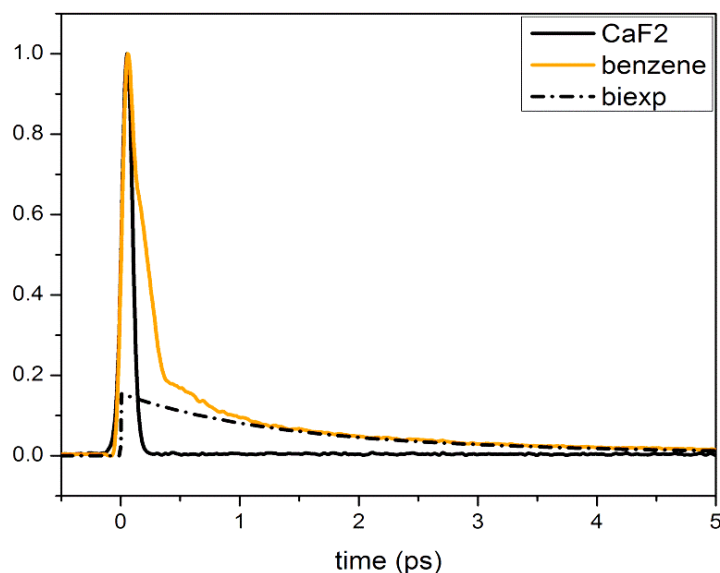


Figure 3: A typical OKE signal in time of benzene.

The timescale for this orientational diffusion is the slowest component of the relaxation process and decays exponentially. The rotational diffusion process is well studied in literature and has been approximated using the Debye function (decaying exponentially in the time domain). A process

modeled by a Debye function assumes a single relaxation time for the molecules undergoing the relaxation process. The diffusive timescales could be accessed in the time transients itself by fitting the data exponentially at longer times. It is common practice to remove the diffusive part from the time transients by subtracting an exponential of the form;

$$\exp\left(-\frac{t}{\tau_{OKE}}\right)\left[1 - \exp\left(-\frac{t}{\tau_{rise}}\right)\right] ; \quad 1$$

Where τ_{OKE} is the orientational diffusion timescales, ranging from picoseconds to nanoseconds depending on the molecule's size and viscosity. τ_{rise} is the rise time associated with the relaxation process; generally, a value between 40 - 200 fs is assumed [7],[8], but the value of τ_{rise} does not affect fitting parameters or the goodness of the fit. In some works, the rise time has been done away with because of its redundancy [9].

Generally, the orientational correlational timescale of a solute in a solvent is given by the Debye-Stokes-Einstein (DSE) relation,

$$\tau = \frac{4\pi r_h^3 \eta}{3k_B T} \quad 2$$

Where η is the solvent viscosity, r_h is the solute hydrodynamic radius, T is the temperature, and k_B is the Boltzmann's constant. Temperature-dependent OKE scans on molecular liquids have shown that the longer relaxation timescales follow DSE [8].

Since OKE essentially measures the collective orientational correlation timescales. The values obtained would differ from those obtained using Raman or NMR spectroscopy since they are sensitive only to single-molecule correlation functions [8], [10]. Both these timescales are related by the equation,

$$\tau_{coll} = \frac{g_2}{j_2} \tau_{sm} ; \quad 3$$

Where τ_{coll} is the collective orientational timescales measured by OKE and τ_{sm} is the single-molecule correlation times. g_2 is the static pair orientational correlation parameter, and j_2 is the

dynamic pair orientational correlation parameter. The value of j_2 is assumed to be unity for simple molecular liquids. g_2 is determined by the degree of parallel ordering in liquids; in the absence of any net ordering, it takes the value of unity.

After removing the diffusive part, the transient left behind is related to the intermolecular motions of the molecules; a Fourier transform of this would yield the reduced spectral density (RSD) in the frequency domain that can be fitted to various phenomenological lineshapes to understand the underlying dynamics. More about analyzing the data in the frequency domain is explained afterward.

However, removing the slowest decaying exponential shows that there is still some exponential character remaining behind in the time transients. This has been called the intermediate region, the origin of which remains elusive. Beyond that, we have the ultrafast dynamics in the sub-ps timescales, originating from intermolecular oscillations that can be librational and translational in character [11].

The OKE spectral density (SD) can be thought of containing the entire dynamical picture of the molecules, extending from the structural relaxations till the lowest GHz frequencies to the intermolecular librations and intramolecular modes at higher THz frequencies. One can envision this as starting with faster individual vibrations of the atoms followed by the libration motions of the cage surrounding the central atom to the structural relaxations at the slowest time scales.

One of the advantages of the OKE experiment is that we can analyze the same dynamics in time as well as in the frequency domain by just doing a Fourier transform deconvolution; pioneered by McMorro and Lotshaw [4]. If the pump and probe originate from the same laser source, the transmitted signal, $T(\tau)$, can be thought of as a convolution of the zero background second harmonic intensity autocorrelation trace $G_0^{(2)}$ and the material response function $R_{ijkl}(t)$. Both $T(\tau)$ and $G_0^{(2)}(t)$ are experimentally measured quantities.

$$T(\tau) = \int_{-\infty}^{\infty} G_0^{(2)}(\tau - t) R_{ijkl}(t) dt \quad ; \quad 4$$

Generally, for the OKE experiments, an autocorrelation trace is obtained by measuring the signal from a CaF₂ crystal, taken exactly at the sample position. Care should be taken that there should be minimal changes in the experimental setup while measuring the sample and the autocorrelation.

The CaF₂ signal can be approximated as the autocorrelation because the Kerr nuclear transient of CaF₂ is almost negligible and is mainly dominated by the electronic contribution, which follows the electric field oscillations of the laser pulse. In some cases, a glass slide [12] or a nonlinear crystal like KDP [13] has also been used to trace the autocorrelation.

Following the Fourier transform relationship, the above equation becomes

$$F\{R_{ijkl}(\tau)\} = \frac{F\{T(\tau)\}c}{F\{G_0^{(2)}(\tau)\}} = D_{ijkl}(\Delta\omega) \quad 5$$

where F denotes the forward complex Fourier transform and $D_{ijkl}(\Delta\omega)$ the frequency domain spectrum of the sample response function $R_{ijkl}(\tau)$. The spectrum thus obtained is free of the finite bandwidth effect of the laser pulse and hence does not depend on the instrument used for obtaining the data.

The sample response function contains contributions from both the nuclear, $r_{ijkl}(t)$, and instantaneous electronic response function, $\sigma_{ijkl}(t)$. The electronic response can be approximated as a δ function,

$$\sigma_{ijkl}(t) = b\delta(t) \quad 6$$

Where b is a constant denoting the scalar amplitude of the electronic hyperpolarizability.

Due to the Born Oppenheimer approximation, the nuclear and the electronic motions are separable,

$$R_{ijkl}(t) = \sigma_{ijkl}(t) + r_{ijkl}(t) ; \quad 7$$

In the frequency domain, the function $D_{ijkl}(\Delta\omega)$ can be expressed as,

$$Im D_{ijkl}(\Delta\omega) = Im F\{r_{ijkl}(t)\} ; \quad 8$$

$$Re D_{ijkl}(\Delta\omega) = b + Re F\{r_{ijkl}(t)\} ; \quad 9$$

Since the Fourier transform of a delta function is 1 and b is a real scalar quantity, the electronic part contributes only to $Re D_{ijkl}(\Delta\omega)$. The $Im D_{ijkl}(\Delta\omega)$, on the other hand, has contributions

only from the nuclear part of the response function, $r_{ijkl}(t)$ is called the nuclear impulse response function and contains all the information about the system's nuclear dynamics [4].

$$r_{ijkl}(t) = 2F^{-1}\{Im D_{ijkl}(\Delta\omega)\} H(t - t_0) \quad 10$$

Where F^{-1} is the inverse Fourier transform, and H is the Heaviside unit step function. Therefore, the nuclear response function can be determined solely by the imaginary part of $D_{ijkl}(\Delta\omega)$, which is called the spectral density (SD).

If we subtract the contribution from the orientational diffusion in the time domain, the remaining part of the response function will give us the reduced spectral density (RSD). The RSD has been fit to a sum of complex lineshapes to describe the underlying dynamics. One such combination is the sum of antisymmetrized Gaussians (AG, equation 11) and an Ohmic lineshape called the Bucaro-Litovitz (BL, equation 12) function.

$$I_{AG}(\omega) = A(\exp\left\{\frac{-2(\omega-\omega_1)^2}{\Delta\omega^2[2 \ln(2)]^{-1}}\right\} - \exp\left\{\frac{-2(\omega+\omega_1)^2}{\Delta\omega^2[2 \ln(2)]^{-1}}\right\}); \quad 11$$

where $\Delta\omega$ is the Gaussian halfwidth, and ω_1 is the Gaussian frequency, and A is the amplitude or relative contribution.

$$I_{BL}(\omega) = B\omega^\alpha \exp\left(-\frac{\omega}{\omega_{BL}}\right); \quad 12$$

where ω_{BL} is the BL frequency, and B is the relative contribution. Many groups have successfully implemented the model to describe the underlying dynamics of liquids [10].

Other models have also been used to describe the RSDs. For example, a sum of underdamped, critically damped, and overdamped harmonic oscillators [14] were used to fit the spectra of CS_2 [15]. Similarly, a sum of Brownian oscillators has also been used to fit the OKE spectral density [16], [17].

Comparison of the models, the ASG+BL and the sum of Brownian oscillators have also been done on aniline, nitrobenzene, and benzonitrile, and it was found that the sum of ASG+BL gave a better fit [10].

Another way of analyzing the frequency domain data is to consider the entire spectral density spanning across entire GHz-THz frequencies [18]. The spectrum is bound by the alpha relaxation at the lowest frequencies extending up to the GHz, which has been modeled by the Debye relaxation model in earlier studies and as an exponential decay in the time-domain analysis. Fitting the time domain data to exponentials seems unpredictable since earlier reports have shown that sometimes up to five exponentials were required to fit the data. Instead of subtracting the exponential decays from the raw time transients, a set of phenomenological functions can be called to fit the complex lineshapes. The Mode Coupling Theory (MCT) approach has been used in some scenarios to fit this broad spectrum. The MCT approach talks about an additional process called the β relaxation in supercooled liquids below the critical temperature, which joins the alpha relaxation and the intermolecular peaks at the higher frequencies. Another feature seen in liquids at room temperature is the presence of an excess wing to the slow α peak. Initially, it was thought that the excess wing in normal molecular liquids and the β relaxation in glass formers are two different processes. Now it is universally accepted that both these have the same origin and are attributed to restricted librations of the molecules in a cage. Analysis of these broad GHz-THz spectra at different temperatures has shown that the β relaxation is present even in pure molecular liquids and at room temperatures but is enveloped inside the more prominent α peak. Even for the glass formers, the β peak begins to separate only at low temperatures and forms a distinct peak only at temperatures below the critical temperature, T_c . The α relaxation can be modeled by the Cole-Davidson (CD) function to account for the excess wing of the α peak. The CD function is a type of modified Debye function with a broadening parameter. A Cole-Cole (CC) function is used to model the β relaxation. The CD and the CC function are reduced from the more general Havriliak-Negami (HN) function.[eq] The intermolecular modes are fit to a sum of Brownian oscillators. However, we must remember that these are not separate processes taking place one at a time, but they all start simultaneously, and there is considerable overlap between them.

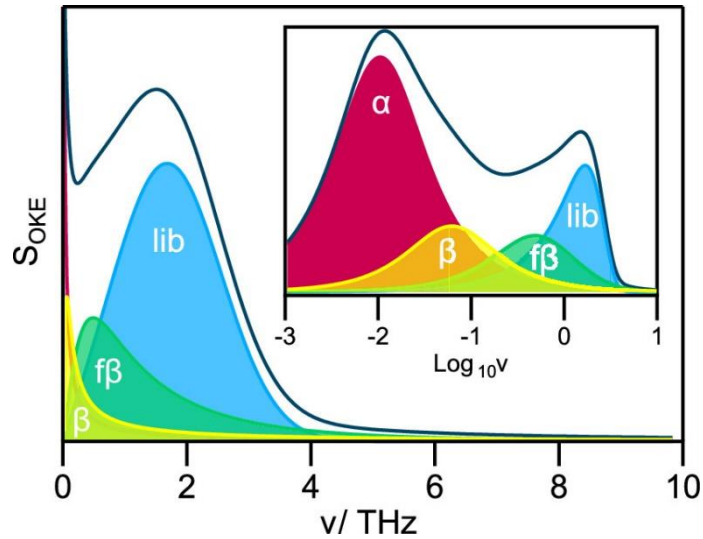


Figure 2: The General schematic of the low-frequency vibrational spectrum of a liquid. The different contributions are the α -relaxation (orientational relaxation), β -relaxation (translational diffusion), the fast- β process (cage-rattling), and librations (refer to text above). The inset shows the same on a logarithmic frequency axis, which is advantageous for highlighting the lowest frequency (gigahertz and lower) region of the spectrum. [19]

2.2 THz-TDS setup using air-photonics for generation and detection of THz radiation

The optical source is a Ti: Sapphire laser (Spitfire Pro XP, Spectra-Physics), with a central wavelength of 800 nm, 50 fs pulse duration, and 1 kHz repetition rate. The total power output of 4W is split into two, where one half is directed to the optical parametric amplifier (OPA), where it is used to generate a wide range of wavelengths that can be used as a pump source for time-resolved THz spectroscopy (TRTS) experiments. The other half is used in the subsequent generation and detection of THz radiation. The latter is again split into two using a pellicle beam splitter (R: T= 8:92); the transmitted beam is used for generation while the reflected one functions as a gate beam to map the THz waveform in time. The transmitted beam from the pellicle beam splitter passes through a 100-micron thick type-I β barium borate (BBO) which generates the second harmonic (2ω) of the fundamental beam (ω). The fundamental, along with its second harmonic, is focused in the air using a plano-convex lens, which creates an intense plasma. The

plasma emits radiation at all frequencies, including at THz frequencies. A high resistivity silicon filter filters out all the other radiations and allows only THz to pass through. The first pair of off-axis parabolic mirrors collimate the THz beam and focuses it into the sample. After absorption of THz radiation by the sample, the transmitted beam is re-collimated by another pair of parabolic mirrors and is focused between a pair of electrodes for detection.

The gate beam travels through an optical delay line (50 mm) before being routed to and focused on the same spot as the THz beam, between the electrodes. An AC bias of 1.5 kV is applied to the electrodes through a high voltage modulator (HVM), modulated at 500Hz, and synchronized to the laser repetition rate. The external bias acts as a local oscillator (LO) necessary for the heterodyned detection of the signal. The THz field induces a second harmonic generation of the gate beam. The second harmonic generated is filtered and detected by a photo-multiplier tube (PMT). For an optimal signal, the spatial and temporal overlap of the THz field and the gate beam has to be monitored precisely. The output from the PMT is amplified by a current amplifier (CA) which also converts it into a slowly varying signal, which is detected using a lock-in amplifier (LIA), locked at the frequency of the LO.

The amplitude of the signal obtained is proportional to the THz electric field. The time-domain THz waveform can be recorded by scanning the optical delay stage present in the gate beam. This gives us the entire THz waveform as a function of the time delay between the pump (THz field in this case) and the gate beam. A simple Fourier transformation of this time-domain signal would give us the complex frequency-domain spectrum.

For a typical THz-TDS experiment, a reference signal (E_{ref}) is collected, which is the THz waveform in air (without any sample) in case of a solid sample or the THz waveform transmitted through an empty sample cell in case of liquid. The sample signal is the transmitted THz waveform through the sample (E_{samp}). Care should be taken that the reference and the sample signal are collected at the same point in space in identical conditions. The ratio of the complex Fourier transform of E_{samp} to E_{ref} gives us the complex refractive index of the sample.

$$\frac{\int E_{samp}(t) dt}{\int E_{ref}(t) dt} = \frac{\tilde{E}_{samp}(\omega)}{\tilde{E}_{ref}(\omega)} = \sqrt{T(\omega)} \exp(i\varphi(\omega)), \quad 13$$

where $T(\omega)$ is the power transmittance, and $\varphi(\omega)$ is the relative phase.

Using the extinction coefficient (k), and the refractive index (n) the other optical constants can also be calculated (equation 14-17).

$$\text{Absorption coefficient: } \alpha = -\frac{1}{d} \ln \left(\frac{E_{sam}(\omega)}{E_{ref}(\omega)} \right)^2 \quad 14$$

$$\text{Extinction coefficient: } k = \frac{\lambda \alpha}{4\pi} = \frac{c \alpha}{2\omega} \quad 15$$

$$\text{Refractive index: } n = 1 + \frac{c}{2\pi\omega d} (\varphi_{sample} - \varphi_{ref}) \quad 16$$

$$\text{Absorbance: } A = \alpha * d \quad 17$$

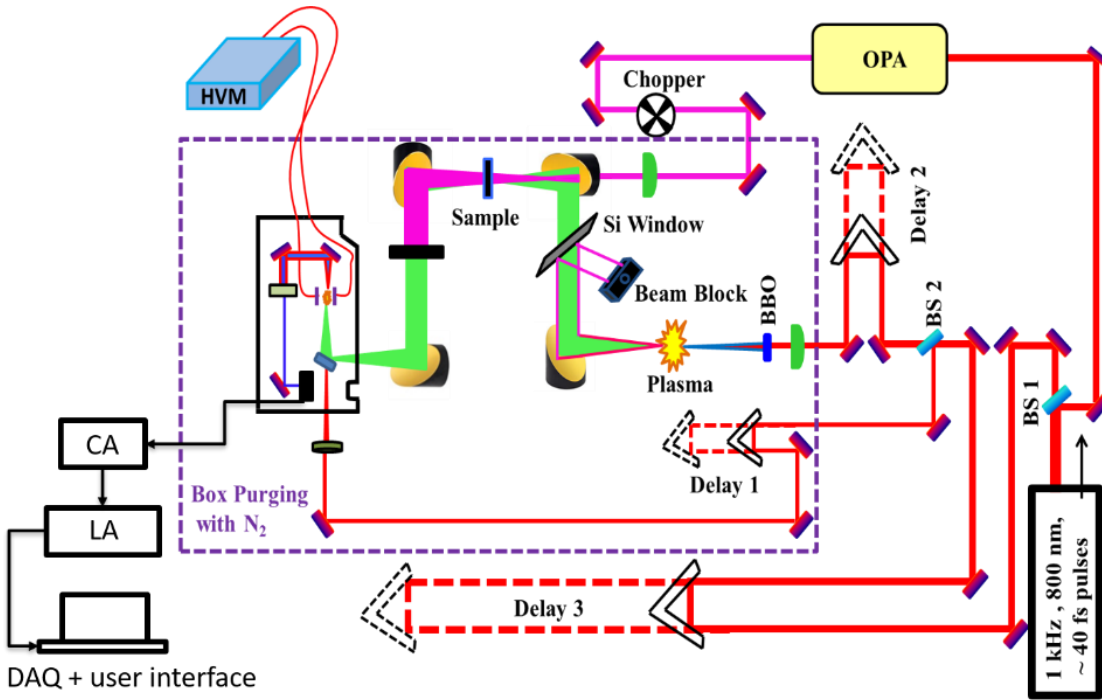


Figure 3: Experimental setup for Time-domain and time-resolved THz spectroscopy using air-photonics for THz generation and detection [20].

2.3 References

1. Wynne, K., et al., *Tunneling of single-cycle terahertz pulses through waveguides*. Optics Communications, 2000. **176**(4): p. 429-435.
2. Giraud, G., et al., *The effects of anion and cation substitution on the ultrafast solvent dynamics of ionic liquids: A time-resolved optical Kerr-effect spectroscopic study*. The Journal of Chemical Physics, 2003. **119**(1): p. 464-477.
3. Kamada, K., et al., *Femtosecond optical Kerr dynamics of thiophene in carbon tetrachloride solution*. Chemical Physics Letters, 1996. **249**(5): p. 329-334.
4. McMorro, D., *Separation of nuclear and electronic contributions to femtosecond four-wave mixing data*. Optics Communications, 1991. **86**(2): p. 236-244.
5. McMorro, D. and W.T. Lotshaw, *The frequency response of condensed-phase media to femtosecond optical pulses: spectral-filter effects*. Chemical Physics Letters, 1990. **174**(1): p. 85-94.
6. Chang, Y.J. and E.W.C. Jr., *Fast responses from "slowly relaxing" liquids: A comparative study of the femtosecond dynamics of triacetin, ethylene glycol, and water*. The Journal of Chemical Physics, 1993. **99**(10): p. 7289-7299.
7. McMorro, D. and W.T. Lotshaw, *Evidence for low-frequency ($\approx 15 \text{ cm}^{-1}$) collective modes in benzene and pyridine liquids*. Chemical Physics Letters, 1993. **201**(1): p. 369-376.
8. Zhong, Q. and J.T. Fourkas, *Optical Kerr Effect Spectroscopy of Simple Liquids*. The Journal of Physical Chemistry B, 2008. **112**(49): p. 15529-15539.
9. Ricci, M., et al., *The fast dynamics of benzene in the liquid phase. Part I. Optical Kerr effect experimental investigation*. Physical Chemistry Chemical Physics, 2001. **3**(14): p. 2795-2802.
10. Smith, N.A. and S.R. Meech, *Optically-heterodyne-detected optical Kerr effect (OHD-OKE): Applications in condensed phase dynamics*. International Reviews in Physical Chemistry, 2002. **21**(1): p. 75-100.

11. Ladanyi, B.M. and Y.Q. Liang, *Interaction-induced contributions to polarizability anisotropy relaxation in polar liquids*. The Journal of Chemical Physics, 1995. **103**(15): p. 6325-6332.
12. Miyata, K., et al., *Large polarons in lead halide perovskites*. Science Advances, 2017. **3**(8): p. e1701217.
13. Kakinuma, S. and H. Shirota, *Dynamic Kerr Effect Study on Six-Membered-Ring Molecular Liquids: Benzene, 1,3-Cyclohexadiene, 1,4-Cyclohexadiene, Cyclohexene, and Cyclohexane*. The Journal of Physical Chemistry B, 2015. **119**(13): p. 4713-4724.
14. McMorro, D., W.T. Lotshaw, and G.A. Kenney-Wallace, *Femtosecond optical Kerr studies on the origin of the nonlinear responses in simple liquids*. IEEE Journal of Quantum Electronics, 1988. **24**(2): p. 443-454.
15. McMorro, D., et al., *Probing the Microscopic Molecular Environment in Liquids: Intermolecular Dynamics of CS₂ in Alkane Solvents*. The Journal of Physical Chemistry, 1996. **100**(24): p. 10389-10399.
16. Mukamel, S., *Principles of Nonlinear Optical Spectroscopy* 1995, New York: Oxford University Press.
17. Tanimura, Y. and S. Mukamel, *Two-dimensional femtosecond vibrational spectroscopy of liquids*. The Journal of Chemical Physics, 1993. **99**(12): p. 9496-9511.
18. Turton, D.A. and K. Wynne, *Structural relaxation in the hydrogen-bonding liquids N-methylacetamide and water studied by optical Kerr effect spectroscopy*. The Journal of Chemical Physics, 2008. **128**(15): p. 154516.
19. Farrell, A.J., et al., *Low-Frequency (Gigahertz to Terahertz) Depolarized Raman Scattering Off n-Alkanes, Cycloalkanes, and Six-Membered Rings: A Physical Interpretation*. The Journal of Physical Chemistry B, 2020. **124**(35): p. 7611-7624.
20. Banerjee, S., Yettapu, G., Sarkar, S., Mandal, P., *Broadband Terahertz Spectroscopy, Modern Techniques of Spectroscopy*. 2021, p 117-142.

3

Structural fluctuations in an azeotrope: Understanding the
benzene-methanol azeotrope

Introduction

The structure and dynamics of molecular liquids have been of interest for a long time. Intermolecular interactions, especially hydrogen bonding, bring about many interesting properties in self-associated liquids. Binary mixtures of two molecular liquids will have various such interactions that give rise to non-ideality. In some cases, when this non-ideality is significant, we observe the formation of an azeotrope. Raoult's Law is only applicable to ideal mixtures, where the forces of attraction between the molecules of the mixture are expected to be the same as that of the pure liquids. However, when we consider real mixtures, the forces acting in a mixture differs from that in the pure liquids, this causes deviation from the Raoult's Law and may result in the formation of an azeotrope. Azeotrope is a special class of liquid mixture that boils at a constant temperature at a constant composition. Azeotropes can be categorized into two scenarios. In the first one, the forces of attraction between the unlike species (let us say A-B), i.e., the adhesive force, are greater than the forces acting between the like species (A-A, B-B). If an azeotrope is formed, it will have a lesser tendency to evaporate out of the bulk. The total vapor pressure of the azeotropic mixture will thus be less than the total vapor pressure in the case of an ideal mixture of A and B. Therefore, we see a negative deviation from the Raoult's Law and the azeotrope formed will be a maximum boiling point type. This effect can be termed as Interaction Strengthening Effect. On the other hand, when the adhesive forces are weaker than the cohesive ones, the solution mixture's total vapor pressure will be more than that of the ideal mixture of the two components. This is the case of Interaction Weakening. In such a case, if formed, the azeotrope will be of the minimum boiling type and will tend to escape out faster than the pure liquids.

The thermodynamic properties of the azeotropes are characteristic of pure, single-component liquids, and their constant composition makes them desirable for a wide range of applications as an industrial solvent. While the physical interpretation of why azeotropes occur can be explained in terms of non-ideality, azeotropes remain a mystery at a molecular level. It is complicated to predict the formation of an azeotrope for a pair of liquids. Studies done on the azeotropic systems are not very conclusive, and therefore a general picture behind their formation is missing.

Our system, benzene- methanol azeotrope, is a minimum boiling homo-azeotrope at 58.3 °C. Pure methanol boils at 64.7 °C and benzene at 80 °C. We see a more significant depression in the boiling point of benzene as compared to that in methanol.

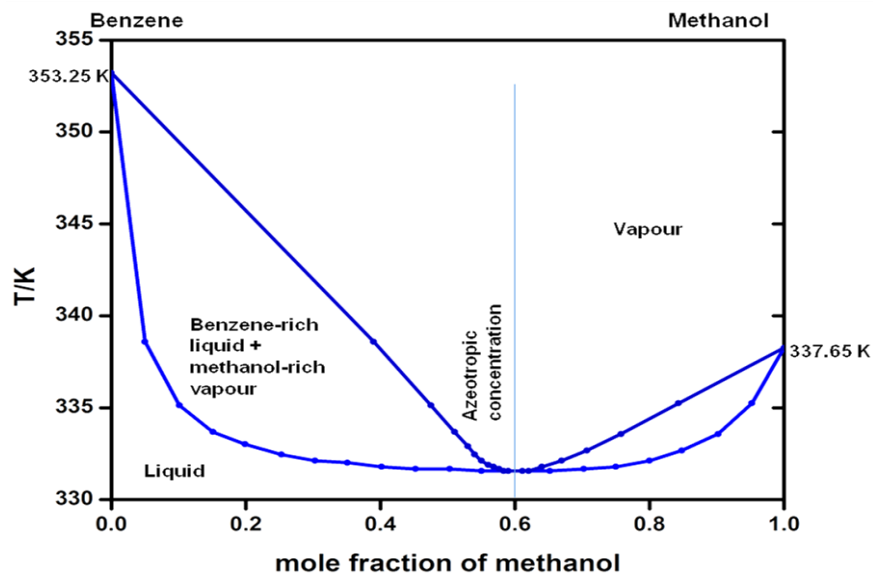


Figure 1: The phase diagram of the benzene-methanol binary liquid system

Thermodynamic studies have deemed the benzene-methanol system as an anomaly. The viscosity concentration plot of the system changes its slope twice [3]. In most hydrocarbon or alcohol binary systems, there is a linear dependence of the viscosity with concentration. Hydrocarbon-alcohol systems show one maxima/minima, which suggests a structural change in the mixture. Only selected methanol systems with hydrocarbons like benzene and toluene show this anomaly, where the viscosity has one maximum at high methanol concentration and crosses over to a minimum at lower concentrations [3]. The crossover point is dependent on temperature [4]. A sign change in the slope of the viscosity concentration plot suggests a major change in the system's molecular structure [3]. Methanol forms large associative hydrogen bonded clusters among each other, and also with benzene, the size and nature of these aggregates formed are dependent on both temperature and concentration. Monte Carlo simulations have shown that [5] aggregation of methanol molecules increases with an increase in methanol concentration, the shape of the self-associating aggregates formed, changes from spherical at low concentrations to chain like in high methanol concentrations. A density functional study of methanol clusters [6] has suggested that clusters of n methanol forming a ring having n number of hydrogen bond is comparatively more

stable than cyclic structures having (n-1) or (n-2) hydrogen bonds with the additional hydrogen bonds dangling outside the ring. The study also claims that from $n = 3$ to $n = 6$, ring clusters are preferred over chains, while for $n > 6$, chains are the most predominant structures. For ring structures (for $n=5$ or $n=6$), calculations show that all the hydrogen bonds try to converge at a value of 27 kJ/mol. The study concluded that a cyclic cluster of five or six methanol molecules is sufficient to mimic the liquid state behavior of methanol.

High level ab-initio calculations have shown that the benzene dimer has two isoenergetic stable structures (the T-shaped and the slipped parallel), dispersion is the major source of attraction between the molecules and the barrier height between the two stable structures is very small [7]. Early experimental measurements have suggested the existence of the T-shaped dimer, which has also been observed in the crystal. But this does not negate the existence of the slipped parallel structure [8],[9],[10]. Benzene has significant quadrupole moment and the interacting quadrupoles play an important role in determining the stable dimer structure, which again point towards both the T-shaped and slipped parallel orientations. Aromatic hydrocarbons can act as proton acceptors and therefore form hydrogen bonds. Spectroscopic studies have shown the presence of benzene-water and benzene-ammonia complexes with the water or ammonia molecule positioned above the benzene plane. The binding energy of the benzene-water complexes formed is significantly lower than the water dimer. In contrast to conventional hydrogen bonds, dispersion plays the major role in stabilizing the benzene-water complexes. This is also the case for CH/ π interactions in the benzene-methane complexes formed. Halogenated methanes have also shown to have high interaction energies when they form complexes with benzene [7].

Previous NMR, IR, and Raman shift studies done on the methanol-benzene azeotrope suggest the formation of complexes between benzene and methanol. Jalilian et al. have proposed a structure such that the benzenes are distributed around the methanol molecules in a way that the hydrogens of the benzene molecule are attracted to the hydroxyl oxygen of the methanol [11]. Ploetz et al. reported large positive Kirkwood–Buff integral values [12] indicating methanol-methanol pairs present in benzene rich mixtures, which would mean that the aggregation of methanol molecules takes place, and the mixture tends towards heterogeneity [13],[14]. Kirkwood-Buff integrals (KBI) radioprovide a connection between microscopic properties and thermodynamic properties of multicomponent fluids. Neutron diffraction measurements along with Empirical Potential Structure Refinement (EPSR) approach and the isotopic substitution technique [15] suggest a

strong association among the methanol molecules forming chain like clusters and benzene is mostly left out of the methanol rich regions even at the azeotropic composition.

A combination study utilizing resonant two-photon ionization, resonant ion-dip infrared and IR-UV hole-burning spectroscopies, have suggested two isomers for the benzene-methanol azeotrope. In both the case the methanol molecules are in a hydrogen bonded trimer chain with the terminal OH forming π hydrogen bond with one of the benzenes, which is in a perturbed T-shaped dimer orientation [16]. Ab-initio methods have also been used to investigate benzene-methanol clusters. To model the azeotrope, several isoenergetic structures, having the benzene dimer in T-shape as well as in the slipped-parallel orientation have also been proposed [17].

A recent study, utilizes Monte Carlo simulations to successfully reproduce the experimental phase diagram of the ethanol-benzene system. One of the necessary and sufficient condition for the occurrence of an azeotrope is the changing of the relative volatilities with the concentration of the components. Analysis of molecular energetics using radial distribution functions (RDF), KBI and Hydrogen bond (HB) analysis, they concluded that at low ethanol concentrations, ethanol molecules try to aggregate among themselves in a sea of benzene. As, the amount of methanol is increased, the cluster size increases leading to microscopic segregation between methanol rich and benzene rich regions. Increasing the ethanol concentration even further leads to a continuous phase of ethanol with the benzene molecules significantly isolated from each other [18].

In this study we have utilized ultrafast spectroscopic techniques like the Optical Kerr Effect (OKE) spectroscopy and THz time domain spectroscopy (THz-TDS) to investigate the azeotropic non-ideality at a molecular level and to understand how the intermolecular dynamics of the azeotrope is different from the other composition mixtures and the neat liquids at these ultrafast timescales.

3.2 Experimental Methods

3.2.1 Samples: All the liquids were purchased from Sigma-Aldrich and were of reagent grade with > 99% purity. Benzene was used without further distillation, while methanol was further distilled. The 2:3 mole ratio benzene-methanol minimum boiling azeotrope was formed and collected via distillation. 3:1, 1:1, 1:2 and 1:4 mole ratio benzene methanol mixtures were also made by taking the appropriate amount of solvents and mixing them together at room temperature. The mixtures are termed as B3M1, B1M1, B1M2 and B1M4, respectively. A 2:3 mole ratio composition (same

as the azeotrope) mixture was also made at room temperature without further distillation. This was called the manually mixed mixture or the MMM.

Another 2:3 composition mixture was heated in a closed environment at the boiling point of the azeotrope. The vapors were not allowed to escape as in distillation, instead they condensed back into the bulk, and this mixture was cooled down and designated as MMM (h).

3.2.2 Optical Kerr Effect Spectroscopy: The details of the experimental setup are given in Chapter 2: Experimental methods and Data analysis. For data collection 1mm thick quartz cuvettes were used. The autocorrelation curve was approximated from the OKE time signal through a 3mm thick CaF₂ crystal. Data analysis was done using MATLAB.

3.2.3 THz-Time Domain Spectroscopy: The details of the experimental setup are given in the Chapter 2: Experimental methods and Data analysis. The sample cell used to record the THz data was made up of silicon windows separated by a 150 micron spacer.

3.3 Result and Discussion

3.3.1 Spectral Density and the dielectric loss spectra: The spectral density of the azeotrope is shown in Figure 2. The OKE spectra contains the dynamical picture of the molecules, from the structural relaxations at the lowest GHz frequencies to the intermolecular librations and intramolecular modes at higher THz frequencies. One can envision this as starting with faster individual vibrations of the atoms followed by the libration motions of the cage surrounding the central atom to the structural relaxations at the slowest time scales. To reiterate, these processes are not taking place one at a time, but start simultaneously, and there is considerable overlap between them.

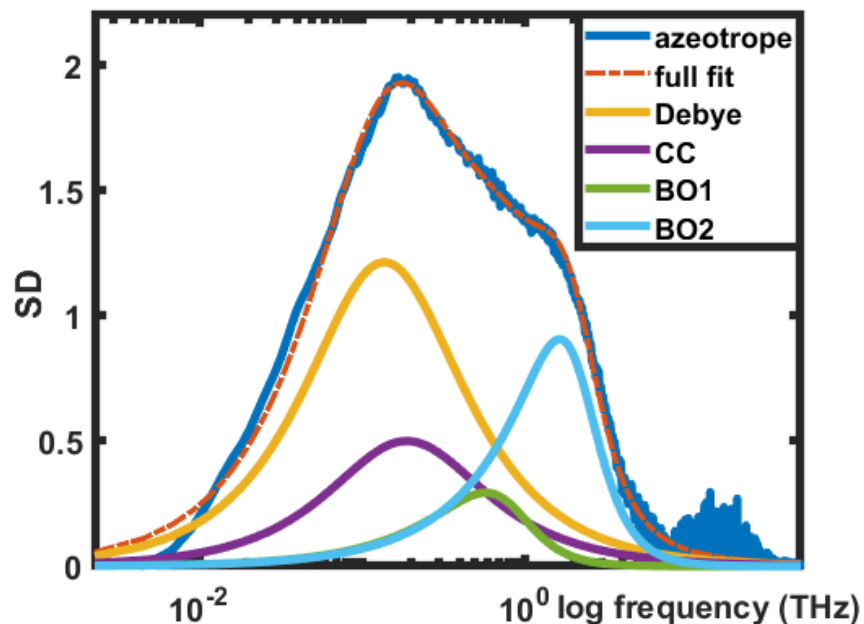


Figure 2: Spectral Density of azeotrope fit to a Debye, CC and two Brownian oscillators.

The spectrum is bound by the alpha relaxation at the lowest frequencies extending up to the GHz, which has been modeled by the Debye relaxation model in earlier studies. The Debye relaxation is an exponential decay in the time domain. A process modeled by a Debye function assumes a single relaxation time for the molecules undergoing the relaxation process; this is, of course, the ideal scenario, earlier reports have shown that up to a sum of five exponentials[] have been used to fit pure molecular liquids. The advantage of the OKE data is that it can be analyzed in both the time and frequency domain. Instead of subtracting the exponential decays from the raw time transients, a set of phenomenological functions can be called to fit the complex lineshapes. The mode coupling theory (MCT) approach has been used in some scenarios to fit this broad spectrum [19]. The MCT approach talks about an additional process called the β relaxation in supercooled liquids below the critical temperature, which joins the alpha relaxation and the intermolecular peaks at the higher frequencies. Another feature that is seen in liquids at room temperature is the presence of an excess wing to the slow α peak. Initially, it was thought that the excess wing in normal molecular liquids and the β relaxation in glass formers are two different processes. Now it

is universally accepted that both these have the same origin and are attributed to restricted librations of the molecules in a cage [19]. Analysis of these broad GHz-THz spectra at different temperatures has led us to see that the β relaxation is present even in pure molecular liquids and at room temperatures but is enveloped inside the more prominent α peak. Even for the glass formers, the β peak begins to separate only at low temperatures and forms a distinct peak only at temperatures below the critical temperature, T_c . The α relaxation can be modeled by the Debye or the Cole-Davidson (CD) function to account for the excess wing of the α peak. The CD function is a modified Debye function with a broadening parameter. A Cole-Cole (CC) function is used to model the β relaxation. The intermolecular modes are fit to a sum of Brownian oscillators. The spectral density of pure benzene was fit to a sum of relaxation and oscillatory lineshapes. A recent study by Farrell et al. has utilized a four-component model to fit the data using a Debye and Cole-Cole function along with two Brownian oscillators. The α and the β relaxation corresponded to the orientational and translational diffusion. The cage rattling motion is known as the fast β process. The fast β , in this case, fits well with a Brownian oscillator. Lastly, another oscillator is used to account for the librational motions [20].

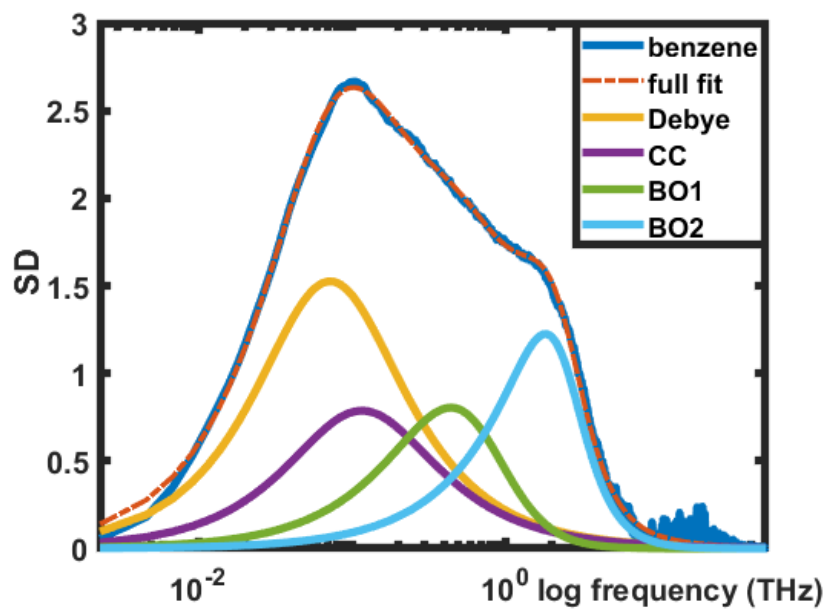


Figure 3: Spectral Density of benzene fit to a Debye, CC and two Brownian oscillators.

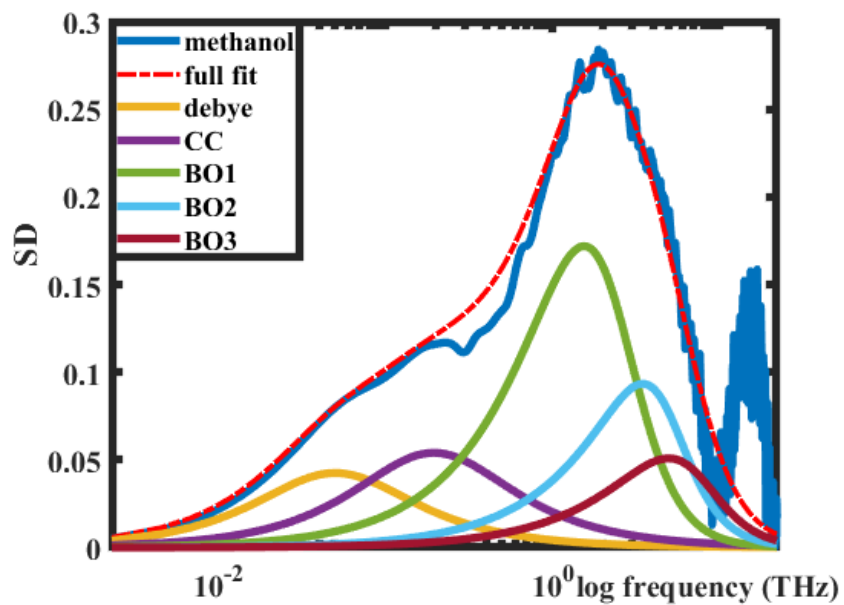


Figure 4: Spectral Density of methanol fit to a Debye, CC and three Brownian oscillators.

The liquids in this study were fit to a sum of Debye, CC and Brownian oscillators. Two oscillators were found sufficient to fit the higher frequency part of the spectra, except for methanol, which required two relaxation peaks and three oscillators, as shown in Figure 2, 3 and 4. The parameters obtained are summarized in Table 1 . The values of the fit that we obtained are similar to the ones previously reported in the literature.

Fukasawa et al. studied the entire GHz-THz spectral range combining the complex dielectric and the Raman spectra of methanol, though the study on the higher frequency side was limited to only 2.5 THz. The spectra obtained was fit to a sum of 3 Debye relaxation processes, (having timescales 51.8 ps, 8.04 ps, and 0.89 ps) and two oscillators (central frequency 55cm⁻¹ and 125 cm⁻¹) [21]. Kampfrath et al. studied methanol using THz Kerr Effect, and the dielectric spectra obtained also fit the above five-component model with similar values [22].

	benzene	azeotrope	B3M1	B1M1	MMM	MMM heated	B1M2	B1M4	methanol
A1 (%)	0.77	1.17	1.30	1.62	1.21	1.54	1.51	1.64	0.03
A2 (%)	0.41	0.48	0.39	0.19	0.39	0.29	0.20	0.30	0.03
A3 (%)	7.63	4.94	14.04	15.36	17.79	15.88	22.26	17.00	17.65
A4 (%)	91.19	93.40	84.27	82.84	80.62	82.29	76.03	81.05	34.81
A5 (%)									47.47
a (CC)	0.01	0	0.00	0.00	0.05	0.00	0.00	0.00	0.00
γ 1 (THz)	1.59	1.27	1.91	1.88	2.10	1.91	2.17	1.91	4.24
γ 2 (THz)	3.50	2.88	3.18	3.24	3.27	3.03	3.03	3.02	7.28
γ 3 (THz)									12.29
τ 2 (ps)	2.20	1.16	1.92	1.46	1.41	1.15	1.36	1.11	3.2
τ 1 (ps)	1.36	0.84	0.96	0.74	0.81	0.80	0.98	0.87	0.82
ω 1 (THz)	0.78	0.81	0.96	1.02	1.10	1.10	1.11	1.13	2.39
ω 2 (THz)	2.44	2.12	2.39	2.47	2.42	2.40	2.41	2.21	4.77
ω 3 (THz)									7.32

Table 1: Parameters of fitting the spectral density of benzene, methanol and their mixtures using a Debye, CC and a sum of BO.

Following the same phenomenological lineshapes for the fitting of the spectral density of the mixtures, we see that the addition of methanol shifts the main α relaxation peak of benzene to higher frequencies with the increase in the amount of methanol in the mixture. The addition of methanol fastens the relaxation process in the mixtures. The spectral densities for the mixtures and azeotrope are narrower and span a smaller frequency range than benzene. Shifting of the α relaxation peak to higher wavenumbers also decreases the difference between the diffusive and the intermolecular regime. Hence any β relaxation, if present, would be wholly overlapped.

The fits obtained from the spectral density was inverse Fourier transformed to see if they fit the time transients. Only fits that were satisfactory in both the frequency and the time domain were considered.

Since THz-TDS response depends on the presence of permanent molecular dipoles, the dielectric loss spectrum is complimentary to the OKE spectral density. This is one of the major advantages of doing a combined THz-TDS and OKE study. The dielectric loss spectra of benzene, methanol and their mixtures obtained from our THz-TDS study is given in Figure 5. The dielectric loss spectra shows a pronounced peak at 3-4THz and shoulders at around 2 and 8 THz. The frequency values of these oscillatory modes also match the central frequencies of the modes in the OKE spectral density.

In a previous dielectric study utilizing THz-TDS, Sarkar et al. fits the complex dielectric spectra of methanol to a Debye and three oscillator model. The lower frequency limit for the data was only up to 0.5 THz; hence the Debye relaxations could not be adequately resolved. The three oscillators at 30 cm^{-1} , 127 cm^{-1} , and 266 cm^{-1} have been assigned (using all-atom MD simulations and ab initio quantum calculations) to the overall motion of alcohol molecules, the alkyl group oscillations and signatures of H-bonded OH groups of alcohol molecules, respectively [23].

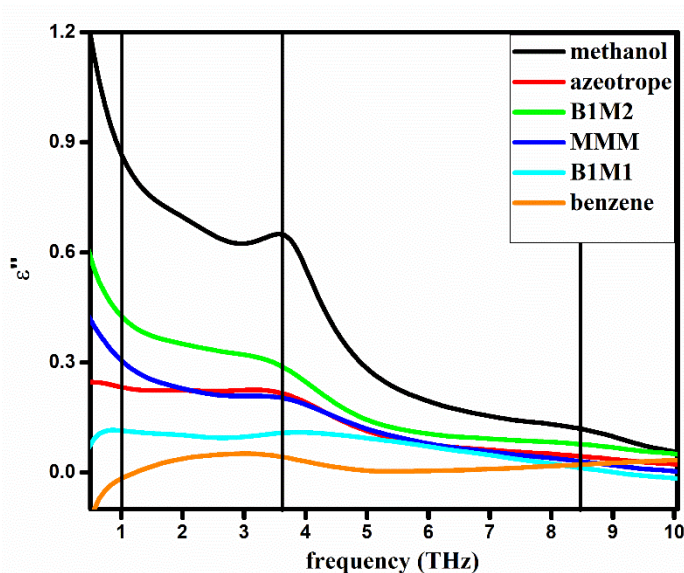


Figure 5: The dielectric loss spectra of benzene, methanol and their mixtures.

The low frequency depolarized Raman spectra by Fukasawa et al. shows a resemblance to their dielectric loss spectra's high-frequency part. They fit the susceptibility spectra to two Debye processes with timescales 2.5 and 0.55 ps, and three Brownian oscillators at 60, 120 and 260 cm^{-1} . The slowest timescale obtained from the Raman spectra is three times faster than the τ_2 of the dielectric study. This relation has also been seen to hold true previously for dipolar aprotic liquids. The relaxation has been attributed to the rotational diffusion of individual methanol molecules. The main peak, corresponding to τ_1 , of the dielectric spectra is not Raman active [21].

The fits that we get for methanol from the OKE spectra match the literature; the high-frequency fits of the dielectric data also complement the previous results. Since our THz-TDS data is limited to only 0.5 THz at the lowest frequency, the fits to the relaxation dynamics were not satisfactory. Dielectric loss is the dissipation of energy through the reorientation of the molecular dipoles due to the applied THz field. Dielectric loss tends to be higher for polar molecules, therefore we see a huge response for methanol. Comparatively, addition of benzene to methanol brings down this response substantially. From the THz-absorbance spectra of the mixtures (Figure 6), we have a better picture of the oscillatory modes and see that the 2 and the 4 THz peaks have not only reduced in amplitude but have also broadened compared to neat methanol. The 8 THz hump is seen for

B1M2 and the azeotrope but goes down for manually mixed mixture. The B1M1 mixture on the other hand, looks totally different from that of methanol and the oscillatory features are almost not discernible.

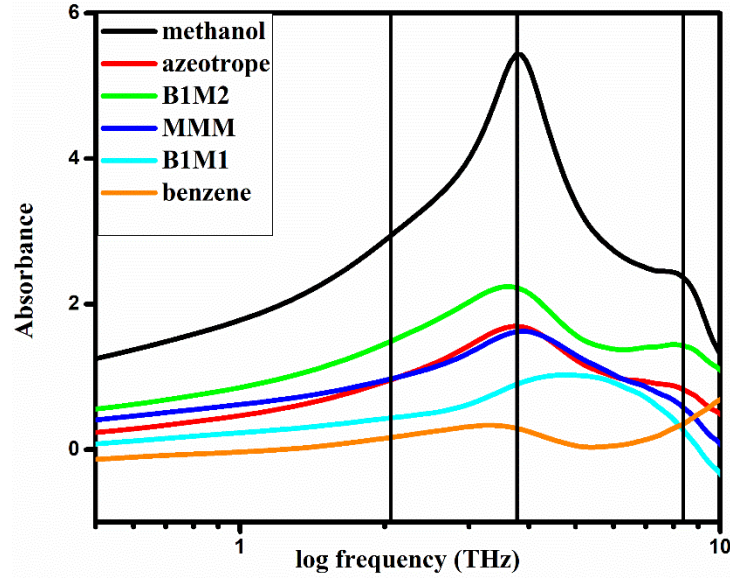


Figure 6: The THz absorbance spectra of benzene, methanol and their mixtures.

3.3.2 Excess dielectric loss spectra: Since the formation of an azeotrope occurs due to deviation from ideality, we decided to calculate the excess spectra using volume fractions of the mixtures [24], [25]. The excess spectra are simply the volume fraction simulated data subtracted from the experimental data. It should essentially give us how the mixtures deviate from ideality.

$$\varepsilon''_{ideal}(\omega) = V_1\varepsilon''_1(\omega) + V_2\varepsilon''_2(\omega) \quad 1$$

$$\text{with } \varepsilon''_{excess} = \varepsilon''_{real} - \varepsilon''_{ideal} \quad 2$$

where V_1 and V_2 are the volume fraction of the pure liquids and ε''_1 and ε''_2 are their dielectric loss at a particular frequency. ε''_{real} is the dielectric loss of the benzene-methanol mixture measured

experimentally at the same frequency. Figure 7 shows the excess dielectric loss calculated for the mixtures and compared to the dielectric loss spectrum of neat methanol.

The excess dielectric loss (ϵ''_{excess}) of the azeotrope and the mixtures are negative upto 4-5THz, crosses the zero line and again goes to negative at higher frequencies. The negative excess indicates that the experimentally observed dielectric loss is less compared to what is expected in the ideal scenario, which is consistent with previous studies of acetonitrile, acetone and alcohols with water [24], [25], [26]. In accordance to the previous works, this difference between the experimentally observed and the expected ideal spectra can be interpreted as the addition of a benzene molecule disrupting the extensive hydrogen bonding that is present in pure methanol. New intermolecular interactions are also formed between methanol and benzene molecules which is characterized by the broadening of the modes. The pronounced dip around 4THz in the (ϵ''_{excess}) spectrum corresponds to reduction from the expected amplitude and subsequent broadening of the particular mode.

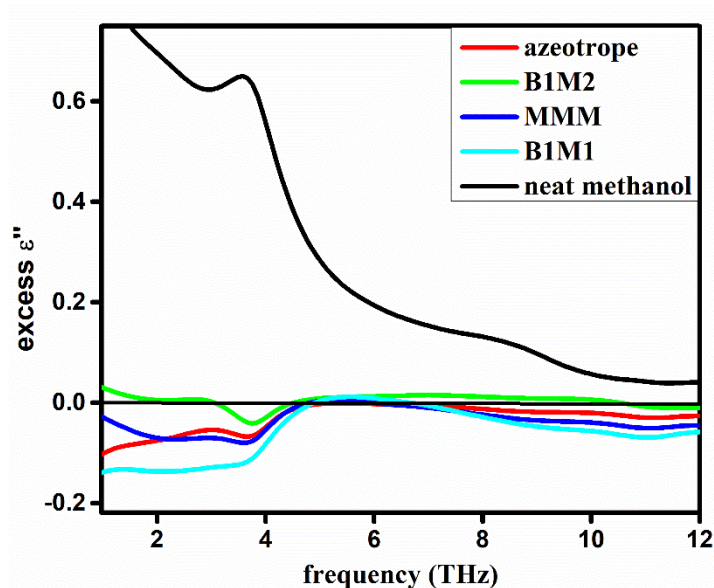


Figure 7: The excess dielectric loss of mixtures compared to neat methanol

3.3.3 Excess and reduced spectral densities: Excess spectra have been used previously to study the OKE spectra of different mixtures of solvents like benzene and hexafluorobenzene [27]. The excess quantities of the mixture are plotted in Figure 8. Higher the amplitude of the excess spectra,

greater is its deviation from ideality. The volume fraction simulated data corresponds to the ideal scenario where the average interaction energy between the unlike species is the same as that between the like ones.

$$SD_{ideal}(\omega) = V_1SD_1(\omega) + V_2SD_2(\omega) \quad 3$$

$$\text{with } SD_{excess} = SD_{real} - SD_{ideal} \quad 4$$

where V_1 and V_2 as stated previously are the volume fraction of the pure liquids and SD_1 and SD_2 are their spectral density (SD) at a particular frequency. SD_{real} is the spectral density of the benzene-methanol mixture obtained experimentally at the same frequency.

The main α peak of the mixtures in the SD_{ideal} plot falls directly below the benzene's main peak, with a reduction in amplitude following the decrease in benzene volume fraction in the mixtures. The higher frequency part in these calculated spectra resembles the shape of the benzene spectra though the decrease in amplitude is lesser compared to the relaxation peak. The actual experimental spectra (SD_{real}) are much more complicated than this, and a direct comparison should give us insights about the interactions between the unlike species.

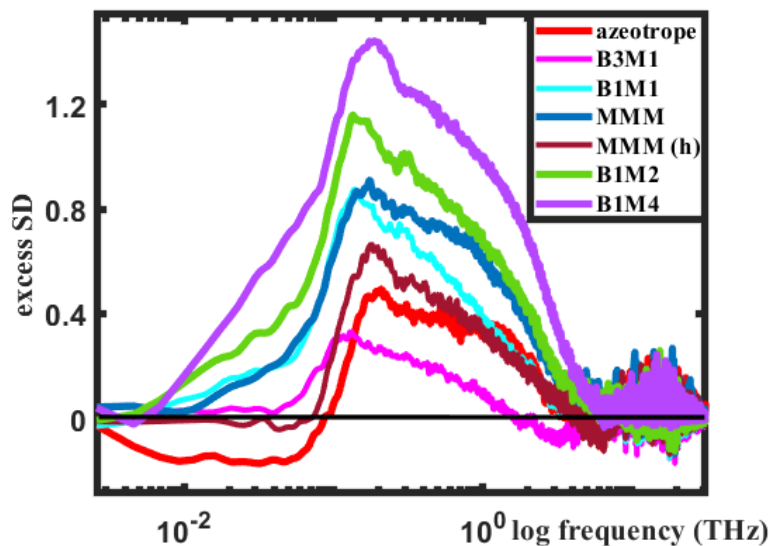


Figure 8: The excess spectral density of benzene, methanol and their mixtures.

We observe that the amplitude of the excess spectra (SD_{excess}) increases in the order of an increase of methanol in the mixture. This indicates that as we increase the amount of methanol, the system becomes even more non-ideal. The mixture with the maximum amount of benzene, B3M1, has the smallest positive excess making it the closest to the ideal scenario. The other most exciting thing to observe in the excess spectra is that only for the azeotrope, the SD_{excess} goes to negative at the lowest frequencies. At these same frequencies, the manually mixed mixture (heated) also goes below the zero line following the azeotrope. The MMM, on the other hand, is quite positive. The low-frequency part where the excess for azeotrope becomes negative corresponds to the low-frequency tail of the α relaxation in benzene. Comparing the same for any other mixture, their SD_{real} is broader compared to the azeotrope, as shown in Figure 9 (fig comparing azeo and B1M1 SD) for B1M1. It contains the full low-frequency tail of the α relaxation, as expected from the V% simulated data.

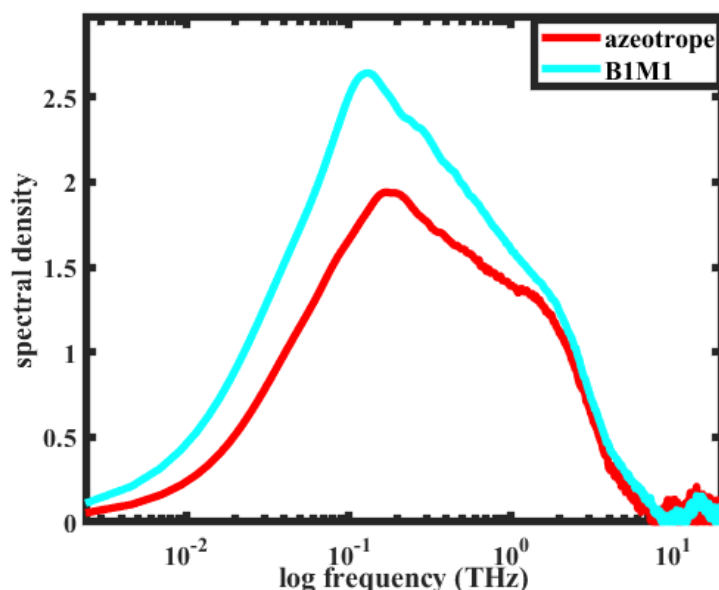


Figure 9: The spectral density of azeotrope and the B1M1 mixture.

The orientational diffusion timescale is the fastest for the azeotrope. For the mixtures, the timescales are a broader distribution since the excess spectral density is positive throughout. Most of the mixtures have a higher concentration of benzene in them, and therefore along with the

benzenes that are in clusters with methanol, there might be excess benzene stacked together like in the pure liquid giving rise to a slower decay than the benzenes that are part of the cluster. The peak frequencies of the α peak is dependent on the concentration and the type of interactions present.

The spectral density that we present here is deconvoluted from the raw normalized OKE transient. Interesting to note is that the amplitude of the azeotrope spectra is quite less compared to the manually mixed and the other mixtures whose amplitudes are comparable to that in pure benzene. This can be because at higher benzene concentrations, the benzene molecules associate with each other forming benzene rich regions, isolating the methanol molecules. As the methanol concentration increases, the spectral density shape also gets skewed at all frequencies. At B1M4, the spectral density amplitude is closer to that of the azeotrope than benzene suggesting that at this concentration, there are enough methanol molecules to disrupt the benzene continuity. The SD_{real} of all the mixtures are more in amplitude than the expected ideal spectra, suggesting that the addition of methanol to benzene enhances the interactions present in benzene.

The spectra are even more complex at higher THz frequencies, where it becomes difficult to separate the overdamped modes that are overlapped with each other. Benzene and methanol both have librational modes around the same frequencies; hence it becomes difficult to attribute a particular mode to specific molecular motions without the help of theoretical calculations. To simplify the spectra further, we subtract the relaxation dynamics from the spectra and compare reduced spectral densities (RSDs) of the mixtures. The shape of the RSDs are not dependent on the functions used to fit the relaxation part. The RSD of benzene, azeotrope, MMM and the mixture with highest methanol content, B1M4 is shown in Fig. 10.

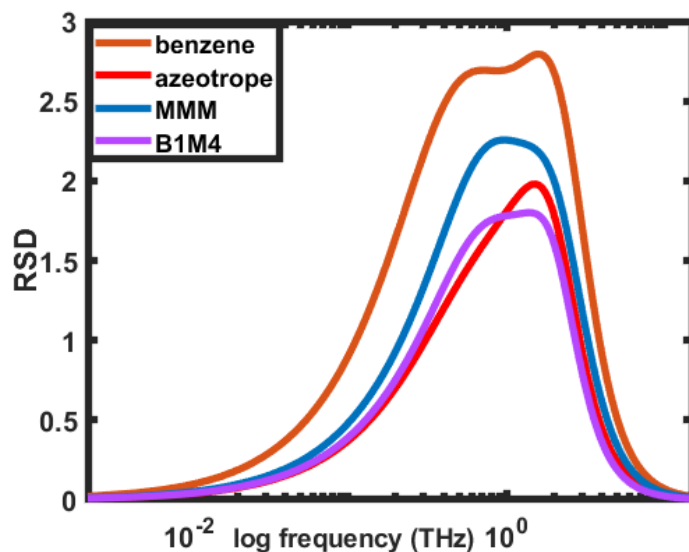


Figure 10: RSD of benzene, azeotrope, MMM and B1M4

Farrell et al. attributes the lowest 20 cm^{-1} shoulder to cage-rattling or the fast β process, and the higher $55\text{-}100\text{ cm}^{-1}$ is the librational peak. The mixtures mostly look similar to each other, with three (B1M2, B1M1 and B3M1) of them almost having the same amplitude. The frequency spread of the mixtures and the azeotrope is comparatively less than the neat liquids. The contribution of the high-frequency librational mode is reduced in the mixtures, which could imply a weakening of the cage structure. The RSD of the azeotrope is different from that of the mixtures as the bimodal character is hardly discernible. The contribution from the fast β process in the azeotrope spectra is very less as can also be seen from the fitting parameters. Even for the mixture, B1M4, which has the highest content of methanol, the bimodal character is still evident.

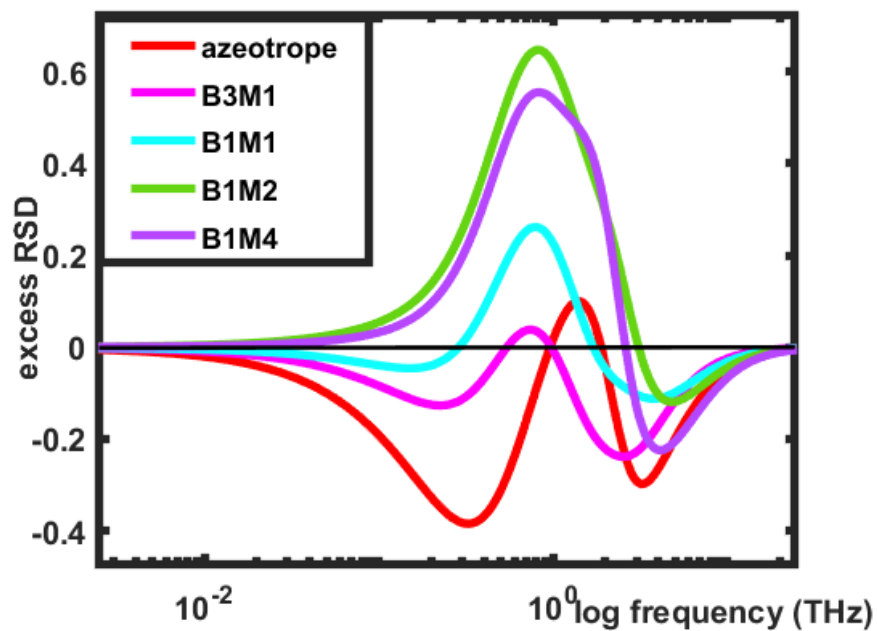


Figure 9: Excess RSD of the mixtures

We analyzed the RSD the same way we did the entire SD, using excess quantity, see Figure 9. We see a huge negative peak for azeotrope and B3M1 for the frequencies lower than 1 THz, while there is a corresponding positive excess for the two mixtures with the highest amount of methanol. Around 1THz, we see a positive excess for all of them, followed by a negative for all mixtures at higher frequencies. To try to correlate these modes to those of the pure liquids, we plotted them together (Figure 10). Comparing benzene and this simulated spectra for azeotrope, we see the lowest frequency mode is the fast β relaxation. The librational mode around 50-100 cm^{-1} is a mix of benzene and methanol intermolecular modes, since both their librational modes lie within proximity of each other.

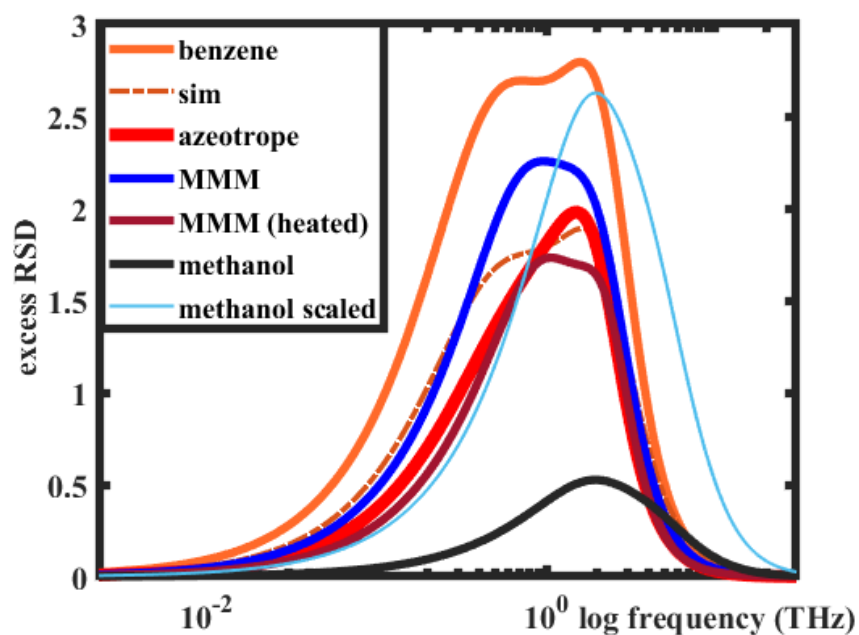


Figure 10: RSD of benzene, azeotrope, MMM, MMM (h) and methanol compared with the simulated spectra for 2:3 mixture.

To talk about how the actual azeotrope spectrum differs from the simulated one, we see that the first negative excess arises due to the absence/reduction of the fast β mode (Figure 10). The cage rattling has significantly reduced in the azeotrope. Since the cage-rattling is a collision-induced process [20], it is inversely proportional to the inter-particle distance. A reduction in the collision-induced part of the spectra can suggest a decrease in the number and/or the strength of the collisions. The librational peak of the azeotrope is slightly red-shifted compared to both the benzene and methanol modes.

On the other hand, the mixtures differ from the azeotrope in that their RSDs are still bimodal in character. The spectra show an increase in the fast β contribution. This is the case for all the other mixtures as well, where the contribution from the cage-rattling mode is more than what is expected after the addition of methanol. The mode is also shifted to higher frequencies. The librational contributions are lesser than the ideal simulated curves but roughly fall around the same

frequencies. The higher frequency negative excess varies for the mixtures depending on the concentration.

Comparing the systems having same composition, namely, i) azeotrope, ii) manually mixed (MMM) and iii) the manually mixed heated to the azeotrope boiling point in a closed environment (MMMh), we see that the MMM differs from the azeotrope having a bimodal character like the other mixtures. The heated mixture also has a bimodal character, but its amplitude is closer to the azeotrope. The MMM SD is higher in amplitude and broader in frequency compared to both azeotrope and the heated mixture. The MMM behaves like any other mixture and is considerably different from both the azeotrope and the heated mixture. The heated mixture, on the other hand, has similarity to both the azeotrope and the MMM. Based on the differences in the same composition mixtures, we propose that formation of an azeotrope is a temperature driven process and that heating the benzene methanol mixture causes the molecules to rearrange in a way such that they are able to cross the energy barrier to form the azeotrope.

The difference between the azeotrope and MMM is also seen in the NMR spectra. Surprisingly, the chemical shifts for all the protons are the same for both the MMM and the heated mixture (Figure 11). A temperature dependent NMR experiment was also carried out for the mixtures and the neat liquids. The temperature dependence of the chemical shifts for the mixtures and the neat liquids are summarized in table 2, 3 and 4.

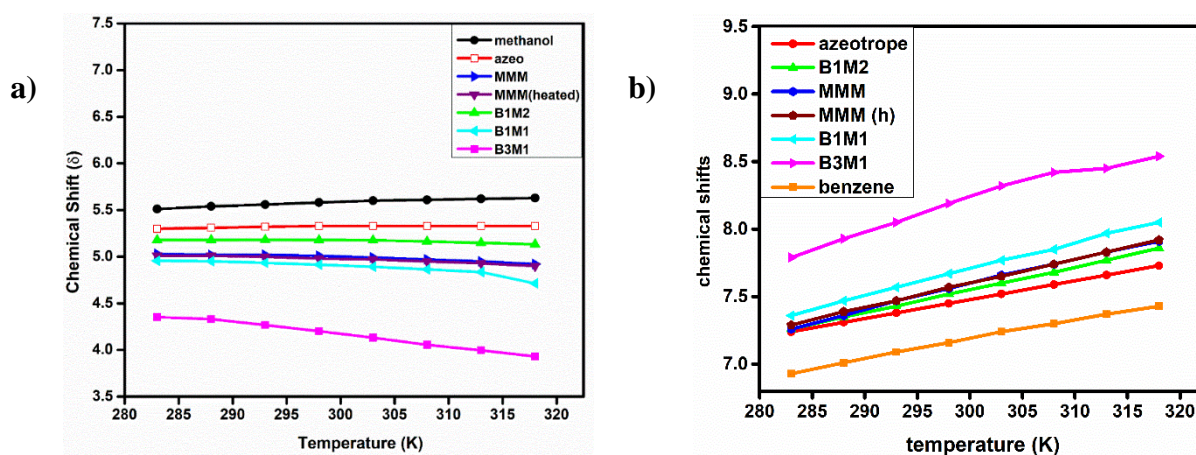


Figure 11: a) The NMR OH chemical shifts of of methanol and the mixtures, b) the NMR CH shift of benzene and the mixture, as a function of temperature.

	methanol	azeotrope	B1M2	MMM	MMM (h)	B1M1	B3M1
283 K	3.39	3.32	3.37	3.38	3.41	3.49	3.9
288 K	3.44	3.39	3.45	3.48	3.51	3.60	4.03
293 K	3.48	3.45	3.54	3.57	3.56	3.70	4.16
298 K	3.54	3.52	3.62	3.66	3.68	3.79	4.28
303 K	3.59	3.59	3.71	3.76	3.77	3.89	4.41
308 K	3.65	3.67	3.79	3.85	3.85	3.97	4.51
313 K	3.69	3.74	3.87	3.93	3.94	4.08	4.54
318 K	3.83	3.73	3.96	4.02	4.03	4.17	4.62

Table 2: Methanol CH₃ chemical shift

	methanol	azeotrope	B1M2	MMM	MMM (h)	B1M1	B3M1
283 K	5.1	5.11	5.13	5.13	5.16	5.17	5.09
288 K	5.1	5.11	5.14	5.14	5.16	5.15	5.08
293 K	5.1	5.12	5.15	5.16	5.16	5.15	5.07
298 K	5.1	5.13	5.15	5.16	5.16	5.16	5.06
303 K	5.11	5.14	5.16	5.16	5.16	5.16	5.04
308 K	5.12	5.14	5.16	5.17	5.17	5.16	5.03
313 K	5.1	5.15	5.17	5.17	5.17	5.16	4.94
318 K	5.09	5.15	5.17	5.17	5.17	5.16	4.86

Table 3: Methanol OH chemical shift

	azeotrope	B1M2	MMM	MMM (h)	B1M1	B3M1	benzene
283 K	7.24	7.26	7.26	7.29	7.36	7.79	6.93
288 K	7.31	7.35	7.36	7.39	7.47	7.93	7.01
293 K	7.38	7.43	7.47	7.47	7.57	8.05	7.09
298 K	7.45	7.52	7.56	7.57	7.67	8.19	7.16
303 K	7.52	7.60	7.66	7.65	7.77	8.32	7.24
308 K	7.59	7.68	7.74	7.74	7.85	8.42	7.3
313 K	7.66	7.77	7.83	7.83	7.97	8.45	7.37
318 K	7.73	7.86	7.91	7.92	8.05	8.54	7.43

Table 4: Benzene CH chemical *shift*

Generally when a hydrogen bond is present, there is a downfield shift of the hydroxyl proton signal towards higher frequencies. For the OH proton of methanol, the mixtures are deshielded with respect to the neat liquid. The azeotrope has chemical shifts almost comparable to that of pure methanol. The CH₃ proton of methanol and the CH proton of benzene are also deshielded in the mixtures compared to the pure liquids. In all cases, the azeotrope is the least deshielded compared to the other composition mixtures. The manually mixed and the heated mixtures have similar values that are different from that of the azeotrope. A greater deshielding of the protons would imply a stronger interaction, the deshielding for the CH and CH₃ protons increase even more with the temperature as is evident from the temperature coefficient (slope) obtained by fitting the temperature vs concentration plot to a linear function. The temperature coefficient increases with the increase of benzene in the mixtures. A positive slope again implies a much stronger interaction. The temperature coefficient of the azeotrope is the lowest among the mixtures and matches that of the pure liquids.

The interaction that the protons undergo (both the CH₃ and the CH proton) is stronger and more extensive in the mixtures compared to in the neat liquids. The intermolecular interactions are getting enhanced when both these liquids are mixed. Although when we talk about hydrogen bonding, generally with an increase in temperature the hydrogen bonded protons deshield less, corresponding to a negative slope. This should be the case for other intermolecular interactions as

well. It has been reported that non-hydrogen bonded amides that are strongly deshielded by neighboring aromatic rings have a more positive temperature coefficient than their expected value[28]. This can be the case in our system also since most of the protons are in a sea of benzene.

	benzene	azeotrope	B3M1	B1M1	MMM	MMM(h)	B1M2	methanol
conc. of benzene	1	0.39	0.75	0.5	0.39	0.39	0.33	0
$\Delta\delta/\delta T$ for CH ₃ proton	0.014	0.014	0.022	0.020	0.019	0.018	0.017	-
$\Delta\delta/\delta T$ for CH proton	-	0.013	0.021	0.019	0.018	0.018	0.017	0.012

Table 5: Temperature coefficient of the CH₃ proton and the CH proton

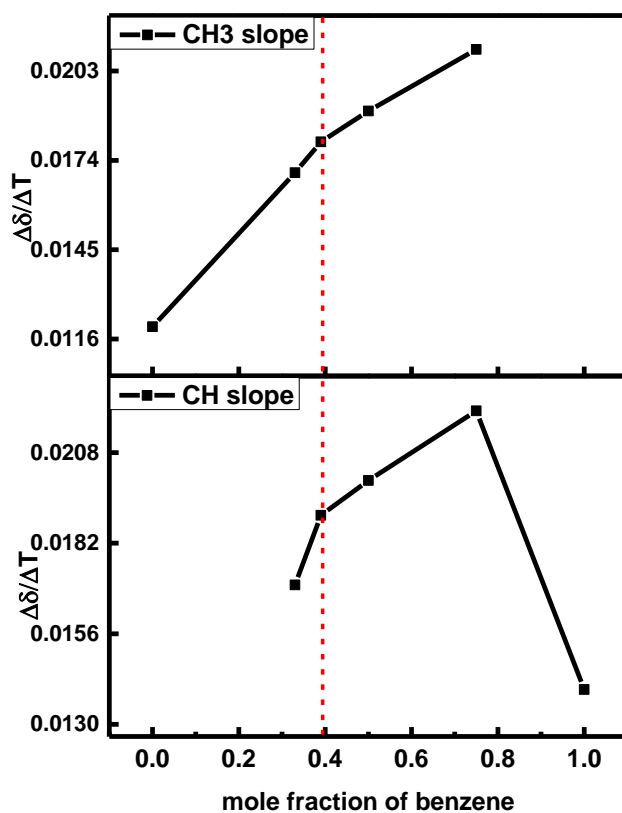


Figure 12: Temperature coefficient (slope) vs mole fraction of benzene

3.4 Conclusion

To summarize, most importantly we were able to show that the formation of an azeotrope is a temperature driven process. We provide experimental proof that the intermolecular dynamics is starkly different for the azeotrope when compared to the MMM and all the other mixtures. The difference of spectra between three identical concentrations, i) the azeotrope ii) the manually mixed mixture and iii) manually mixed heated in a closed environment, is fascinating. The MMM when heated in a closed environment, goes through molecular rearrangement, reaches the top of the potential energy curve but without an outlet for it to vaporize, it condenses with an equal probability of existing as MMM or as an azeotrope. We provide experimental proof that at ultrafast timescales the intermolecular dynamics of benzene-methanol azeotrope is different than other mixtures.

3.5 References

1. A D Buckingham, a. and B.D. Utting, *Intermolecular Forces*. Annual Review of Physical Chemistry, 1970. **21**(1): p. 287-316.
2. Dessent, C.E.H. and K. Müller-Dethlefs, *Hydrogen-Bonding and van der Waals Complexes Studied by ZEKE and REMPI Spectroscopy*. Chemical Reviews, 2000. **100**(11): p. 3999-4022.
3. Eslamian, M. and M.Z. Saghir, *Thermodiffusion in binary and ternary nonpolar hydrocarbon + alcohol mixtures*. Journal of Non-Equilibrium Thermodynamics, 2012. **37**(4): p. 329.
4. Irving, H.M.N.H. and R.B. Simpson, *The viscosity of mixtures of benzene and methanol*. Journal of Inorganic and Nuclear Chemistry, 1972. **34**(7): p. 2241-2247.
5. Adachi, Y. and K. Nakanishi, *Monte Carlo Study of the Self-association of Methanol in Benzene*. Molecular Simulation, 1991. **6**(4-6): p. 299-310.
6. Boyd, S.L. and R.J. Boyd, *A Density Functional Study of Methanol Clusters*. Journal of Chemical Theory and Computation, 2007. **3**(1): p. 54-61.
7. Tsuzuki, S., *Interactions with Aromatic Rings*, in *Intermolecular Forces and Clusters I*, D.J. Wales, Editor. 2005, Springer Berlin Heidelberg: Berlin, Heidelberg. p. 149-193.
8. Janda, K.C., et al., *Benzene dimer: A polar molecule*. The Journal of Chemical Physics, 1975. **63**(4): p. 1419-1421.
9. Steed, J.M., T.A. Dixon, and W. Klemperer, *Molecular beam studies of benzene dimer, hexafluorobenzene dimer, and benzene-hexafluorobenzene*. The Journal of Chemical Physics, 1979. **70**(11): p. 4940-4946.
10. Arunan, E. and H.S. Gutowsky, *The rotational spectrum, structure and dynamics of a benzene dimer*. The Journal of Chemical Physics, 1993. **98**(5): p. 4294-4296.
11. Jalilian, M.R. and S.F. Tayyari, *Spectra and structure of binary azeotropes VI-benzene-methanol*. Spectrochimica Acta Part A: Molecular and Biomolecular Spectroscopy, 2009. **73**(5): p. 828-832.
12. Ploetz, E.A., N. Benteitis, and P.E. Smith, *Kirkwood-Buff integrals for ideal solutions*. The Journal of Chemical Physics, 2010. **132**(16): p. 164501.

13. Newman, K.E., *Kirkwood–Buff solution theory: derivation and applications*. Chemical Society Reviews, 1994. **23**(1): p. 31-40.
14. Perera, A., et al., *Kirkwood-Buff integrals of aqueous alcohol binary mixtures*. The Journal of Chemical Physics, 2006. **124**(12): p. 124515.
15. Shephard, J.J., et al., *Microstructures of negative and positive azeotropes*. Physical Chemistry Chemical Physics, 2016. **18**(28): p. 19227-19235.
16. Pribble, R.N., C. Gruenloh, and T.S. Zwier, *The ultraviolet and infrared spectroscopy of (benzene)₂-(CH₃OH)₃ isomeric clusters*. Chemical Physics Letters, 1996. **262**(5): p. 627-632.
17. Matisz, G., et al., *Coordination of Methanol Clusters to Benzene: A Computational Study*. The Journal of Physical Chemistry A, 2011. **115**(38): p. 10556-10564.
18. Li, D., et al., *Molecular Mechanism for Azeotrope Formation in Ethanol/Benzene Binary Mixtures through Gibbs Ensemble Monte Carlo Simulation*. The Journal of Physical Chemistry B, 2020. **124**(16): p. 3371-3386.
19. Turton, D.A. and K. Wynne, *Universal nonexponential relaxation: Complex dynamics in simple liquids*. The Journal of Chemical Physics, 2009. **131**(20): p. 201101.
20. Farrell, A.J., et al., *Low-Frequency (Gigahertz to Terahertz) Depolarized Raman Scattering Off n-Alkanes, Cycloalkanes, and Six-Membered Rings: A Physical Interpretation*. The Journal of Physical Chemistry B, 2020. **124**(35): p. 7611-7624.
21. Fukasawa, T., et al., *Relation between Dielectric and Low-Frequency Raman Spectra of Hydrogen-Bond Liquids*. Physical Review Letters, 2005. **95**(19): p. 197802.
22. Kampfrath, T., et al., *The Nature of the Dielectric Response of Methanol Revealed by the Terahertz Kerr Effect*. The Journal of Physical Chemistry Letters, 2018. **9**(6): p. 1279-1283.
23. Sarkar, S., et al., *Broadband terahertz dielectric spectroscopy of alcohols*. Chemical Physics Letters, 2017. **678**: p. 65-71.
24. Venables, D.S. and C.A. Schmuttenmaer, *Far-infrared spectra and associated dynamics in acetonitrile–water mixtures measured with femtosecond THz pulse spectroscopy*. The Journal of Chemical Physics, 1998. **108**(12): p. 4935-4944.

25. Venables, D.S. and C.A. Schmuttenmaer, *Spectroscopy and dynamics of mixtures of water with acetone, acetonitrile, and methanol*. The Journal of Chemical Physics, 2000. **113**(24): p. 11222-11236.
26. Li, R., et al., *Mesoscopic Structuring and Dynamics of Alcohol/Water Solutions Probed by Terahertz Time-Domain Spectroscopy and Pulsed Field Gradient Nuclear Magnetic Resonance*. The Journal of Physical Chemistry B, 2014. **118**(34): p. 10156-10166.
27. Neelakandan, M., D. Pant, and E.L. Quitevis, *Reorientational and intermolecular dynamics in binary liquid mixtures of hexafluorobenzene and benzene: femtosecond optical Kerr effect measurements*. Chemical Physics Letters, 1997. **265**(1): p. 283-292.
28. Cierpicki, T. and J. Otlewski, *Amide proton temperature coefficients as hydrogen bond indicators in proteins*. Journal of Biomolecular NMR, 2001. **21**(3): p. 249-261.

4

Water and water-urea dynamics

4.1 Introduction

The water-urea system displays several exciting properties and has garnered much attention over the previous years. Aqueous urea solutions have been widely used to denature protein [1-4]. Although the presence of urea is considered detrimental to the structure of macromolecules, it is also used by cells as an osmolyte in certain water-stressed organisms, mostly in combination with methylamines (like Trimethylamine N-oxide (TMAO)) [5]. The counteracting action of TMAO against urea in a 1:2 ratio is more beneficial to the cells than urea or TMAO alone [5] [6]. An in-depth understanding of the urea-water interactions would aid the understanding of more complex systems of biological importance. Hydrocarbons dissolve in aqueous urea solutions more efficiently than compared to pure water [7-11]. Micelle formation is also significantly decreased at high urea concentrations [12, 13]. To understand these properties, it is important to understand the interactions existing between urea, water, and the solute molecule. One of the critical questions that still remains unanswered is what effect urea has on the hydrogen-bonded structure of water. The underlying molecular origin of protein denaturation by urea, although well studied, is still ambiguous. Two different mechanisms have been used to describe the denaturation process. The first mechanism, the direct mechanism, suggests that the unfolding of the protein occurs due to a direct interaction of urea with the protein backbone or/and the polar and non-polar sidechains via hydrogen bonding or through favorable Van der Waals attraction [14-25]. Therefore, the protein-water and the protein-urea interactions play a vital role in the denaturation process. However, it is also known that urea denaturation starts only at a specific concentration of urea which suggests that the urea-water interaction is also an important factor in the denaturation process. Hence, alternatively, the indirect mechanism has also been proposed in which it is assumed that urea disrupts the water structure, thus making the protein hydrophobic residues more readily solvated [10, 26].

Water molecules are bound to each other due to an extensive hydrogen-bond network forming ice-like tetrahedral clusters. In an attempt to explain the remarkable properties of the aqueous urea system, earlier thermodynamics studies proposed two models in 1960. One is known as the indirect method or the Frank-Frank model (or the FF model), which suggests that water generally coexists in two states, the dense disordered state and the clathratelike ordered state [10]. The addition of urea disrupts the equilibrium and shifts it to exist as the disordered state. Therefore, urea is generally referred to as the structure-breaker for water. It is assumed that hydrocarbons generally

dissolve only in the disordered state of water, and their solubility, therefore, increases with the addition of urea.

The second model, the direct method also called the SKSS model proposed by Schellman [27], Kresheck and Scheraga [28], and Stokes [29], attributes the properties of the urea-water system to the preferential interaction of the urea molecules with a third component, for example, a protein or a solute molecule. This model mainly focuses on the urea-urea interaction and does not take into account the structure of water.

The aqueous urea system is well studied in literature, using both experimental and theoretical methods. An important question throughout the literature is the degree to which urea perturbs the highly directional water hydrogen bond network. The activity coefficient of urea is constant throughout its solubility range on the molar scale [30, 31], which indicates that the urea-water system is relatively ideal and that the urea-water interactions are energetically well-balanced with the water-water and the urea-urea interactions. This ideality has been supported by some experimental techniques like NMR [32], calorimetry [22], THz absorption [33], dielectric spectroscopy [34], pump-probe IR spectroscopy [35], and neutron diffraction experiment, and also from computer simulations. Due to this, the FF model of urea disrupting the water structure has started to lose favor. Stumpe et al. using MD simulations, has shown that urea enhances the water structure in terms of hydrogen-bond energetics and that the main driving force behind protein denaturation is the direct interaction between urea and urea protein (the SKSS model) [18].

To understand this urea-water ideality, it has been suggested that urea substitutes a water dimer in the hydrogen bond network [35]. However, densitometry measurements comparing the partial molar volumes of water and urea show that a urea molecule replaces not about 2 but 2.45 water molecules [36]. Therefore the argument of urea being a structure breaker or maker still remains unresolved. Idrissi reviewed the water-urea system using MD simulations and spectroscopy [37] that urea acts as a structure breaker. This point of view has also been supported by various techniques like NMR [38], Raman spectroscopy [39] [40, 41], viscosity measurements [42, 43], and molecular dynamics simulations [44].

Several theoretical studies also suggest that urea enhances the hydrogen bond network of water [45] [46, 47]. The concept of a solute molecule being a structure breaker or maker in itself has not been very well-defined, and its interpretation may vary significantly in literature. As such, the

effect urea has on water, although controversial, is a very important system to probe because of its unique properties and biological importance.

Time-resolved Optical Kerr effect (OKE) spectroscopy is a powerful spectroscopic technique to study the hydrogen-bonded structure and dynamics of complex aqueous systems in the picosecond timescales. OKE spectral density can resolve protein water dynamics from 100GHz to up to 10 THz, including relaxation and librational dynamics of bulk water and water-protein interactions. The aqueous urea system has been studied using Optical Kerr effect spectroscopy before [48, 49]. The time-domain analysis of the OKE transients by Idrissi et al. [49] attributes the slowest relaxation time to the reorientation of a urea molecule about a principal axis lying in the plane of the molecule. This slow relaxation timescale increases with the increase in urea concentration. The analysis of the faster relaxation dynamics, on the other hand, shows an increase in anisotropy with an increase of urea mole fraction. This increase in anisotropy is due to the formation of highly directional hydrogen bond interaction. The frequency-domain analysis shows that two different types of concentration regimes are present in the aqueous urea system depending on the concentration of urea in the solution. This is also in line with the work done by Mazur et al. [48], who have also analyzed the OKE frequency domain spectra of different concentrations of urea solutions. At low urea concentration, the OKE spectral density retains the bimodal character of the water spectrum, which suggests that the water structure at this concentration remains unaffected in the presence of urea. At higher concentrations (which is generally used for protein denaturation), most water molecules are part of the solvation shell of urea; along with the slowing down of the picosecond relaxation dynamics, there is also a redshift of the H-bond stretching frequency present in the pure water spectrum (175 cm^{-1} for neat water). These changes have been associated with a disruption of water structure at high urea concentrations. The authors have also attributed the slow relaxation dynamics at higher concentrations to be associated with confined water molecules.

In the present study, we have also probed the water-urea system using OKE spectroscopy at varying urea concentrations. We have analyzed the entire OKE spectrum in the frequency domain to get a better understanding of the urea-water dynamics in the broad GHz-THz region.

4.2 Experimental Methods

4.2.1 Samples: Urea was purchased from Sigma-Aldrich. A stock solution of 9M urea was made using Millipore water and filtered using 0.22 μm syringe filter. Solutions of subsequent molarities were made by diluting the stock solution.

4.2.2 Optical Kerr Effect Spectroscopy: The details of the Optical Kerr effect spectroscopy setup are given in Chapter 2: Experimental Methods and Data analysis. For data collection, 1mm thick quartz cuvettes were used. The autocorrelation curve was approximated from the OKE time signal through a 3mm thick CaF_2 crystal. Data analysis was done using MATLAB.

4.3 Results and Discussion: The OKE response for water is significantly less compared to that from benzene; this is due to its molecular polarizability being almost isotropic. Thus, the OKE signal obtained for water would mostly have contributions from the intermolecular or collision-induced dynamics. The time transients for water have been seen to follow the stretched behavior proposed by MCT, which generally is observed for glass-forming liquids but can also be used to explain the spectra of molecular liquids [50],[51]. The stretching parameter obtained on fitting the relaxation part to a derivative of a stretched exponential remained constant throughout the temperature range studied [50].

In the frequency domain, the log-log plot of the SD shows that along with a relaxation peak attributed to translational diffusion or cage-rattling motion (β relaxation), water has two additional intermolecular modes corresponding to the hydrogen bond bend or the transverse acoustic (TA) phonon mode and the hydrogen bond stretch or the longitudinal acoustic (LA) phonon mode. Beyond 20 THz librational bands start appearing [52]. Understanding water dynamics on its own and in the presence of different biologically important solutes is fundamental because water plays a crucial role in many biological functions.

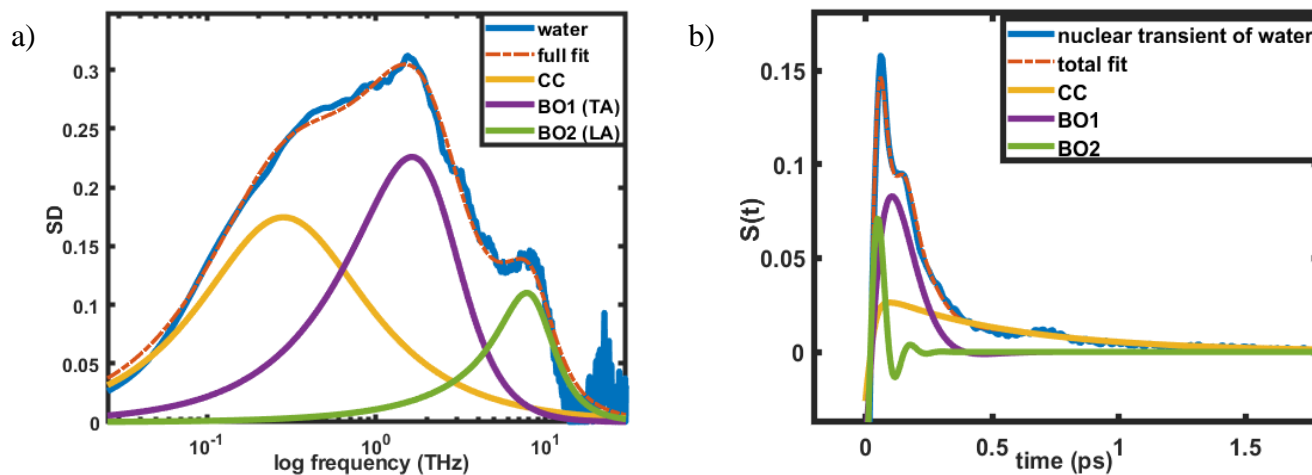


Figure 1: a) OKE spectral density (SD) of water and their fits to CC (Cole-Cole) and two Brownian oscillators (BO) b) the corresponding nuclear time transient with the fits.

Figure 1a) shows the frequency-dependent log-log plot of the spectral density of water as processed from the OKE time domain data that we obtained. The data fits well to the scheme of functions described above. A Cole-Cole function is used to fit the low-frequency shoulder corresponding to translational diffusion (β relaxation) with a characteristic timescale of 0.55 ps, and two Brownian oscillators fit the hydrogen bond bend and stretch modes. As described in Chapter 2, the spectral density is processed by first removing electronic hyperpolarizability from the time-domain data. Figure 1 b) shows the corresponding nuclear transient of the OKE data. Figure 2 shows the GHz-THz spectral density of different concentrations of urea in water compared to neat water. The addition of urea to water sees the emergence of a new peak at the lowest GHz frequencies, which was earlier attributed to the reorientational diffusion of the urea molecules. With the increase in urea concentration, this process increases in amplitude and starts to dominate the dynamics. The librational frequencies (around 1-10 THz), on the other hand, do not show a corresponding increase with concentration.

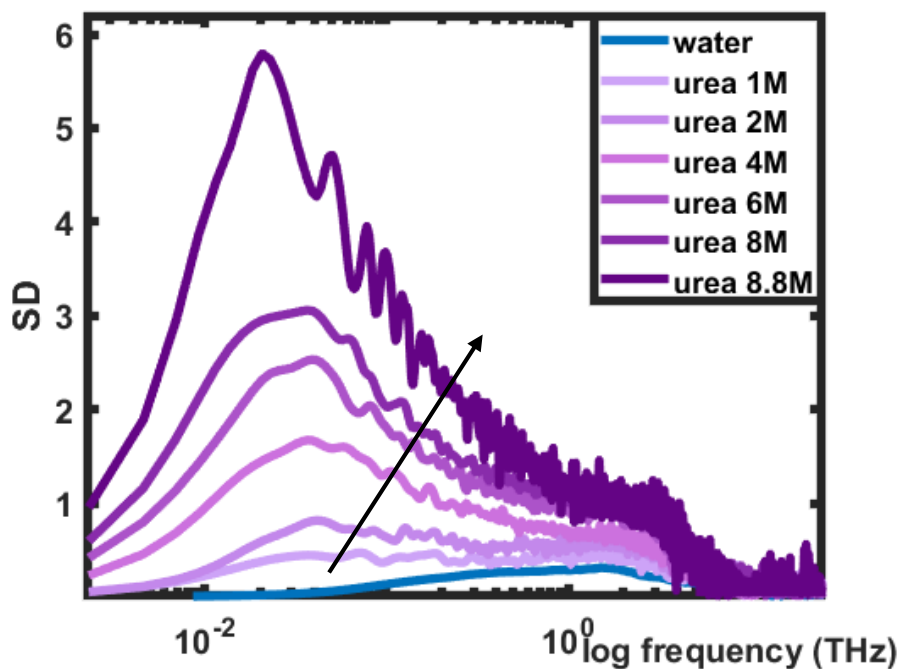


Figure 2: The spectral density of different concentrations of aqueous urea solutions compared to neat water (blue)

Generally, all anisotropically polarizable molecular liquids show a similar type of dynamics with the α relaxation (or the orientational diffusion) flanking the GHz end of the frequency spectrum, the intermediate dynamics (or the β relaxation) due to translational diffusion and the librational modes at the higher THz frequencies. As seen from the spectrum of molecular liquids, the orientational diffusion band and the librational modes are of the same magnitude since the same molecular anisotropic polarizability tensor determines them. Thus it has been argued [53] that if the increased amplitude of the GHz band is caused solely by the orientational diffusion of the solute molecule, then the librational frequencies should also show changes of equal magnitude, which is not the case in these concentrated aqueous urea solutions. The GHz frequency band is pretty broad even at lower concentrations of urea, where a significant change in the water structure is not expected.

Ramakrishnan et al. have studied the aqueous TMAO system [53], their OKE spectral density also shows a prominent broad peak at the GHz frequencies. According to the calculations based on the Debye-Stokes-Einstein theory, if this band is due to the orientational diffusion, it should follow a Debye relaxation and have a peak at 5.4 GHz. Measurements using dielectric relaxation spectroscopy have shown the TMAO diffusion peak to be expected at around 8THz [54]. However, the OKE SD shows a broad band spanning from 1 to 100 GHz, even at low concentrations. This is consistent with what we see in our OKE SD of urea solutions as well. Therefore, this slow dynamics is related to the slowing down of the dynamics of water molecules in close interaction with the solute molecule.

The spectral density was fit to a sum of Debye, Cole-Cole, and three Brownian oscillators. The Debye function was used to fit the lowest GHz band, while the Cole-Cole function fit the intermediate β relaxation. The three Brownian oscillators fit the higher frequency modes. To get a clear picture of how the β relaxation and the oscillatory modes change with concentration, we need to subtract the reorientational peak and analyze the reduced spectral densities (RSD). Figure 3 shows the spectral density of 8M urea with the corresponding fit. The SD of 1M urea required a sum of Debye, Cole-Cole, and two Brownian oscillators. A third oscillator was also required to fit the high-frequency end of the spectrum from beyond this concentration. From 2M to 8 M, a sum of Debye, CC, and three oscillators were used. At 8.8 M, the saturated solution of urea, the high-frequency librational mode (corresponding to the water librational mode), is no longer present, and only two oscillators can fit the data along with the relaxation dynamics. The fit parameters are summarized in Table1.

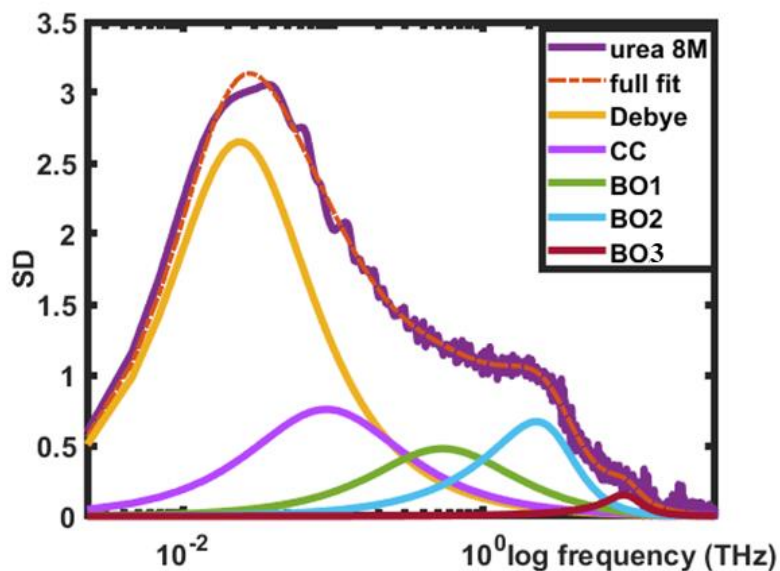


Figure 3: Spectral density of 8M aqueous urea solution and its corresponding fit to a sum of Debye, Cole-Cole, and three Brownian oscillators.

The peak at GHz frequency shifts to even lower frequencies with the increase in urea concentration in the solution. This is due to the slowing down of the water dynamics. The molecular polarizability of water is almost isotropic; hence the OKE response of pure water is very less. The addition of urea to water gives rise to a significant increase in the OKE response of the solutions. The slow water GHz frequency peak is therefore highly anisotropic, and this is a result of interaction between urea and water molecules via highly directional hydrogen bonding. The librational peaks (hydrogen bond bend and stretch) are not much perturbed except at the saturated concentration of 8.8M. The hydrogen bond stretch of water (LA phonon mode) at 8.75 THz shifts to lower frequencies till 6M concentration and is totally absent in the 8.8M solution. This is an indication that at 8.8M urea solution forms the upper limit, and the water hydrogen structure is disrupted as most of the water molecules would in some way be part of a urea solvation shell. We calculated the reduced spectral densities (RSD) of the solutions by subtracting the GHz frequency band from the spectrum to get a clearer view of the high-frequency modes. Figure 4 shows the RSD of the urea solutions compared to the SD of pure water.

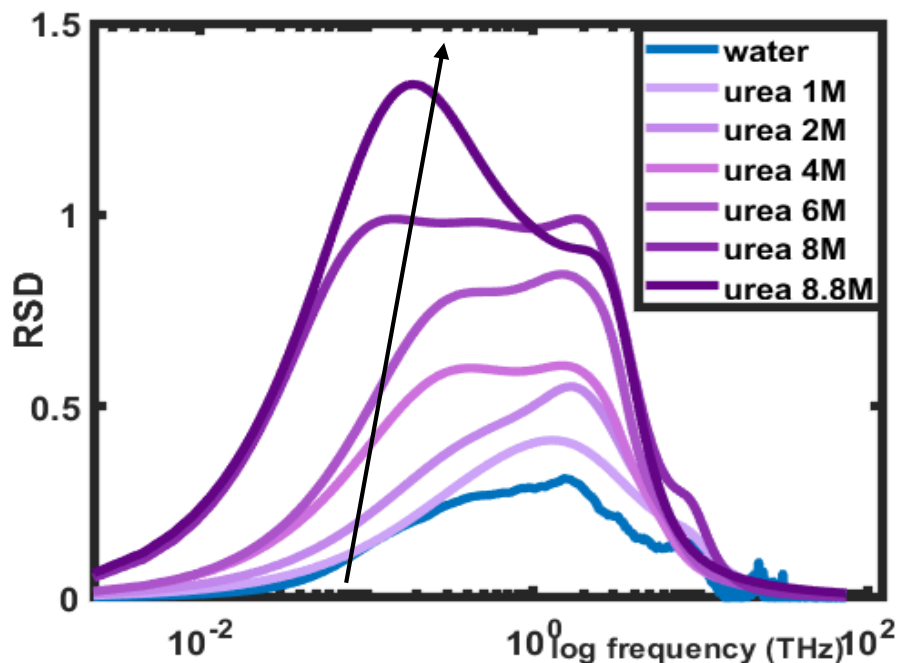


Figure 4: The reduced spectral density of different concentrations of aqueous urea solutions compared to neat water (blue)

The RSD shows a marked increase in the amplitude of the intermediate β relaxation mode. With increasing urea concentration, the translational diffusion timescale associated with this mode becomes slightly faster, initially up to 2M concentration, and then slows down for higher concentrations. Also, beyond 1M concentration, an additional oscillator is required to fit the higher frequency end of the spectrum. DFT calculations done by Mazur et al. for urea and urea plus specific water saw a new mode at 73 cm^{-1} ($\sim 2 \text{ THz}$) corresponding to a Raman active out of plane bending mode of the urea-water complex. Another similar mode was found pertaining to urea dimers at 99 cm^{-1} (3 THz). Additional calculations revealed a third mode at a similar position arising due to a urea dimer structure connected by two intervening water molecules. The most important thing here is that this particular mode (ω_2) arises only when the urea molecules are hydrogen-bonded either to one another or to water and is not present in the isolated molecule.

Therefore the additional librational mode present above 1M urea concentration can be due to urea-urea or urea-water complexes or both forming an extended hydrogen bond network. For the saturated 8.8M urea solution, most of the water molecules are associated with urea causing a disruption of the water structure which is evident from Figure 4, which shows a decrease in the amplitude of the librational modes compared to the increase in translational diffusion band. The spectrum of 8.8M urea is also different in terms of that the hydrogen bond stretch of pure water at 8.75 THz is absent in the 8.8M saturated urea solution. This is another indication that the water dynamics at such a high concentration is totally different from bulk water.

	water	1M	2M	4M	6M	8M	8.8M
A1 (%)	--	0.16	0.55	1.50	1.48	0.81	3.36
A2 (%)	0.11	0.12	0.35	0.60	0.42	0.20	0.99
A3 (%)	19.86	8.60	11.65	21.01	25.59	8.14	9.49
A4 (%)	--	--	43.62	39.89	43.84	54.24	86.16
A5 (%)	80.03	91.12	43.83	36.99	28.68	36.61	--
a	0	0.1	0.16	0.12	0.09	0.06	0.11
γ1 (THz)	3.86	3.01	2.44	2.86	4.07	4.77	3.03
γ2 (THz)	--	--	4.36	3.31	3.18	5.34	3.98
γ3 (THz)	7.16	12.73	4.53	4.67	5.53	4.99	--
τ1 (ps)	--	3.68	3.72	4.74	5.20	6.13	7.80
τ2 (ps)	0.55	0.25	0.37	0.56	0.63	0.88	0.95
ω1 (THz)	2.39	2.38	1.96	1.98	2.01	1.82	1.59
ω2 (THz)	--	--	3.22	3.05	2.87	3.27	3.23
ω3 (THz)	8.75	8.69	6.27	5.66	6.56	9.33	--

Table 1: Fit parameters of the spectral density of urea solutions and pure water fit to a sum of Debye, Cole-Cole, and Brownian oscillators.

4.4 Conclusion

In conclusion, we see that at concentrations used for denaturing proteins, the water dynamics is affected by the presence of urea. At all concentrations studied here, we see a prominent peak at the GHz frequency corresponding to the slowing down of the dynamics of water molecules associated with urea. With increasing urea concentration, this mode shows a marked increase in amplitude, and the timescale associated with the dynamics slows down even further. This slowdown indicates that these water molecules remain in the solvation shell of urea for a longer time. Beyond 2M, the translational diffusion timescales (β relaxation) also show a slight slowing down. The β relaxation amplitudes also increase with concentration; this increase is due to the increase in anisotropy due to the hydrogen bonding interaction between urea and water molecules. Beyond 1M, the higher frequency end sees the emergence of a new mode that has been attributed to urea-urea or urea-water complexes in previous studies.

From this study, we can say that the OKE response of urea solutions at all concentrations shows solute-induced effects. As pointed out in earlier studies, we also see the existence of two concentration regimes. At the lowest concentration of 1M, urea interacts with the water molecules, which is evident from the slowdown of the dynamics. But the water structure remains unaffected as the librational frequencies are hardly perturbed in this concentration. As the concentration increases, we see the slow relaxation modes becoming more prominent at the expense of the librational modes. This change in dynamics becomes more prominent from 4M concentration, as evident from the increasing amplitude and broadening of the translational diffusion mode (Figure 4). The hydrogen bond bend and stretch of pure water show a slight redshift in the higher urea concentration solutions. All these changes can be associated with the disruption of water structure beyond 2M concentration of urea solution.

References:

1. Creighton, T.E., *Protein Structures and Molecular Properties*, 2nd ed. 1993: W.H. Freeman and Co.
2. McKenzie, H.A. and G.B. Ralston, *The denaturation of proteins: Two state? Reversible or irreversible?* *Experientia*, 1971. **27**(6): p. 617-624.
3. Brandts, J.F. and L. Hunt, *Thermodynamics of protein denaturation. III. Denaturation of ribonuclease in water and in aqueous urea and aqueous ethanol mixtures*. *Journal of the American Chemical Society*, 1967. **89**(19): p. 4826-4838.
4. Tanford, C., *Contribution of Hydrophobic Interactions to the Stability of the Globular Conformation of Proteins*. *Journal of the American Chemical Society*, 1962. **84**(22): p. 4240-4247.
5. Yancey, P., et al., *Living with water stress: evolution of osmolyte systems*. *Science*, 1982. **217**(4566): p. 1214-1222.
6. Canchi, D.R. and A.E. García, *Cosolvent Effects on Protein Stability*. *Annual Review of Physical Chemistry*, 2013. **64**(1): p. 273-293.
7. Wallqvist, A., D.G. Covell, and D. Thirumalai, *Hydrophobic Interactions in Aqueous Urea Solutions with Implications for the Mechanism of Protein Denaturation*. *Journal of the American Chemical Society*, 1998. **120**(2): p. 427-428.
8. Schellman, J.A., *A simple model for salvation in mixed solvents: Applications to the stabilization and destabilization of macromolecular structures*. *Biophysical Chemistry*, 1990. **37**(1): p. 121-140.
9. Kuharski, R.A. and P.J. Rosky, *Solvation of hydrophobic species in aqueous urea solution: a molecular dynamics study*. *Journal of the American Chemical Society*, 1984. **106**(20): p. 5794-5800.
10. Frank, H.S. and F. Franks, *Structural Approach to the Solvent Power of Water for Hydrocarbons; Urea as a Structure Breaker*. *The Journal of Chemical Physics*, 1968. **48**(10): p. 4746-4757.
11. Watlafer, D.B., et al., *Nonpolar Group Participation in the Denaturation of Proteins by Urea and Guanidinium Salts. Model Compound Studies*. *Journal of the American Chemical Society*, 1964. **86**(3): p. 508-514.

12. Schick, M.J., *Effect of Electrolyte and Urea on Micelle Formation*1. The Journal of Physical Chemistry, 1964. **68**(12): p. 3585-3592.
13. Bruning, W. and A. Holtzer, *THE EFFECT OF UREA ON HYDROPHOBIC BONDS: THE CRITICAL MICELLE CONCENTRATION OF n-DODECYLTRIMETHYLAMMONIUM BROMIDE IN AQUEOUS SOLUTIONS OF UREA*1. Journal of the American Chemical Society, 1961. **83**(23): p. 4865-4866.
14. Carr, J.K., et al., *Structure and Dynamics of Urea/Water Mixtures Investigated by Vibrational Spectroscopy and Molecular Dynamics Simulation*. The Journal of Physical Chemistry B, 2013. **117**(42): p. 13291-13300.
15. Yang, Z., et al., *Coherent Microscopic Picture for Urea-Induced Denaturation of Proteins*. The Journal of Physical Chemistry B, 2012. **116**(30): p. 8856-8862.
16. Zhou, R., et al., *Comment on "Urea-Mediated Protein Denaturation: A Consensus View"*. The Journal of Physical Chemistry B, 2011. **115**(5): p. 1323-1326.
17. Graziano, G., *How does trimethylamine N-oxide counteract the denaturing activity of urea?* Physical Chemistry Chemical Physics, 2011. **13**(39): p. 17689-17695.
18. Stumpe, M.C. and H. Grubmüller, *Urea impedes the hydrophobic collapse of partially unfolded proteins*. Biophysical journal, 2009. **96**(9): p. 3744-3752.
19. Hua, L., et al., *Urea denaturation by stronger dispersion interactions with proteins than water implies a 2-stage unfolding*. Proceedings of the National Academy of Sciences, 2008. **105**(44): p. 16928-16933.
20. Das, A. and C. Mukhopadhyay, *Atomistic Mechanism of Protein Denaturation by Urea*. The Journal of Physical Chemistry B, 2008. **112**(26): p. 7903-7908.
21. Klimov, D.K., J.E. Straub, and D. Thirumalai, *Aqueous urea solution destabilizes Abeta(16-22) oligomers*. Proceedings of the National Academy of Sciences of the United States of America, 2004. **101**(41): p. 14760-14765.
22. Batchelor, J.D., et al., *Impact of Protein Denaturants and Stabilizers on Water Structure*. Journal of the American Chemical Society, 2004. **126**(7): p. 1958-1961.
23. Tobi, D., R. Elber, and D. Thirumalai, *The dominant interaction between peptide and urea is electrostatic in nature: A molecular dynamics simulation study*. Biopolymers, 2003. **68**(3): p. 359-369.

24. Felitsky, D.J. and M.T. Record, *Thermal and Urea-Induced Unfolding of the Marginally Stable Lac Repressor DNA-Binding Domain: A Model System for Analysis of Solute Effects on Protein Processes*. *Biochemistry*, 2003. **42**(7): p. 2202-2217.
25. Zou, Q., S.M. Habermann-Rottinghaus, and K.P. Murphy, *Urea effects on protein stability: hydrogen bonding and the hydrophobic effect*. *Proteins*, 1998. **31**(2): p. 107-15.
26. Frank, H.S. and M.W. Evans, *Free Volume and Entropy in Condensed Systems III. Entropy in Binary Liquid Mixtures; Partial Molal Entropy in Dilute Solutions; Structure and Thermodynamics in Aqueous Electrolytes*. *The Journal of Chemical Physics*, 1945. **13**(11): p. 507-532.
27. Schellman, J.A., *The thermodynamics of urea solutions and the heat of formation of the peptide hydrogen bond*. *C R Trav Lab Carlsberg Chim*, 1955. **29**(14-15): p. 223-9.
28. Kresheck, G.C. and H.A. Scheraga, *The Temperature Dependence of the Enthalpy of Formation of the Amide Hydrogen Bond; the Urea Model*. *The Journal of Physical Chemistry*, 1965. **69**(5): p. 1704-1706.
29. Stokes, R., *Thermodynamics of aqueous urea solutions*. *Australian Journal of Chemistry*, 1967. **20**(10): p. 2087-2100.
30. Kokubo, H., et al., *Molecular Basis of the Apparent Near Ideality of Urea Solutions*. *Biophysical Journal*, 2007. **93**(10): p. 3392-3407.
31. Felitsky, D.J. and M.T. Record, *Application of the Local-Bulk Partitioning and Competitive Binding Models to Interpret Preferential Interactions of Glycine Betaine and Urea with Protein Surface*. *Biochemistry*, 2004. **43**(28): p. 9276-9288.
32. Shimizu, A., et al., *NMR studies on dynamic behavior of water molecule in aqueous denaturant solutions at 25 °C: Effects of guanidine hydrochloride, urea and alkylated ureas*. *Journal of Molecular Liquids*, 2000. **85**(3): p. 269-278.
33. Funkner, S., M. Havenith, and G. Schwaab, *Urea, a Structure Breaker? Answers from THz Absorption Spectroscopy*. *The Journal of Physical Chemistry B*, 2012. **116**(45): p. 13374-13380.
34. Hayashi, Y., et al., *Liquid Structure of the Urea–Water System Studied by Dielectric Spectroscopy*. *The Journal of Physical Chemistry B*, 2007. **111**(5): p. 1076-1080.
35. Rezus, Y.L.A. and H.J. Bakker, *Effect of urea on the structural dynamics of water*. *Proceedings of the National Academy of Sciences*, 2006. **103**(49): p. 18417-18420.

36. Gucker, F.T., F.W. Gage, and C.E. Moser, *The Densities of Aqueous Solutions of Urea at 25 and 30° and the Apparent Molal Volume of Urea*¹. *Journal of the American Chemical Society*, 1938. **60**(11): p. 2582-2588.
37. Idrissi, A., *Molecular structure and dynamics of liquids: aqueous urea solutions*. *Spectrochimica Acta Part A: Molecular and Biomolecular Spectroscopy*, 2005. **61**(1): p. 1-17.
38. Finer, E.G., F. Franks, and M.J. Tait, *Nuclear magnetic resonance studies of aqueous urea solutions*. *Journal of the American Chemical Society*, 1972. **94**(13): p. 4424-4429.
39. Hoccart, X. and G. Turrell, *Raman spectroscopic investigation of the dynamics of urea–water complexes*. *The Journal of Chemical Physics*, 1993. **99**(11): p. 8498-8503.
40. Idrissi, A., et al., *The effect of temperature on urea–urea interactions in water: a molecular dynamics simulation*. *Journal of Molecular Liquids*, 2004. **110**(1): p. 201-208.
41. Walrafen, G.E., *Raman Spectral Studies of the Effects of Urea and Sucrose on Water Structure*. *The Journal of Chemical Physics*, 1966. **44**(10): p. 3726-3727.
42. Herskovits, T.T. and T.M. Kelly, *Viscosity studies of aqueous solutions of alcohols, ureas, and amides*. *The Journal of Physical Chemistry*, 1973. **77**(3): p. 381-388.
43. Rupley, J.A., *The Effect of Urea and Amides upon Water Structure*¹. *The Journal of Physical Chemistry*, 1964. **68**(7): p. 2002-2003.
44. Idrissi, A., et al., *The Effect of Urea on the Structure of Water: A Molecular Dynamics Simulation*. *The Journal of Physical Chemistry B*, 2010. **114**(13): p. 4731-4738.
45. Idrissi, A., F. Sokolić, and A. Perera, *A molecular dynamics study of the urea/water mixture*. *The Journal of Chemical Physics*, 2000. **112**(21): p. 9479-9488.
46. Stumpe, M.C. and H. Grubmüller, *Aqueous Urea Solutions: Structure, Energetics, and Urea Aggregation*. *The Journal of Physical Chemistry B*, 2007. **111**(22): p. 6220-6228.
47. Chitra, R. and P.E. Smith, *Molecular Association in Solution: A Kirkwood–Buff Analysis of Sodium Chloride, Ammonium Sulfate, Guanidinium Chloride, Urea, and 2,2,2-Trifluoroethanol in Water*. *The Journal of Physical Chemistry B*, 2002. **106**(6): p. 1491-1500.
48. Mazur, K., I.A. Heisler, and S.R. Meech, *THz Spectra and Dynamics of Aqueous Solutions Studied by the Ultrafast Optical Kerr Effect*. *The Journal of Physical Chemistry B*, 2011. **115**(11): p. 2563-2573.

49. Idrissi, A., et al., *Time resolved optical Kerr effect analysis of urea–water system*. The Journal of Chemical Physics, 2001. **114**(15): p. 6774-6780.
50. Torre, R., P. Bartolini, and R. Righini, *Structural relaxation in supercooled water by time-resolved spectroscopy*. Nature, 2004. **428**(6980): p. 296-299.
51. Turton, D.A. and K. Wynne, *Universal nonexponential relaxation: Complex dynamics in simple liquids*. The Journal of Chemical Physics, 2009. **131**(20): p. 201101.
52. Turton, D.A., et al., *Rattling the cage: Micro- to mesoscopic structure in liquids as simple as argon and as complicated as water*. Journal of Molecular Liquids, 2011. **159**(1): p. 2-8.
53. Ramakrishnan, G., et al., *Spectrum of Slow and Super-Slow (Picosecond to Nanosecond) Water Dynamics around Organic and Biological Solutes*. The Journal of Physical Chemistry Letters, 2017. **8**(13): p. 2964-2970.
54. Hunger, J., et al., *Complex Formation in Aqueous Trimethylamine-N-oxide (TMAO) Solutions*. The Journal of Physical Chemistry B, 2012. **116**(16): p. 4783-4795.

5

Protein-water interactions and protein denaturation by urea

5.1 Introduction

Understanding the mechanism of protein folding and unfolding is an active research area in biophysical chemistry [1, 2]. The conformational changes occurring in proteins range from sub-picosecond timescales to beyond seconds [3-5]. Protein motions that take place in milliseconds to seconds are called the promoting motions, the timescale characteristic of biochemical reactions; they are diffusive in nature. These motions affect the activation free-energy barrier by changing the tertiary structure of the protein. Dynamical motions, on the other hand, are fast and take place at femtosecond to picosecond timescales. These motions bring about changes in the secondary structure of the macromolecule and determine the probability of barrier crossing in the transition state [6]. These low-frequency dynamical motions associated with the protein's structural flexibility can be probed with ultrafast spectroscopy [7, 8] and play an essential role in its folding and biological function [9].

Water is a natural solvent and plays a vital role in many biological processes like enzyme activity, protein folding-refolding, and denaturation. Interfacial water has a significant effect on the protein's internal structure and dynamics. It is essential to know the time scales characteristic of both the local protein rearrangements and water dynamics within the solvation shell to understand the protein-water interactions. Since water dynamics, including the hydrogen bond vibrations, their making and breaking, and their rotational and translational diffusion occur in sub-picosecond and picosecond timescales, the fluctuations in the water network can serve as an excellent probe to understand the solvation of proteins. While probing the structural dynamics of proteins, much emphasis has been given to understanding the changes occurring in the protein structure itself; thus, we tend to forget the role of the solvent molecules [10]. The folding process itself is mediated by the motions of the water molecules [11], causing collective low-frequency modes of protein and water to be strongly correlated to each other [12-15]. Protein-water dynamics have also been studied by Optical Kerr effect (OKE) spectroscopy. Mazur et al. showed that while at low protein concentrations, the water structure is preserved, but a high concentration of protein also disrupts the water structure. They also attributed the slowest relaxation to interaction-induced hydrogen bonding between protein and water solvating it. This relaxation time increases with the concentration of solute, and at high concentrations was even retarded by a factor of eight compared to bulk water [16]. Wynne and coworkers also reported collective low-frequency vibrational

modes of various globular proteins [6] and of a solvated lysozyme-ligand binding complex [17]. They were also able to show a frequency shift in the OKE spectra due to the helix-to-coil transformation of a polypeptide [18].

Protein folding makes the native three-dimensional structure possible that is biologically functional. The study of how a protein folds and is held together by different molecular interactions is of utmost interest. Similarly, the way proteins are unfolded in the presence of external stress - protein denaturation – also plays a crucial role in understanding many critical biological processes. Protein misfolding and aggregation causes a large number of neurodegenerative diseases in humans. Protein aggregates are oligomeric complexes of misfolded intermediates formed during the denaturation process, held together by all kinds of non-covalent interactions. It is still unclear whether the unfolding process triggers the aggregation in proteins or oligomerization causes conformational changes in the protein. Over the last decade, protein denaturation studies have gained importance in understanding protein dynamics and establishing the structural understanding that could be used for protein designing. Urea is a chaotropic agent [19-22] and a well-known denaturant for proteins [23]. The molecular picture behind urea-induced chemical denaturation of the proteins is still poorly understood. Urea may bind with the protein directly, competing with the native interactions already present, thereby causing the denaturation. This is called the direct mechanism [24-27]. In this case, urea binds to and stabilizes the denatured state preferentially, causing the misfolding. The other probable mechanism is called the indirect model, where urea affects the structure of the solvent, in this case, water [20, 28-30]. It disrupts the structure of water and solvates the hydrophobic protein residues leading to denaturation.

Ultrafast time-resolved Optical Kerr effect (OKE) spectroscopy is a powerful spectroscopic technique to study the hydrogen-bonded structure and dynamics of complex aqueous systems in the picosecond time scales. In this study, we investigate the protein-water dynamics and the mechanism behind the chemical denaturation of three proteins of different hydrophobicities- lysozyme, BSA, and trypsin, by urea.

5.2 Experimental Methods

5.2.1 Samples: Urea was purchased from Sigma-Aldrich. A stock solution of 9M urea was made using Millipore water and filtered using 0.22 μm syringe filter. Solutions of subsequent molarities were made by diluting the stock solution. Lysozyme, BSA, and trypsin were purchased from Sigma-Aldrich and dissolved in water without purification. The samples were filtered with syringe filters (0.22 μm pore diameter to remove dust particles and impurities and to prevent light scattering).

5.2.2 Optical Kerr Effect Spectroscopy: The details of the Optical Kerr effect spectroscopy setup are given in Chapter 2: Experimental Methods and Data analysis. For data collection, 1mm thick quartz cuvettes were used. The autocorrelation curve was approximated from the OKE time signal through a 3mm thick CaF_2 crystal. Data analysis was done using MATLAB.

5.3 Results and Discussion:

5.3.1 Protein-water dynamics

a) Lysozyme: Previous theoretical studies on Lysozyme (Lys) have identified a low-frequency vibrational mode at 3-4 cm^{-1} (~ 100 GHz) and have attributed it to a delocalized hinge-bending mode that affects the binding cleft [31-33]. Identifying such a low-frequency mode in an aqueous solution would be difficult with spectroscopy because such protein mode would be coupled to the solvent dynamics, making it overdamped. Crystalline lysozyme studied using Raman and THz spectroscopy show peaks at around 1-3 THz [9] [34-36]; however, it is difficult to predict if these modes are due to the crystal packing or are of any biological importance. Raman spectroscopy on aqueous lysozyme solutions [34, 36, 37] also shows presence of modes in the THz frequency region, but their biological relevance is also under scrutiny. Turton et al. have utilized OKE spectroscopy and have identified two underdamped delocalized oscillators involving at least a dozen protein residues [17]. Their MD simulation, even though it has not been able to reproduce the lysozyme spectra, shows the presence of vibrational modes between 1-3 THz region.

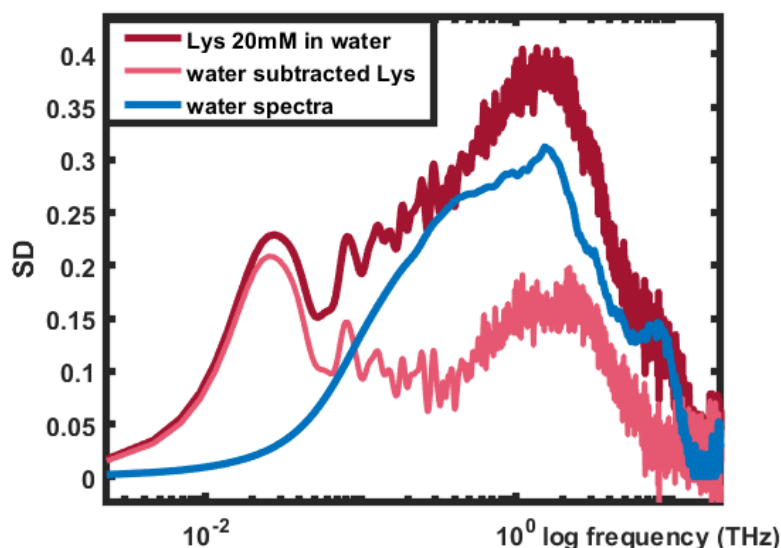


Figure 1: Spectral density (SD) of aqueous 20 mM (the highest concentration soluble in water) Lysozyme compared with the SD of neat water. The lighter pink curve corresponds to the solvent subtracted spectra of the same concentration.

The OKE spectral density (SD) of 20 mM aqueous lysozyme solution is shown in Figure 1, along with the SD of neat water. The solvent subtracted spectrum is also calculated by subtracting the pure solvent spectrum from the aqueous solution spectrum. The solvent subtraction has been done keeping in mind the weight percentage of the protein in the solution [6].

From the 20 mM Lys SD, the first prominent feature to notice is the presence of slower dynamics extending upto 10 GHz. Even for small globular proteins like lysozyme, due to their large moment of inertia, their reorientational dynamics will show up around MHz frequencies [38]. The high-frequency tail of this process, as seen in the previous OKE study [17], is not seen in our spectra. The authors have also regarded this high-frequency tail as unreliable. The slow dynamics that we do see in our OKE spectra therefore, can be attributed to the retardation of the water molecules diffusing within the protein hydration layer. This water dynamics in the protein hydration layer is often termed as “slow water”. This slow water diffusion has a characteristic timescale of 5.8 ps.

As described in the previous chapters, a sum of Debye, Cole-Cole (CC) and Brownian oscillators (BO) have been utilized to fit the aqueous lysozyme spectra (Figure 2).

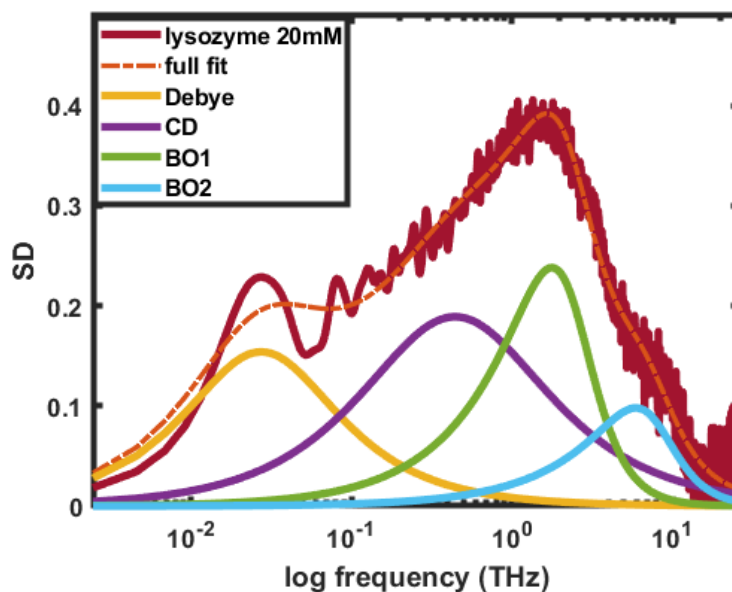


Figure 2: The spectral density of aqueous 20 mM lysozyme solution fitted to a sum of Debye, Cole-Cole, and two Brownian oscillators.

Figure 3, shows the aqueous lysozyme spectra at a low concentration of 3 mM, compared to neat water. This is the lowest concentration of lysozyme in water that we have taken in this study. The low concentration SD looks quite different from the high concentration one, in ways that it almost resembles the pure water spectrum. The slow diffusive water dynamics is negligible at this concentration. Looking at this data, we can say that at these low concentrations, the water structure is mostly preserved. The diffusive process timescale of the slow water is concentration-dependent, with the increase in the lysozyme concentration, the slow water diffuses at an even slower rate. A clearer understanding of the higher frequency modes can be gathered by comparing the reduced spectral densities of the two different concentration regimes with the SD of pure water (Figure 4).

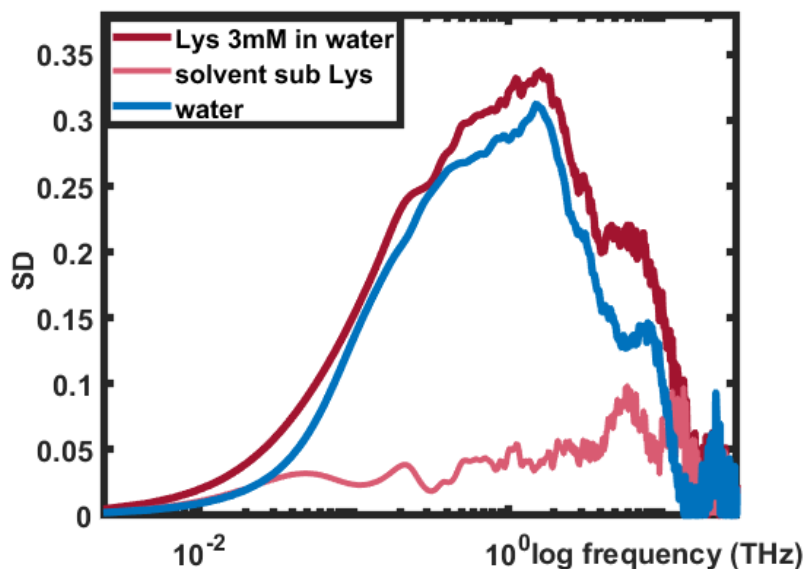


Figure 3: Spectral density (SD) of aqueous 3 mM Lysozyme compared with the SD of neat water. The lighter pink curve corresponds to the solvent subtracted spectra of the same concentration.

	A1 (%)	A2 (%)	A3 (%)	A4 (%)	a	γ_1 (THz)	γ_2 (THz)	τ_1 (ps)	τ_2 (ps)	ω_1 (THz)	ω_2 (THz)
Water	--	0.11	19.86	80.03	0	3.86	7.16	--	0.55	2.39	8.75
Lys 20mM	0.09	0.13	19.03	80.76	0.11	3.49	10.91	5.82	0.36	2.39	7.77
Lys 3mM	0.01	0.06	8.76	91.17	0.04	3.67	10.84	2.89	0.48	2.27	8.75

Table 1: The fitting parameters of pure water and the aqueous solution of 20 mM and 3 mM lysozyme solutions.

A close inspection of the Reduced Spectral Density (RSD) shows that at low concentrations, the librational dynamics of water is not perturbed. Although compared to water, the amplitude of the higher frequency librational mode has increased, which can be attributed to the increase in anisotropy due to interaction between protein surfaces and water molecules. At high concentrations of lysozyme, the water dynamics is slightly disrupted, as can be seen from the redshift of the librational band and the decrease in the amplitude.

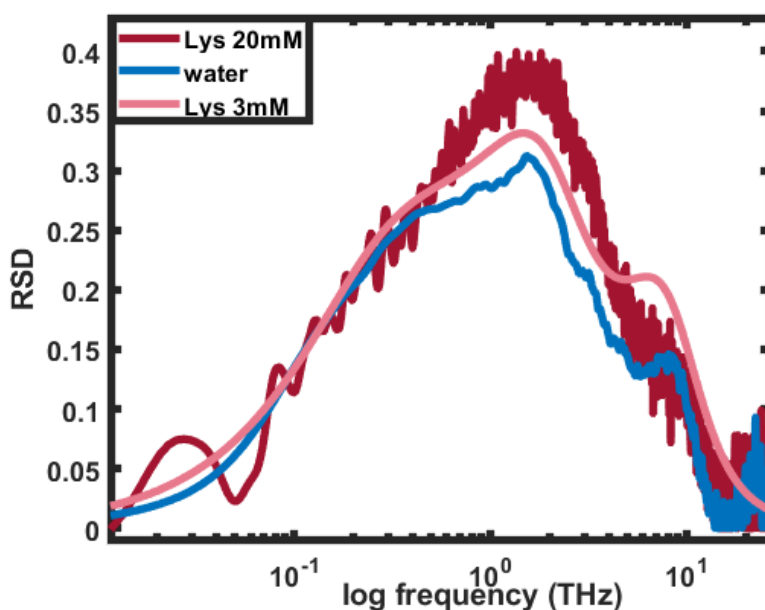


Figure 4: Reduced Spectral density (RSD) of aqueous 20 mM and 3 mM Lysozyme compared with that of neat water.

b) Bovine serum albumin (BSA): Similarly, for BSA, Figure 5 shows the spectral density of the highest concentration soluble in water, 4 mM aqueous BSA solution compared to neat water. As in lysozyme, we see a slow diffusive water dynamics, though it appears at a slightly lower frequency with a characteristic timescale of 1.75 ps. It differs from the lysozyme spectra in having a greater OKE response which can be seen from the increased amplitude of the spectral density compared to pure water. The BSA spectral density is also fitted using a sum of Debye, Cole-Cole, and two Brownian oscillators (Figure 6). The slow dynamics attributed to the “slow water”

diffusing within the protein hydration layer is present at both high and low concentration regimes of the BSA. The timescales do not show a marked difference with a change in concentration.

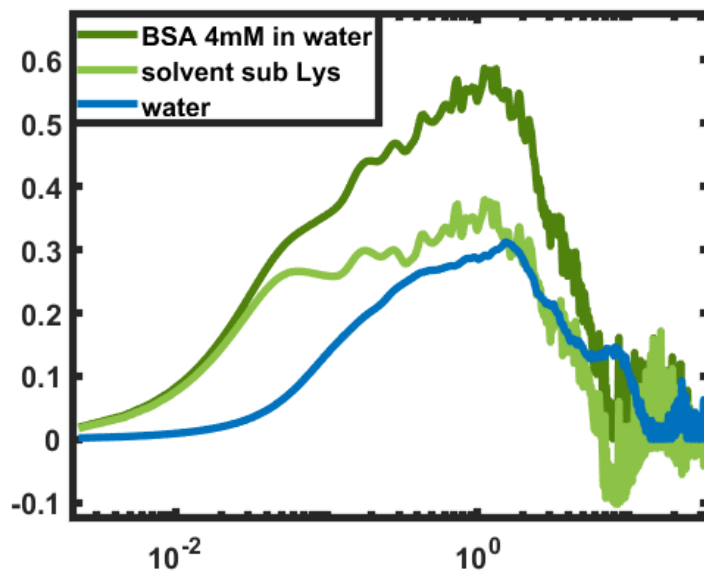


Figure 5: Spectral density (SD) of aqueous 4 mM (the highest concentration soluble in water) BSA compared with the SD of neat water. The lighter green curve corresponds to the solvent subtracted spectra of the same concentration.

	A1 (%)	A2 (%)	A3 (%)	A4 (%)	a	γ 1 (THz)	γ 2 (THz)	τ 1 (ps)	τ 2 (ps)	ω 1 (THz)	ω 2 (THz)
Water	--	0.11	19.86	80.03	0	3.86	7.16	--	0.55	2.39	8.75
BSA 4mM	0.14	0.23	26.74	72.90	0.04	2.85	5.20	1.75	0.28	2.39	5.62
BSA 1mM	0.04	0.06	11.07	88.83	0	3.77	12.26	1.19	0.26	2.61	9.04

Table 2: The fitting parameters of pure water and the aqueous solution of 4 mM and 1 mM BSA solutions.

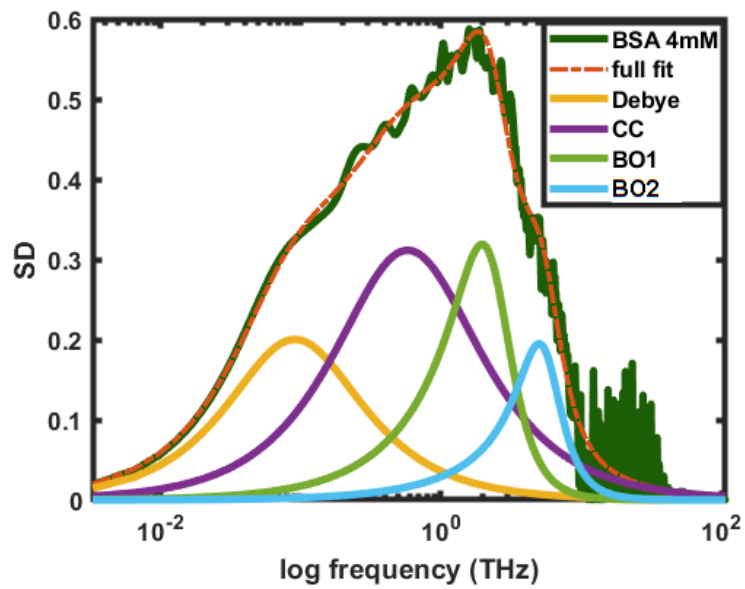


Figure 6: The spectral density of aqueous 4 mM BSA solution fitted to a sum of Debye, Cole-Cole, and two Brownian oscillators.

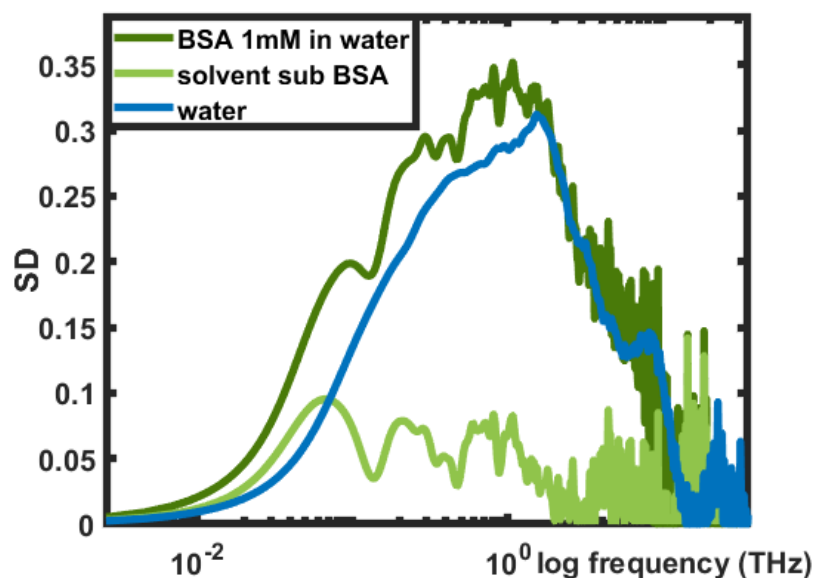


Figure 7: Spectral density (SD) of aqueous 1 mM BSA compared with the SD of neat water. The lighter green curve corresponds to the solvent subtracted spectra of the same concentration.

To get a clearer view of the higher frequency dynamics, we analyzed and compared the reduced spectral densities of the aqueous solutions of 4 mM and 1 mM BSA with the SD of pure water (Figure 8). From the reduced spectral densities, we can see that the water structure is disrupted in the presence of BSA. At low concentrations, the structure is still mostly preserved with only slight changes. The high concentration, on the other hand, shows a complete disruption of the water structure, with the librational frequencies showing a marked redshift. The RSD of 4 mM BSA solution looks absolutely different from the SD of pure water. The increased amplitude observed in the RSD is due to the increased anisotropy of the protein-water interactions.

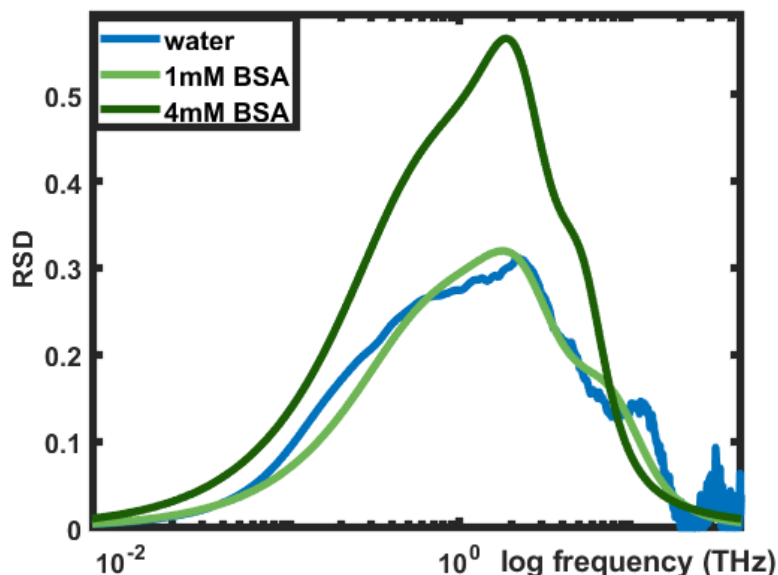


Figure 8: Reduced Spectral density (RSD) of aqueous 4 mM and 1 mM BSA compared with that of neat water.

c) Trypsin: The third protein that we have studied using OKE spectroscopy is trypsin. Only one concentration (1.4 mM) of this protein was studied because it was very difficult to dissolve the protein in water due to the very high hydrophobicity of Trypsin. Figure 9, shows the spectral density of 1.4 mM aqueous trypsin solution compared to the SD of pure water. From figure 9, we can see that the trypsin SD resembles the water spectra at the higher librational frequencies. But compared to the previous proteins, there is no slow dynamics of the diffusing hydration water and the β relaxation of the water spectrum (corresponding to the translational diffusion water molecules) also shows a marked decrease in the trypsin spectra.

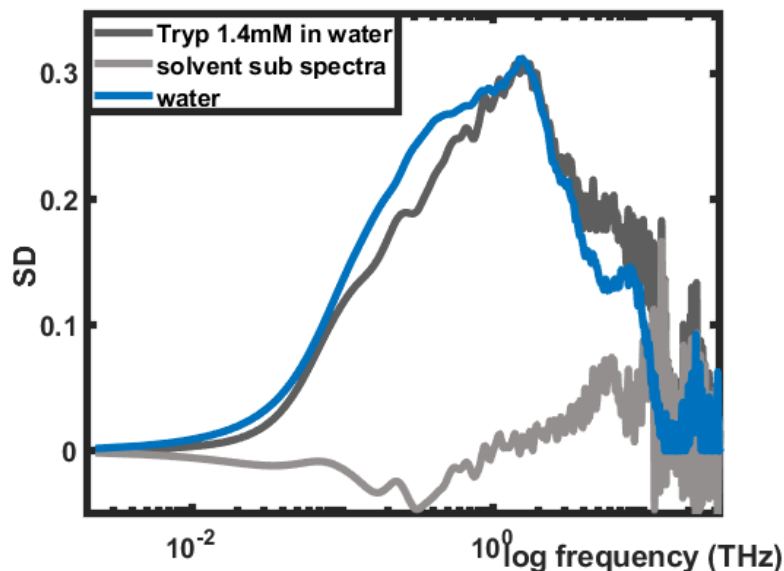


Figure 9: Spectral density (SD) of aqueous 1.4 mM (the highest concentration soluble in water) trypsin compared with the SD of neat water. The lighter grey curve corresponds to the solvent subtracted spectra of the same concentration.

A Cole-Cole and two Brownian oscillators were used to fit the Trypsin spectra. The Debye function was not used because of the absence of slow dynamics (Figure 10).

	A2 (%)	A3 (%)	A4 (%)	a	γ_1 (THz)	γ_2 (THz)	τ_2 (ps)	ω_1 (THz)	ω_2 (THz)
Water	0.11	19.86	80.03	0	3.86	7.16	0.55	2.39	8.75
Trypsin 1.44mM	0.06	8.75	91.19	0.14	3.74	11.14	0.40	2.30	9.1

Table 3: The fitting parameters of pure water and the aqueous solution of 1.4 mM Trypsin.

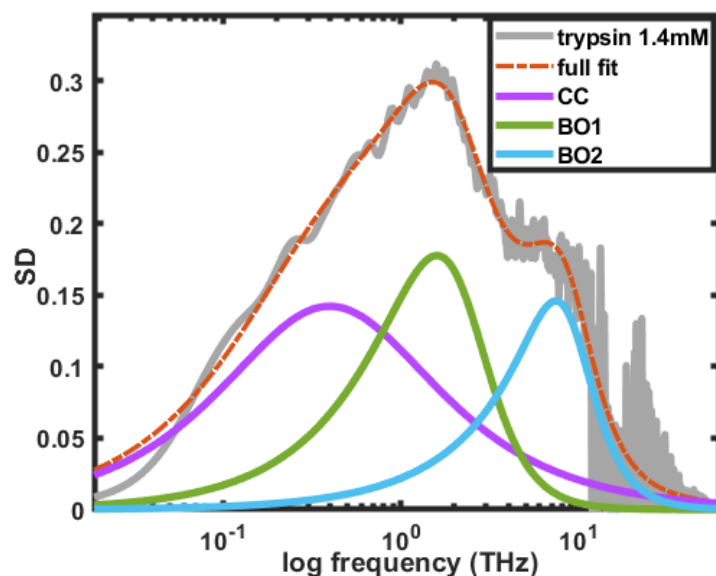


Figure 10: The spectral density of aqueous 1.4 mM Trypsin solution fitted to a sum of Cole-Cole and two Brownian oscillators.

5.3.2 Protein dynamics in urea solutions: The degree of hydrophobicity of the surface of the proteins that we have studied can be ordered as trypsin > lysozyme > BSA, with BSA being the most hydrophilic [16]. This also becomes evident when practically making the protein solutions in water and in urea water systems.

Figure 11 shows the spectral density of BSA in 8.8 M urea, whereas the SDs of BSA in 6 M urea, and in 2 M urea are shown in Figure 12. The solvent subtraction, in this case, is done by subtracting the proportionate weight fraction of the particular concentration urea solution spectra from the protein urea solution. The idea of looking at the solvent-subtracted spectra is to understand what is happening to the solute molecules. Experimentally, in the present OKE spectroscopy setup, it would not be possible to separate out the solvent and solute effects. Solvent spectra subtraction should essentially solve this issue. But this is not the case; rather solvent spectra subtraction only takes out the bulk solvent contribution from the spectra. Therefore the subtracted spectra that are being left behind are characteristic of the solute and the solute-solvent solvation dynamics.

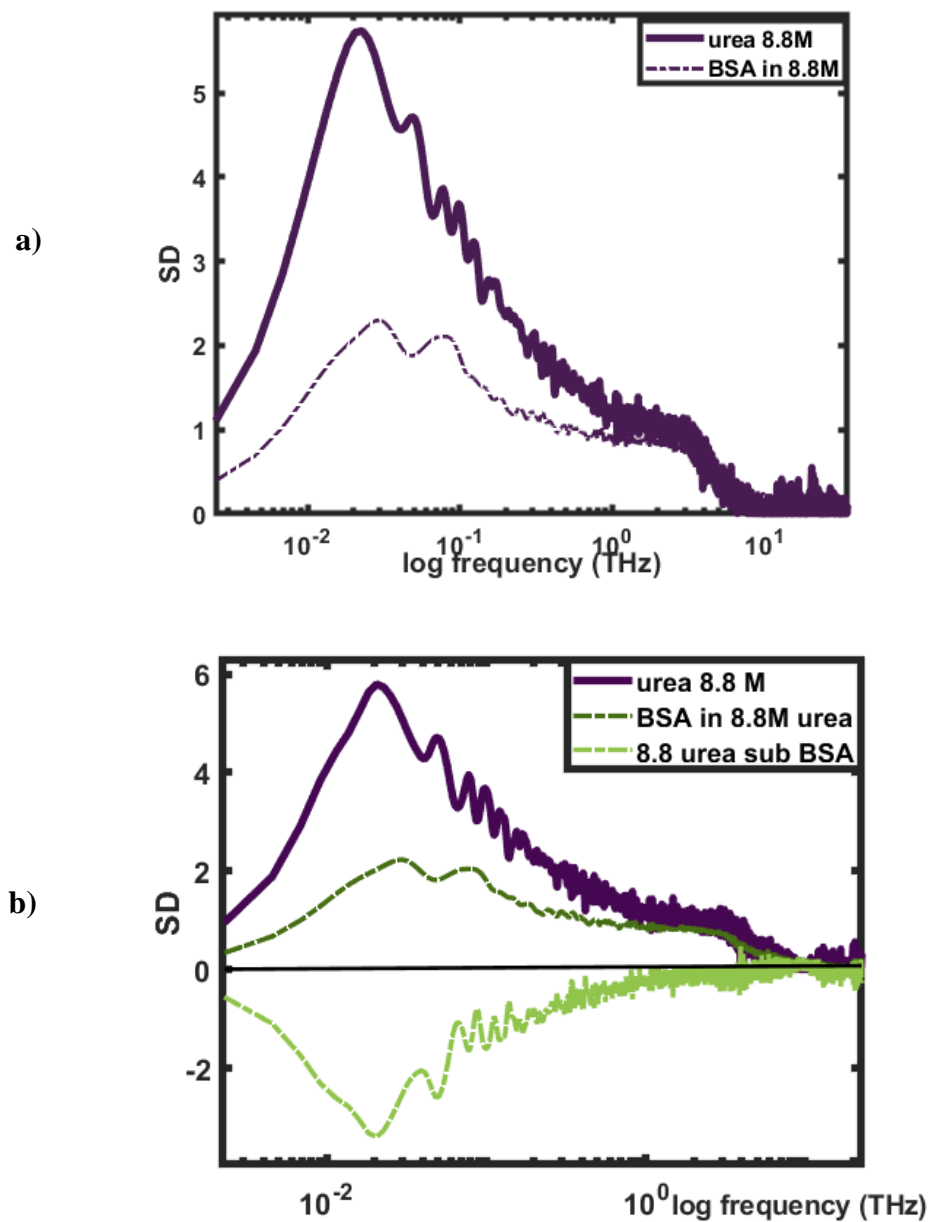


Figure 11: a) The spectral density of BSA in 8.8 M “saturated” urea solution compared to the SD of 8.8 M urea solution. b) along with the light green curve corresponding to the solvent subtracted spectra.

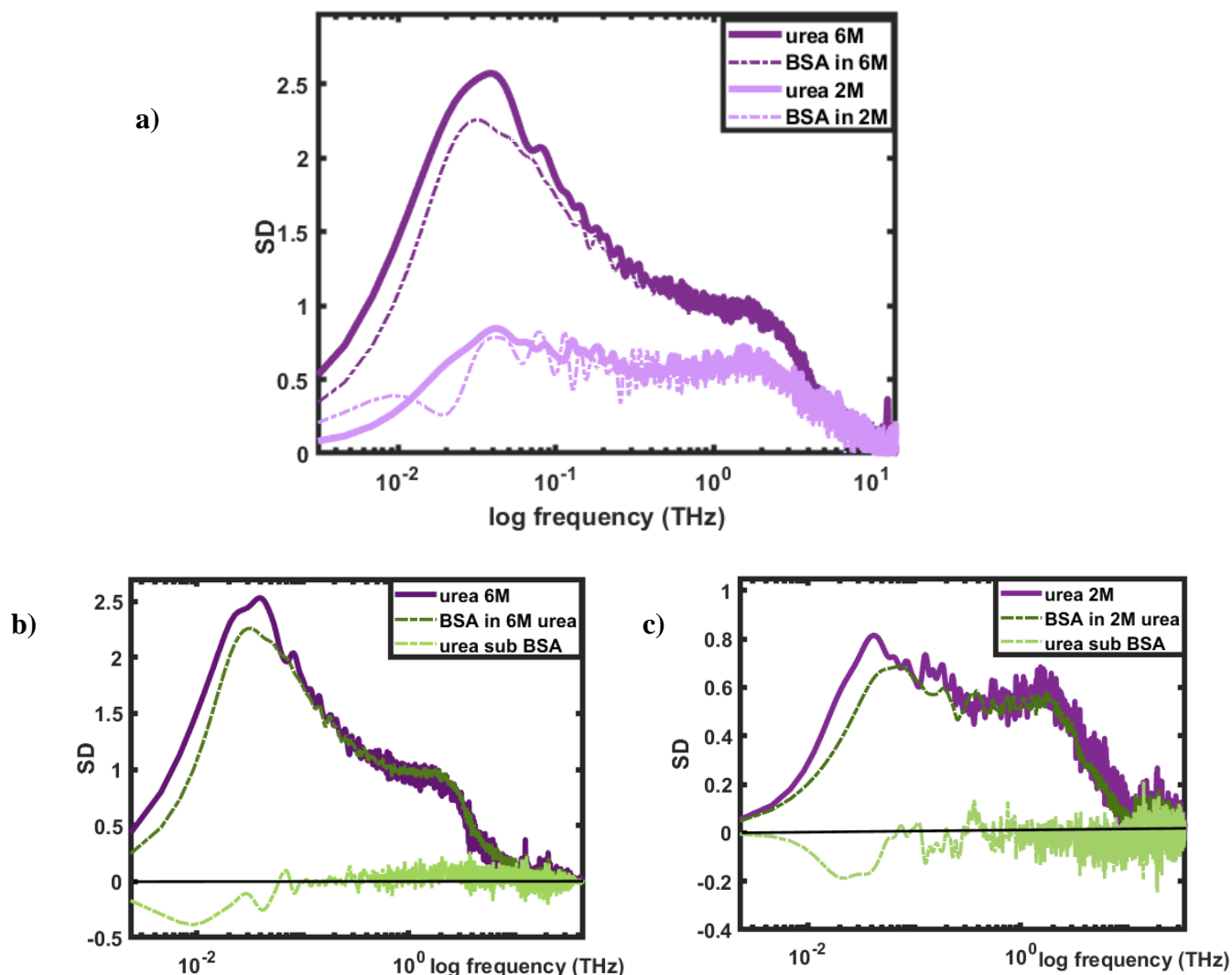


Figure 12: a) The spectral density of BSA in 6 and 2 M urea solution compared to the SD of 6 and 2 M urea solution. b) and c) along with the light green curve corresponding to the solvent subtracted spectra.

One of the most important feature that is noticeable from the spectral densities of the protein-urea solutions (Figures 11 and 12) is that at different urea concentrations, the interaction between the protein and the solvent is remarkably different. In this case, the solvent refers to the aqueous urea system.

In the previous chapter we have learnt that the dominating peak of the urea solutions at the lowest frequencies (between 10-100 GHz) correspond to the slowing down of the dynamics of water molecules which are in close interaction with urea. In Figure 11, the spectral density of BSA in the highest concentration (8.8 M) of urea, the lowest frequency GHz peak shows a tremendous decrease when compared to the SD of urea of equivalent molarity. While a decrease in the amplitude of the SD is expected since the addition of the solute will bring down the relative molarity of urea in the solution. But when the spectral densities are compared at different concentrations, the decrease in the SD amplitude at 8.8 M concentration is not proportionate.

The solvent subtracted (SS) spectra show a huge negative feature at the lowest frequencies for the 8.8 M concentration (Figure 11 b), while for the other two concentrations, the SS spectra (Figure 12 b and c) is almost close to zero with a slight negative feature at the lowest frequencies. The high-frequency librational modes, on the other hand, remain unaffected at all concentrations, which could suggest that the response from the bulk solvent remains unperturbed.

Therefore, the interactions between the protein, urea, and water are strongly dependent on the urea concentration. In Chapter 4, where we studied the urea-water dynamics, we have seen that from 2M urea and beyond, the water structure is disrupted by the presence of urea. In the present chapter, this aqueous urea system (with a disrupted water network when compared to pure bulk water) is our solvent. At the highest concentration of 8.8 M, the only change noticeable on the addition of BSA is the marked decrease of the lowest frequency mode. This particular mode in the urea solution corresponds to the diffusion of the “slow” water molecules in the hydration shell of urea. The marked decrease in the amplitude on the addition of BSA could be due to a decrease in the anisotropy polarization, brought about by the direct interaction of urea with the protein.

At lower concentrations, the addition of protein doesn't bring out a substantial change in the urea spectral density. The decrease in amplitude could be attributed due to the decrease in the relative molarity of the solution. At these concentrations, the protein is denatured by urea following the indirect mechanism. Figure 13, shows the spectral density of trypsin in 8M urea solution, compared to the SD of the equivalent urea concentration.

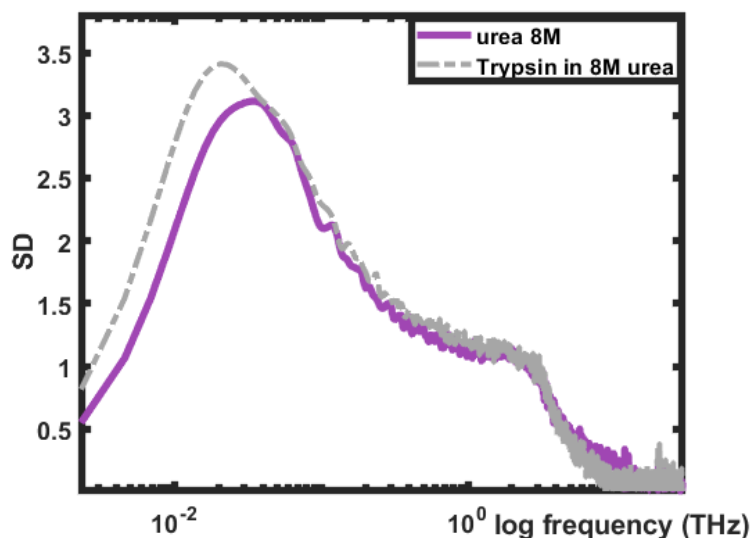


Figure 13: The spectral density of trypsin in 8.8 M “saturated” urea solution compared to the SD of 8.8 M urea solution.

Here (Figure 13), we see something quite different from what we observed for the BSA in urea solution. The addition of trypsin to 8 M urea causes an increase in the spectral density, particularly in the lowest frequency region. There is also a slight redshift of the peak, indicating further slowing down of dynamics, and it is also accompanied by a slight broadening of this diffusive peak of the slow water. The difference between trypsin and BSA is their hydrophobicity at the surface of the macromolecule. While BSA is the most hydrophilic among the three, trypsin is the most hydrophobic. This can be the reason behind the increased anisotropy of this mode on the addition of trypsin.

Figure 14 shows the spectral densities of trypsin added to lower concentrations (6 M and 2 M) of urea. At 6 M urea concentration, the changes on the addition of trypsin are somewhat similar to the 8 M scenario. At 2 M urea concentration, the dynamics are different compared to the higher concentrations. The SD across the entire frequency range shows a decrease in amplitude.

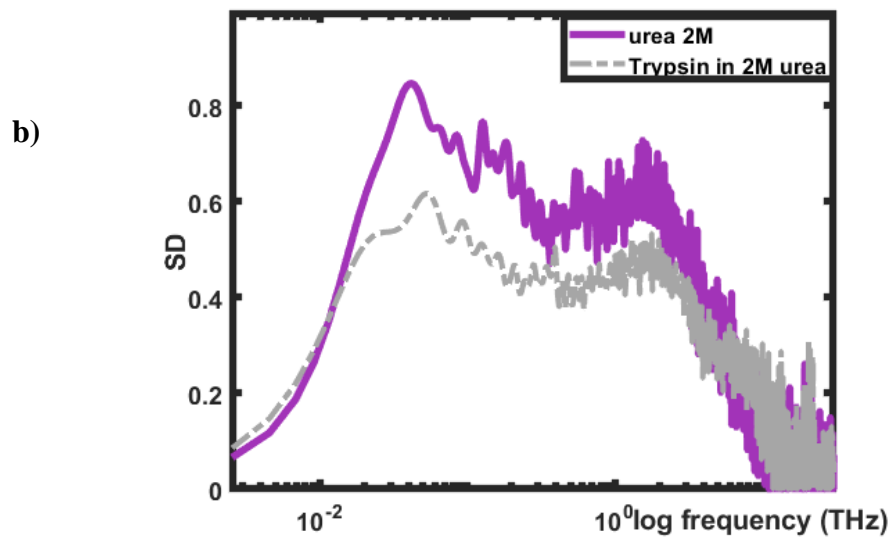
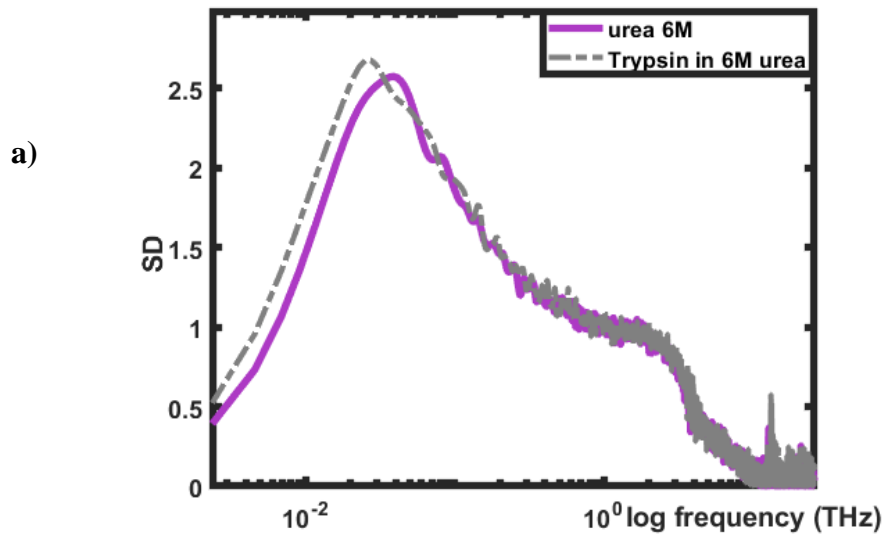


Figure 14: The spectral density of trypsin in a) 6 M and b) 2 M urea solution compared to the SD of 6 M and 2 M urea solution.

5.4 Conclusion:

To conclude, we utilized Optical Kerr effect spectroscopy to study the protein-water system and consecutively understand the mechanism behind the denaturation of protein by urea.

The major take-home message from this chapter is that we were able to shed some light on the controversial direct/indirect argument of urea denaturation of protein. As we see, the mechanism is highly dependent on not only the concentration of the urea solution but also on the type of protein that is being denatured. For BSA, at the 8.8 M, we see evidence of the direct interaction of urea with the protein, while at lower concentrations, the indirect mechanism comes into play. The changes in the spectral densities on the addition of the protein to aqueous urea solution also depend on the hydrophobicity of the protein.

We were also able to understand the effects different proteins have on the water structure at different concentrations. At low protein concentrations, the water structure is mostly preserved. Increasing the concentrations leads to a redshift of the water librational modes indicating that the water structure has been disrupted. This is more pronounced in the case of BSA than in lysozyme. Higher protein concentrations also saw an emergence of a low-frequency mode attributed to the slow diffusion of the water molecules present in the hydration shell of the protein.

5.5 References

1. Wolynes, P.G., W.A. Eaton, and A.R. Fersht, *Chemical physics of protein folding*. Proc Natl Acad Sci U S A, 2012. **109**(44): p. 17770-1.
2. Dill, K.A., et al., *The protein folding problem*. Annual review of biophysics, 2008. **37**: p. 289-316.
3. Lange, O.F., et al., *Recognition dynamics up to microseconds revealed from an RDC-derived ubiquitin ensemble in solution*. Science, 2008. **320**(5882): p. 1471-5.
4. Yang, H., et al., *Protein Conformational Dynamics Probed by Single-Molecule Electron Transfer*. Science, 2003. **302**(5643): p. 262-266.
5. Agarwal, P.K., et al., *Network of coupled promoting motions in enzyme catalysis*. Proceedings of the National Academy of Sciences, 2002. **99**(5): p. 2794-2799.
6. Giraud, G., J. Karolin, and K. Wynne, *Low-Frequency Modes of Peptides and Globular Proteins in Solution Observed by Ultrafast OHD-RIKES Spectroscopy*. Biophysical Journal, 2003. **85**(3): p. 1903-1913.
7. Lipps, F., S. Levy, and A.G. Markelz, *Hydration and temperature interdependence of protein picosecond dynamics*. Physical Chemistry Chemical Physics, 2012. **14**(18): p. 6375-6381.
8. He, Y., et al., *Evidence of protein collective motions on the picosecond timescale*. Biophysical journal, 2011. **100**(4): p. 1058-1065.
9. Acbas, G., et al., *Optical measurements of long-range protein vibrations*. Nature Communications, 2014. **5**(1): p. 3076.
10. Kauzmann, W., *Some Factors in the Interpretation of Protein Denaturation*||The preparation of this article has been assisted by a grant from the National Science Foundation, in *Advances in Protein Chemistry*, C.B. Anfinsen, et al., Editors. 1959, Academic Press. p. 1-63.
11. Denisov, V.P., B.-H. Jonsson, and B. Halle, *Hydration of denatured and molten globule proteins*. Nature Structural Biology, 1999. **6**(3): p. 253-260.

12. Luong, T.Q., et al., *Do hydration dynamics follow the structural perturbation during thermal denaturation of a protein: a terahertz absorption study*. Biophysical journal, 2011. **101**(4): p. 925-933.
13. Heyden, M. and M. Havenith, *Combining THz spectroscopy and MD simulations to study protein-hydration coupling*. Methods, 2010. **52**(1): p. 74-83.
14. Schmidt, D.A., et al., *Rattling in the Cage: Ions as Probes of Sub-picosecond Water Network Dynamics*. Journal of the American Chemical Society, 2009. **131**(51): p. 18512-18517.
15. Born, B., et al., *The terahertz dance of water with the proteins: the effect of protein flexibility on the dynamical hydration shell of ubiquitin*. Faraday Discussions, 2009. **141**(0): p. 161-173.
16. Mazur, K., I.A. Heisler, and S.R. Meech, *Water Dynamics at Protein Interfaces: Ultrafast Optical Kerr Effect Study*. The Journal of Physical Chemistry A, 2012. **116**(11): p. 2678-2685.
17. Turton, D.A., et al., *Terahertz underdamped vibrational motion governs protein-ligand binding in solution*. Nature Communications, 2014. **5**(1): p. 3999.
18. Hunt, N.T., et al., *The Dynamics of Water–Protein Interaction Studied by Ultrafast Optical Kerr-Effect Spectroscopy*. Journal of the American Chemical Society, 2007. **129**(11): p. 3168-3172.
19. Idrissi, A., *Molecular structure and dynamics of liquids: aqueous urea solutions*. Spectrochimica Acta Part A: Molecular and Biomolecular Spectroscopy, 2005. **61**(1): p. 1-17.
20. Hoccart, X. and G. Turrell, *Raman spectroscopic investigation of the dynamics of urea–water complexes*. The Journal of Chemical Physics, 1993. **99**(11): p. 8498-8503.
21. Idrissi, A., et al., *The effect of temperature on urea–urea interactions in water: a molecular dynamics simulation*. Journal of Molecular Liquids, 2004. **110**(1): p. 201-208.
22. Idrissi, A., et al., *The Effect of Urea on the Structure of Water: A Molecular Dynamics Simulation*. The Journal of Physical Chemistry B, 2010. **114**(13): p. 4731-4738.
23. Pace, C.N., *Determination and analysis of urea and guanidine hydrochloride denaturation curves*. Methods Enzymol, 1986. **131**: p. 266-80.

24. Rose, G.D., et al., *A backbone-based theory of protein folding*. Proceedings of the National Academy of Sciences, 2006. **103**(45): p. 16623-16633.
25. Carr, J.K., et al., *Structure and Dynamics of Urea/Water Mixtures Investigated by Vibrational Spectroscopy and Molecular Dynamics Simulation*. The Journal of Physical Chemistry B, 2013. **117**(42): p. 13291-13300.
26. Yang, Z., et al., *Coherent Microscopic Picture for Urea-Induced Denaturation of Proteins*. The Journal of Physical Chemistry B, 2012. **116**(30): p. 8856-8862.
27. Zou, Q., S.M. Habermann-Rottinghaus, and K.P. Murphy, *Urea effects on protein stability: hydrogen bonding and the hydrophobic effect*. Proteins, 1998. **31**(2): p. 107-15.
28. Frank, H.S. and F. Franks, *Structural Approach to the Solvent Power of Water for Hydrocarbons; Urea as a Structure Breaker*. The Journal of Chemical Physics, 1968. **48**(10): p. 4746-4757.
29. Frank, H.S. and M.W. Evans, *Free Volume and Entropy in Condensed Systems III. Entropy in Binary Liquid Mixtures; Partial Molal Entropy in Dilute Solutions; Structure and Thermodynamics in Aqueous Electrolytes*. The Journal of Chemical Physics, 1945. **13**(11): p. 507-532.
30. Finer, E.G., F. Franks, and M.J. Tait, *Nuclear magnetic resonance studies of aqueous urea solutions*. Journal of the American Chemical Society, 1972. **94**(13): p. 4424-4429.
31. Bruccoleri, R.E., M. Karplus, and J.A. McCammon, *The hinge-bending mode of a lysozyme-inhibitor complex*. Biopolymers, 1986. **25**(9): p. 1767-1802.
32. Levitt, M., C. Sander, and P.S. Stern, *Protein normal-mode dynamics: trypsin inhibitor, crambin, ribonuclease and lysozyme*. J Mol Biol, 1985. **181**(3): p. 423-47.
33. Brooks, B. and M. Karplus, *Normal modes for specific motions of macromolecules: application to the hinge-bending mode of lysozyme*. Proceedings of the National Academy of Sciences of the United States of America, 1985. **82**(15): p. 4995-4999.
34. Hédoux, A., et al., *Evidence of a two-stage thermal denaturation process in lysozyme: a Raman scattering and differential scanning calorimetry investigation*. J Chem Phys, 2006. **124**(1): p. 14703.
35. Urabe, H., et al., *Low-frequency Raman spectra of lysozyme crystals and oriented DNA films: dynamics of crystal water*. Biophysical journal, 1998. **74**(3): p. 1533-1540.

36. Genzel, L., et al., *Low-frequency Raman spectra of lysozyme*. Biopolymers, 1976. **15**(1): p. 219-225.
37. Perticaroli, S., et al., *Broadband depolarized light scattering study of diluted protein aqueous solutions*. J Phys Chem B, 2010. **114**(24): p. 8262-9.
38. Cametti, C., et al., *Dielectric Relaxation Spectroscopy of Lysozyme Aqueous Solutions: Analysis of the δ -Dispersion and the Contribution of the Hydration Water*. The Journal of Physical Chemistry B, 2011. **115**(21): p. 7144-7153.

6

Summary and Outlook

6.1 The Bigger Picture

The primary motivation behind the work carried out in this thesis was to explore and therefore contribute to understanding at least some aspects of the broad regime of intermolecular interactions occurring in the liquid phase. The liquid phase itself is dynamic in nature with short-range ordering and disordering at slower timescales, which leads to a range of local microscopic environments. Many interesting phenomena exist in real life, which is a direct manifestation of intermolecular interactions. Using ultrafast spectroscopy, we probed some of these fascinating systems, where intermolecular interactions play a significant role, with hopes of getting a clearer picture of the dynamics, especially the hydrogen-bond dynamics existing in the liquid state.

Ultrafast spectroscopy provides remarkable insights into the fast dynamics and structural fluctuations occurring in the sub-picosecond and the picosecond timescales. These fast timescales are generally characteristic of the fluctuations occurring in the weak non-covalent interactions, the most important one being the highly directional hydrogen bonding. Terahertz time-domain spectroscopy and Optical Kerr Effect spectroscopy, the spectroscopic techniques utilized in this thesis, are excellent probes to help us unravel the intermolecular interaction-induced dynamics in the condensed phase.

Dynamics occurring in different types of molecular liquids and their binary mixtures have garnered much attention over the years. One interesting phenomenon that we see in mixtures of molecular liquids is the formation of an azeotrope. Azeotropes, or constant boiling mixtures, are liquid mixtures of two or more components, having the same concentration in the vapor and the liquid phase at one particular temperature. Using ultrafast spectroscopy, we were able to shed some light on the molecular level understanding behind the formation of an azeotrope. According to the data presented here, we were able to provide experimental proof that the formation of an azeotrope is a temperature-driven process.

Water is the most essential liquid necessary for the existence of life as we know it. The interesting properties of water arise from its extensive hydrogen-bonding network, with the molecules forming ice-like tetrahedral structures. The effect solutes have on the structure of water is an active area of research. Urea is a biologically important solute and has been termed a chaotropic agent; here, in this work, we obtained a clear picture of how urea disrupts the structure of water. We were

also able to see the effect different proteins have on the dynamics of water. Understanding the water dynamics in the presence of solutes like urea is a necessary first step to understand the process urea induced denaturation in protein, the mechanism behind it is one of the most controversial debates in biophysical chemistry. With spectroscopy in the terahertz regime, we were able to see a dependence on urea concentration, and the type of protein used determines the mechanism that the denaturation process will follow.

Terahertz spectroscopy, especially Optical Kerr effect spectroscopy, has therefore proved to be an excellent experimental technique to probe the low-frequency dynamics and the structural fluctuations occurring in the fast femtosecond-picosecond timescales in complex liquid systems. Having said that, OKE spectroscopy does suffer from its own limitations of being a 1D spectroscopic technique. The broad OKE or THz spectra obtained generally give a good picture of the dynamics of the system, but it is impossible to separate the specific processes that contribute to the broadening. The 45° polarization geometry utilized here gives us the anisotropic part of the polarizability tensor, which is made up of both molecular rearrangements and interaction-induced terms. Therefore, the best way to analyze these spectra is by doing a lineshape analysis- fitting the broad spectra to a sum of functions to understand the underlying lineshapes at this GHz-THz frequency range.